UNIVERSITA' POLITECNICA DELLE MARCHE

FACOLTA' DI INGEGNERIA

Corso di Laurea Magistrale **Biomedical Engineering**

Machine Learning Interpretation of Surface Electromyography Signal to Classify Gait Sub-phases

Relatore:

Prof. Sandro Fioretti

Correlatore:

Prof. Francesco Di Nardo

Prof. Christian Morbidoni

Tesi di laurea di:

Filippo Ventura

A.A. **2021** / **2022**

To my family and to all the people who have been close to me on this journey

"Be the change that you wish to see in the world."
— Mahatma Gandhi

TABLE OF CONTENTS

Introduction

Human walking is an intuitive daily-life operation which consists of a cyclic movement of the lower limbs [1,2]. Human gait is accomplished by the coordinated activity of many muscles acting at the hip, knee and ankle joints, which can be described as a sequence of events that requires specific muscles activations [3]. Surface electromyography (sEMG) is acknowledged as a non-invasive approach specifically developed to monitor muscle activity and provide an essential contribution to the characterization of the neuromuscular system [4]. To accomplish a spatial/temporal characterization of muscular recruitment during walking, the signal characterizing foot-floor contact and clearance have to be assessed. This process begins with the need of quantifying the duration of the main phases and sub-phases of human walking. The current gold standard method for the detection of these gait events involves the use of ground reaction force measured by force platforms. Further methods typically involved for gait phases identification are foot-switch sensors, stereo-photogrammetric systems and inertial measurements units (IMUs) [4]. Stereo–photogrammetric systems present high costs of the instrumentation, limited number of cycles observed, and/or invasiveness of experimental set-up, while wearable sensors can require particular care for the correct placement and the need of specific calibration procedures, not consistent with the timing of clinical practice [4]. In the recent years, artificial-intelligence techniques, machine and deep learning models, have been proposed for the classification of gait phases and the prediction of gait events from surface electromyographic signal that contains rich information about muscle excitation [1-16]. This approach would contribute to reduce burden for patient, simplify clinical protocols, and make test faster, specifically in the evaluation of neuro-muscular diseases or for walking-aid devices where the acquisition of myoelectric signals is largely advised [8]. The spatial/temporal characterization of human walking necessarily involves the classification of the two main gait phases, stance and swing, and the consequent assessment of the corresponding transition events, heel-strike (HS, from swing to stance) and toe-off (TO, from stance to swing). Stance and swing identify the functional subdivisions of total limb activity within the gait cycle, thus precisely identifying HS and TO events is important to analyse the gait activity [4]. Usually, stance phase can be further subdivided into three sub-phases, i.e., Initial Stance phase, Mid Stance phase and Terminal Stance phase (Luo et al. [9]), the Initial Stance phase corresponds to the Initial Stance phase in the present work). The Initial Stance phase begins with the heel strike and continues until the foot is completely in contact with the ground. The event that marks the end of the Initial Stance and the beginning of the mid stance phase is the counter lateral toe off. The mid stance phase corresponds to the phase in which the foot is completely resting on the ground. During heel rise event, the terminal stance phase begins until the subsequent toe off.

Once the foot is completely raised from the ground the swing phase begins until the next initial contact. In literature, many studies have been performed on the development of approaches based on machine learning and deep learning techniques for the binary classification of the gait cycle, stance and swing [2,4,5,7,8,10,11,14], with the estimation of the related transition events between the two phases [4,5,7,8,11]. Nevertheless, several works have been proposed for the classification of the different sub-phases of the gait using machine learning algorithms and complex neural network architectures [1,3,9,12,13,15]. However, to our knowledge none of the studies present in the literature provides an estimate of the transition instants between the step sub-phases. Although deterioration of classification performances and events detection compared to a simpler binary classification is expected (average classification accuracy reached by Di Nardo et al. in [7] is 96.10%, while the work of Luo et al. [9] has never exceeded the average level of accuracy of 94.10%), the possibility to provide a 4-phase classification of gait should be exploited in order to provide new insights in different fields such as rehabilitation, clinics, and ergonomics.

Thus, the present study aims to introduce a novel approach based on artificial-intelligence techniques in order to classify gait sub-phases and to identify transition events between these consecutive gait phases using essentially sEMG signals. In details, the sEMG signals collected from the Tibialis Anterior, Gastrocnemius Lateralis, Rectus Femoris, Vastus Lateralis and Hamstring muscles of both legs are processed and organized to feed two supervised learning classifiers implemented in cascade: a Support Vector Machine (SVM) binary classifier to discriminate between stance and swing phases followed by a further SVM 3-classes classifier to identify the three sub-phases of the stance. The output of the second classifier only returns the predictions of the three sub-phases of stance, which are concatenated with the prediction of the swing phases obtained from the first model. This approach is applied to a database composed of sEMG signals acquired during ground walking of 31 young able-bodied subjects recruited at the Movement Analysis Laboratory of Università Politecnica delle Marche. The dataset is freely available consulting the public repository of medical research data PhysioNet. The purpose is to classify the main 4 gait sub-phases, Initial Stance (Class 1), Mid Stance (Class 0), Terminal Stance (Class 2) and Swing (Class 3), and to identify transition events between consecutive gait sub-phases, i.e., Heel Strike (HS), Counter Lateral Toe Off (CTO), Heel Rise (HR) and Toe Off (TO). Classification and prediction performances are evaluated based on standard classification metrics widely used in literature [4,5,7,8,11]: Accuracy Precision, Recall, F1-Score and Mean Absolute Error (MAE). In order to test the reliability of classifications and predictions, results are compared with the ones achieved applying to the same dataset two different approaches reported in literature [4,5,7,8,11].

Machine learning implementation and pre-processing steps were conducted using respectively Google Colab®, a hosted Jupyter notebook service that requires no setup to be used, providing access free of charge to computing resources including GPUs, and MATLAB_R2020b®. Pandas and Numpy libraries were used to import RMSS data and to process and convert them into the format used to train the models

CHAPTER 1: Related Works

The correct identification of gait phases is a prerequisite to achieve a spatial/temporal characterization of muscular recruitment during walking. The adoption of sEMG-based approaches to this issue could help reduce the number of sensors necessary for a complete gait protocol, while limiting the clinical encumbrance, time-consumption, and cost. Recently, artificial intelligence approaches are increasingly used for the classification of gait phases based on the availability of only sEMG signals. Machine learning approaches, implemented for the estimation of gait events from EMG signals during walking, seems to be a very efficient tool to estimate spatial/temporal gait parameters. The study of Di Nardo et al. [7] proposed an intra-subject approach for binary classifying gait phases and related gait events (Heel Strike, HS and Toe Off, TO) using a Multilayer Perceptron (MLP) neural network trained using the envelope of the surface electromyography (sEMG) signals. An average classification accuracy of 96.1% and mean absolute value (MAE) of 14.4 ± 4.7 ms and 23.7 ± 11.3 ms in predicting HS and TO timing were reached. Moreover, the intra-subject approach was compared with the inter-subject approach on the same population, showing a significant improvement (1.4%) in classification and gait events detection. Another study, proposed by Di Nardo et al. [8], shows a mean classification accuracy of 93.4% and mean absolute error of 21.6 ± 7.0 ms and 38.1 ± 15.2 ms for HS and TO prediction, using an MLP classifier fed with vectors composed of 20 ms windows for each sEMG signal of each muscle. Morbidoni et al. [4] reached an average classification accuracy of 93.4%, and a mean absolute error (MAE) of 21.6 ms and 38.1 ms for HS and TO, respectively. Morbidoni et al. also proposed a previous study [6] where three different MLP models are tested reaching value of mean overall accuracy equals to 95.18%. In [5], the intra-subject approach was able to provide, in the hemiplegic population, a mean overall classification accuracy of 97% and a prediction of HS and TO events, in terms of MAE of 14.8 ± 3.2 ms for HS and 17.6 ± 4.2 ms for TO and F1-score of 95% for HS and 92% for TO. In the study proposed by Nazmi et al. [10], a MLP model achieved 87.5% for learned data and 77% for unlearned data of classification accuracy in discriminating stance and swing phase using different time domain features. A second study proposed by Nazmi et al. [11] used a three-layer MLP trained with 5 time domain features achieving a percentage of classification accuracy of 87.4%. Identification of the timing of HS and TO was performed obtaining a MAE (for unlearned subject) of 35 ± 25 ms ms and 49 ± 15 ms, respectively. The work of Ziegler et al. [14] addressed a classification of stance phase and swing phase using a support vector machine (SVM) classifier trained with a feature calculated from the bilateral EMG signals of muscle pairs, called weighted signal difference. The presented method shows promising results with classification accuracies of up to 96%. Ghalyan et al. [2] tested several machine learning models to classify stance and swing phases using raw EMG signals. The results were compared with

the accuracy of the classification obtained using the same classifiers with the application of a median filter to the raw EMG data. K-Nearest Neighbours (K-NN) reported the highest overall accuracy values (99.8%) with a big improvement over the raw data.

For what concerns multiple gait phases recognition, Luo et al. [9] proposed a neural network-based sEMG signal classifier combining long-short term memory (LSTM) with MLP to determine 4 gait phases. Experimental results show that this method achieved average classification accuracies of 94.10% and 87.25% for subjects walking in a flat terrain at 5 and 3 km/h, respectively. Ying et al. [1] used a SVM classifier to determine 5 phases after EMG data denoising and feature extraction. Results reported a mean overall classification accuracy over three subjects of 88.78%. In [12], Wei et al. indicated that the recognition performance of mean absolute value and zero crossing (features set) achieved an average classification accuracy of 89.40% when using a SVM classifier to classify 5 different gait phases. A second study proposed by Wei et al. [13] showed that time and frequency domain feature sets of sEMG signals achieved high accuracy of 7 gait phases recognition (95.58% flat terrain at 1.4 km/h, 97.63% at 2.0 km/h and 98.10% at 2.6 km/h) using a SVM classifier. In the study of Meng et al. [3], instead, a Hidden Markov Model (HMM) is used to recognize 5 different gait phases using time domain features of the sEMG signal. Results are reported in terms of mean recognition error, which achieved the lowest value of 8.15% using a mean absolute value and waveform length as feature set. In the study of Kyeong et al. [15] four sensor combinations were used to classify 6 and 7 gait phases, reaching a classification accuracy of 97.8%. Vastus medialis and gastrocnemius were the most effective combinations of two muscle types among the five sEMG sensor locations on the legs. Finally, Lauer et al. [16] proposed an adaptive neuro-fuzzy inference system (ANFIS) with a supervisory control system (SCS) was used to predict the occurrence of 7 gait events from sEMG signals. Using one EMG signal and its derivative from each leg as its inputs, the ANFIS with SCS was able to predict all gait events in seven out of the eight children, with an overall accuracy in predicting gait events ranged from 98.6% to 95.3%.

CHAPTER 2: Joint Movements and Muscle Activations of Lower Limbs

Human walking can be described as a cyclic pattern of body movements which advances an individual's position. Assuming that all walking cycles are about the same, studying the walking process can be simplified by investigating one walking cycle [17]. The walk is therefore given by a cyclic succession of alternating rhythmic movements that allows us to move our body forward trying to maintain the muscles energy consumption as low as possible.

2.1 Gait Analysis

The **gait cycle** is defined as the time interval between two successive occurrences of one of the repetitive events of walking. Walking uses a repetitive pattern of limb movements that allows the body to advance while maintaining the stability in support. During the progression of the body, one limb act as support, while the other advances, then the two lower limbs exchange their roles. When the oscillating foot touches again the ground at next support, the contralateral foot is in contact with the ground allowing the progressive transfer of the body wight. This sequence of events is defined as gait cycle. Normally, the beginning of the gait cycle is identified with initial contact which correspond, for a normal person, with the **Heel Strike** (HS) event.
Each gait cycle is divided principally in two phases:

- *Stance*
- *Swing*

The stance phase (60% of the entire gait cycle) identifies the period characterized by the contact of the foot with the ground and the average duration of this phase ranges approximately between 0.59 to 0.67 s, while the swing phase (40% of the entire gait cycle) corresponds to the interval in which the foot is raised from the ground for the progression and lasts, on average, 0.38 to 0.42 s. The event that identifies the swing phase is the **Toe-off** (TO), during which the foot rises completely from the ground [18]. This macro-division of gait cycle refers to just one leg and it is reported in ***Figure 2. 1***.

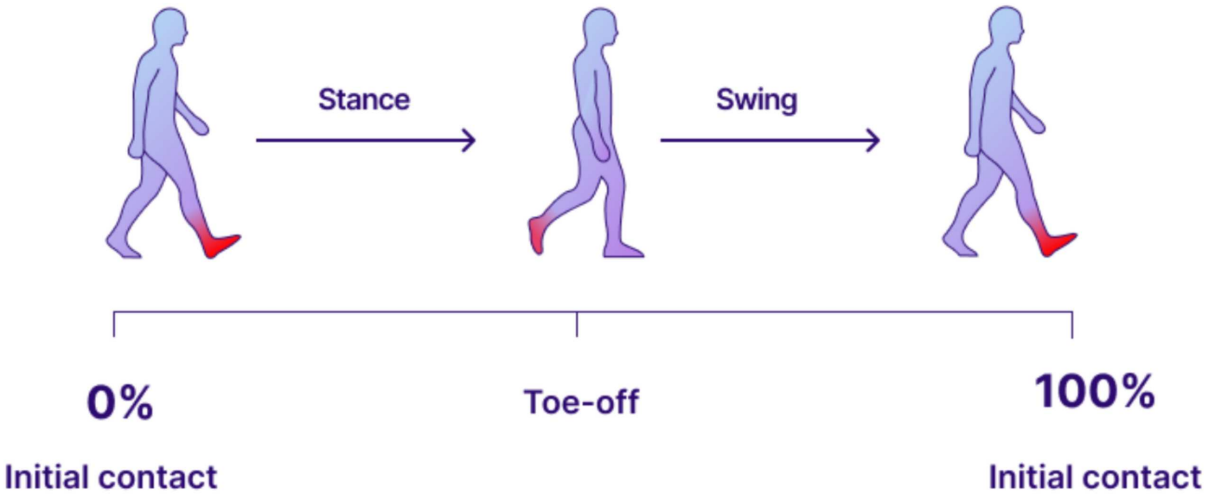

Figure 2. 1 *Main phases of the gait cycle and corresponding transition events*

The gait cycle, also defined as stride, is the interval between two consecutive initial contacts accomplished by the same limb [19]. Each stride consists of two steps. At the midpoint of the stride, the other foot touches the ground to begin the next stance phase (***Figure 2. 2***).

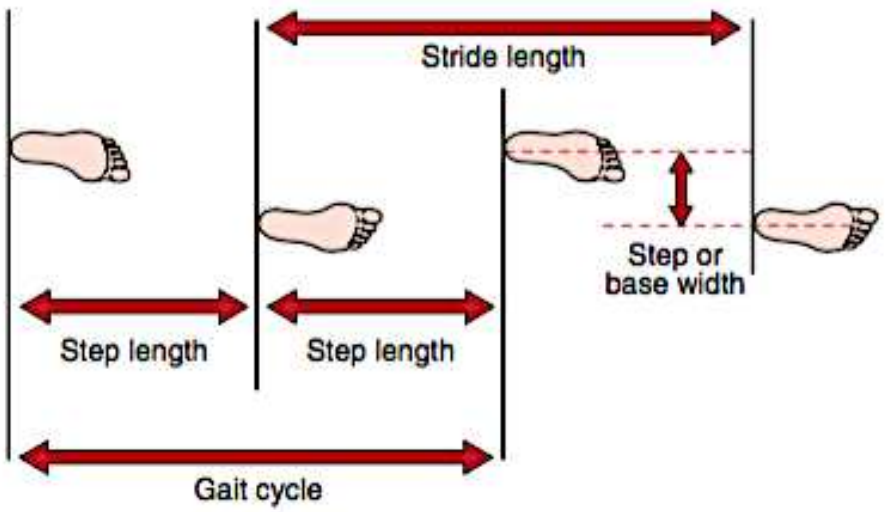

Figure 2. 1 *Stride length: distance between two successive placement of the same foot and it consists of two steps. Base width: the side-to-side distance between the line of the two feet.*

The stance phase is divided in three intervals according to the sequence of foot contact with ground. The beginning and the end of the support phase both include a period of bilateral contact (or **double support**), lasting about 10% of the gait cycle, while the intermediate sequence is characterized by the contact of only one foot with the ground (or **single support**), lasting about 40% of the entire gait

(***Figure 2. 3***). The single support phase begins when the opposite foot detaches from the ground for the oscillation and the entire body weight is supported by the stance limb [18].

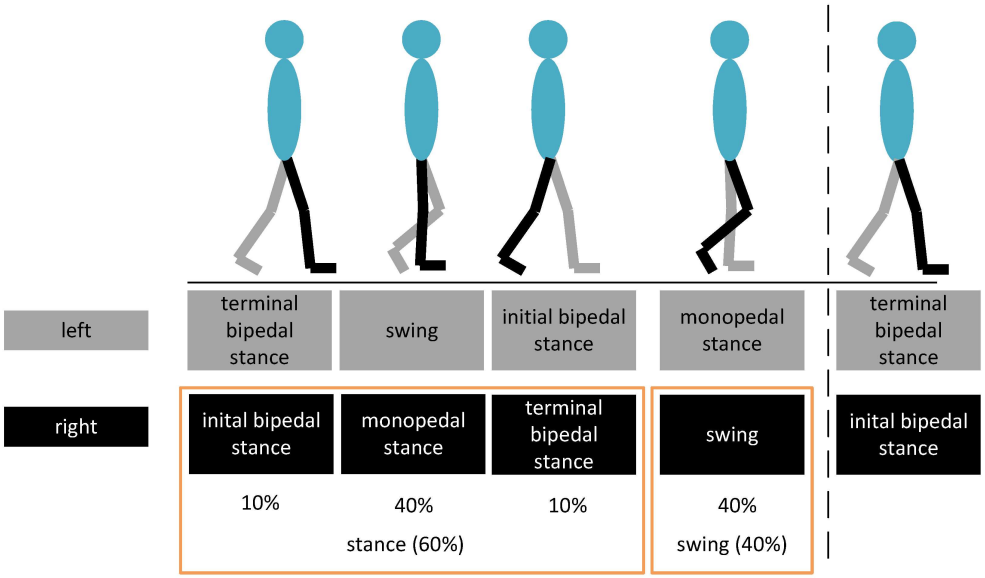

Figure 2. 2 *Gait division in single (40%) and double support (10%) phases and swing (40%) phases*

The increase in walking speed is a variable that affects the time parameters of the gait cycle, in particular by extending the duration of the single support phase and reducing those of the double support [1].

2.1.1 Gait Phases

At each step the alignment between trunk, foot in single support and the progression of each segment of the opposite oscillating limb varies continuously in order to ensure the basic functions required by the walking task. This determines a series of motion patterns made by the hip, knee and ankle joints. The gait cycle contains 8 functional schemes that are defined as sub-phases in relation to the basic swing and stance phases. Each of the 8 sub-phases (***Figure 2. 4***) has a precise **functional objective** and is characterized by a specific synergistic movement pattern to achieve this goal [18]. These functional objectives consist mainly in:

- Weight acceptance
- Stability during the single support phase
- Lower limbs progression

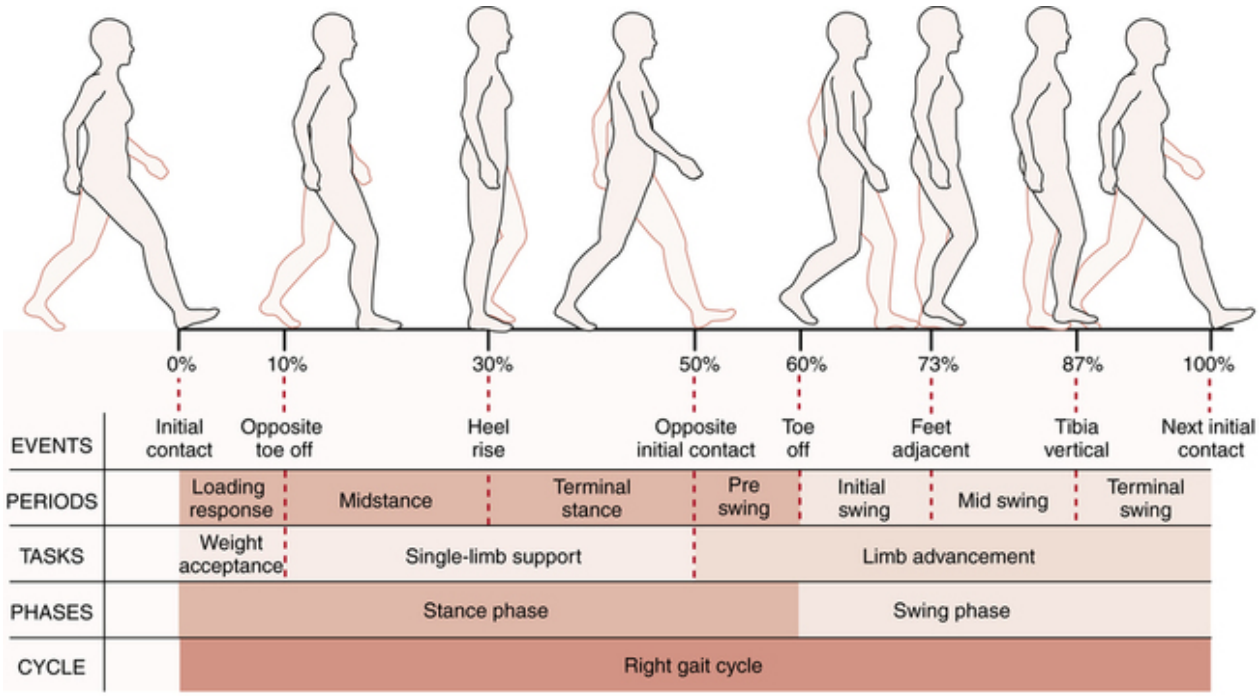

Figure 2. 3 *Gait sub-phases and corresponding transition events*

Weight acceptance

It is characterized by the necessity to rely on three different functional schemes: impact absorption, initial stability of the limb and preservation of progression [18]. The 2 gait phases include:

PHASE 1. INITIAL CONTACT (0-2% of the gait cycle)

Initial contact is the start of the loading response (or the "weight acceptance") and the event that identifies this phase is the heel strike, which is the temporal instant when the heel touches the ground. It is also the beginning of the stance period and the first part of the initial double-leg support period [18]. The goal at this stage is to correctly position the limbs so as to make it possible to roll the heel.

PHASE 2. LOADING RESPONSE (2-12% of the gait cycle)

Loading response is the rest of the initial double-leg support period, it begins with the initial contact and continues until the opposite foot raises from the ground. The goals of this period are the absorption of the impact, stability under load and conservation of progression [18].

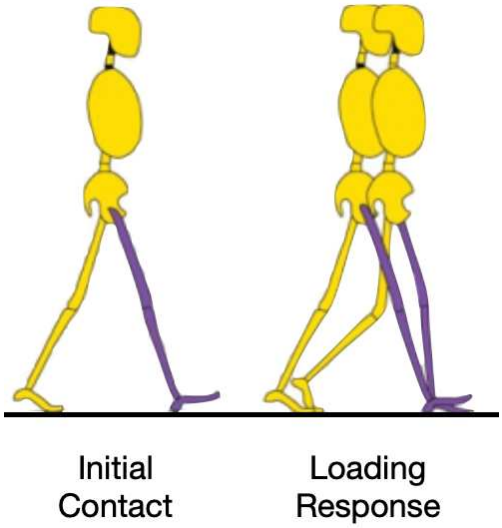

Figure 2. 4 *Reference limb is the violet limb. 1. Initial Contact. The ankle is dorsiflexed (neutral position), the knee is extended, and the hip flexed. The ground contact is made with the heel. 2. Loading Response. the ankle plantar flexion limits the heel rocker by forefoot contact with the ground.*

Single support

The detachment of the contralateral limb during its swing phase determine the beginning of the single support for the stance limb [18].

PHASE 3. MID STANCE (12-31% of the gait cycle)

The gait event that identifies the mid stance phase is the **Counter Lateral Toe Off** (CTO). This is the first part of the single-leg support period. Stability is a major concern as the base of support will decrease significantly and the center of gravity will move to its highest point through leg extension [19]. This phase begins when the opposite foot rises from the ground and finishes when the body weight is aligned with the forefoot [18]. During this period the goal is to maintain the progression over the stance limb and the stability of the trunk and limb itself.

PHASE 4. TERMINAL STANCE (31-50% of the gait cycle)

This phase begins with the **Heel Rise** (HR) gait event. This is the second part of the single-leg support period. Stability is still a concern as well as the heel strike of the opposite foot [19]. It begins with the lifting of the heel from the ground and continues until the contralateral foot touches the ground. The functional objective of this phase concerns the progression of the trunk over the foot in support [18].

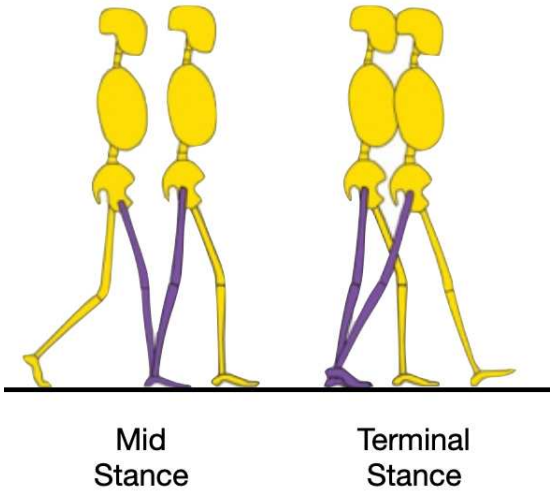

Figure 2. 5 *Mid Stance. Hip and Knee are extended. The limb advances by ankle dorsiflexion (ankle rocker). Terminal Stance. Knee and hip increase extension. The heel rises and the limb advances over the forefoot rocker.*

Lower limb progression

The correct positioning of the swinging limb occurs with three main movement of lifting, advancing and preparing for the subsequent support phase.

PHASE 5. PRE-SWING (50-60% of the gait cycle)

Opposite initial contact (OI) characterizes the onset of the pre-swing phase. In this phase the body weight is transferred, which unloads the swinging limb. All the movements and muscular actions that occur in this period are aimed at preparing the oscillation [18]. During this phase, we also have the maximum propulsion in terms of the anterior-posterior force as we prepare to propel our foot off the ground [19]. This phase begins with the initial contact of the opposite foot and continues until the detachment of the homolateral toes. The functional objective is the preparation of the limb positioning for the swing phase [18].

PHASE 6. INITIAL SWING (60-73% of the gait cycle)

The gait event that identifies this phase is the **Toe Off**. This is the first part of the swing period and the goals are the lifting of foot from the ground allowing the entire leg to flex and the progression of the limb. This overall flexion decreases the moment of inertia of the leg and increases the angular velocity of the swinging leg [19]. It begins when the foot rises from the ground and finishes when the swinging limb is parallel to the opposite foot.

PHASE 7. MID SWING (74-87% of the gait cycle)

Mid swing begins after the two feet are adjacent and parallel each other. The corresponding gait event is known as **Feet Adjacent** (FA). This is the second part of the swing period in which the contralateral leg is in single support, with a small support base. This period stars when the swinging limb is opposite the loading limb and ends when the shank is vertical to the ground. The functional objectives consist in the advancement of the limb and the lifting of the foot from the ground (avoiding sliding) as well as maintaining stability on the supporting foot [18].

PHASE 8. TERMINAL SWING (85-100% of the gait cycle)

Terminal swing begins when the shank is vertically aligned. The gait event is called **Tibia Vertical** (TV). This is the third and last part of the swing period that begins when the shank is vertical to the ground and finishes when the foot touches again the ground during the next initial contact. The progression of the swinging limb is complete when the leg is in front of the thigh [18]. In this phase the main goals are the completion of the progression and the preparation of the swinging limb for the subsequent support.

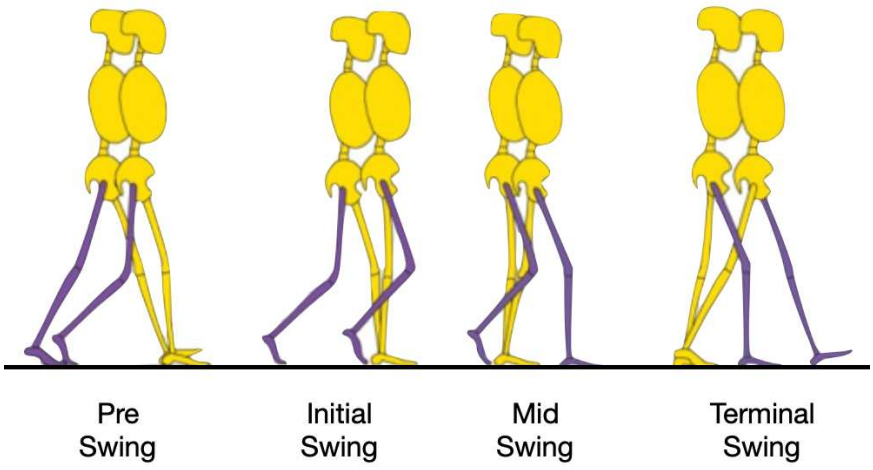

Figure 2. 6 *Pre-Swing. Ankle plantar flexion increases, greater knee flexion and loss of hip extension. Initial Swing. The foot leaves the ground. Limb advances due to hip flexion and increased knee flexion. The ankle partially dorsiflexes. Mid Swing. The ankle continues dorsiflexing reaching the neutral position. The knee extends in response to gravity, while the limb advances anterior to the body weight line thanks to hip flexion. Terminal Swing. The ankle reaches the neutral position, the limb advancement is completed thank to knee extension, the hip keeps its earlier flexion.*

2.2 Energy Conservation

Human locomotion is a very complex and demanding task where the body is forced every time to manage some very important situations such as the (1) generation of a propulsive force to favour the progression of the lower limbs, (2) the maintenance of balance and stability of the body despite continuous postural variations and (3) the absorption of the trauma caused by the impact of the foot with the ground. The muscles contract continuously during walking allowing to provide the necessary stability and mobility to the lower limbs (and to the whole body) during each gait cycle, and at the time they are released, when possible, for **energy conservation**. The efficiency in carrying out any activity represents the relationship between the work performed and the energy expended. In walking, this latter is represented by the muscular activity aimed at maintaining stability in support through the control of the fall of the centre of gravity and the advancement of the limb oscillating during the progression of the body [18]. In a normal gait cycle, two mechanisms act to conserve energy:

- Modulation of the alignment of the gravity line
- Selective muscular control

2.2.1 Control of the Center of Gravity

The six optimizations used to minimize the excursions of the center of gravity were called the **determinants of gait** and they are all integrated together during each gait cycle. The combined effect is a much smoother trajectory for the center of gravity (COG) and a much lower energy expenditure. The determinants of gait reduce the vertical excursions of the trunk by about 50% and the horizontal excursions by about 40%. The first, second and sixth determinants concern the rotations around hip joint axes, while the third, fourth and fifth determinants include movements at the level of the knee, ankle and foot [20].

1. ***Pelvic rotation***

Pelvic rotation around a vertical axis reduces the angle of hip flexion and extension, which in turn reduces the vertical movement of the hip (and COG). If the pelvis did not rotate, the entire stride length would depend only on hip flexion and extension. The forward motion depends on the total angle through which the hip joint moves from flexion to extension. Since the forward motion is equal to the stride length, it follows that the greater the stride length, the greater the flexion and extension angles of the hip, and the more the hip will move vertically between its highest and lowest positions. Pelvic rotation allows greater stride length for the same amount of hip flexion of the advancing limb and hip extension of the retreating limb [20]. This allows for a longer stride length without significantly affecting the center of gravity (***Figure 2. 8***).

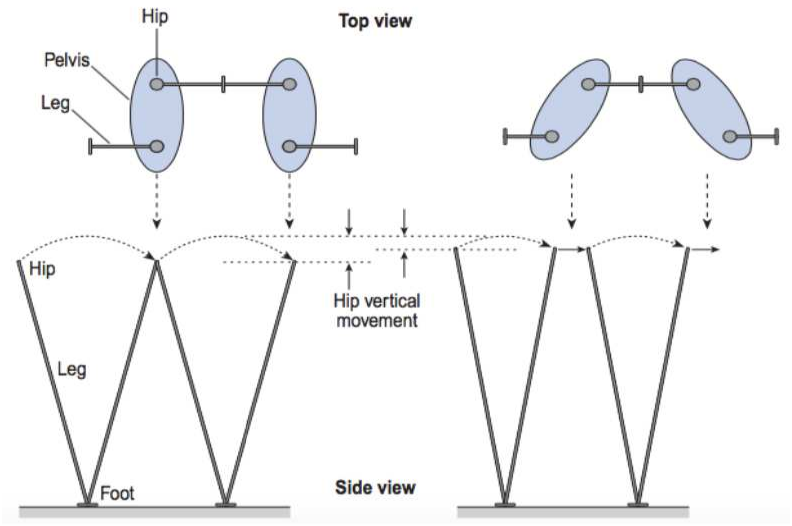

Figure 2. 7 *Pelvic rotation: rotates around its vertical axis reducing the angle of hip flexion and extension*

1. Pelvic tilt

The second determinant of gait is the way in which the pelvis tilts about an anteroposterior axis. Through a positive inclination there is a reduction of the lateral displacement of the COG. It is observed during swing phase. As the pelvis of the swinging leg is lowered the abductors of the contralateral/stance hip contract to control pelvic tilt. The pelvis drops 4-5 degrees towards the swinging leg. This drop decreases the vertical displacement of the center of mass during single limb support. Since the height of the trunk depends on the average height of the two-hip joint, the pelvic obliquity reduces the total vertical excursion of the trunk (and thus of the COG) [20]. The maximal tilting is at mid swing (***Figure 2. 9***).

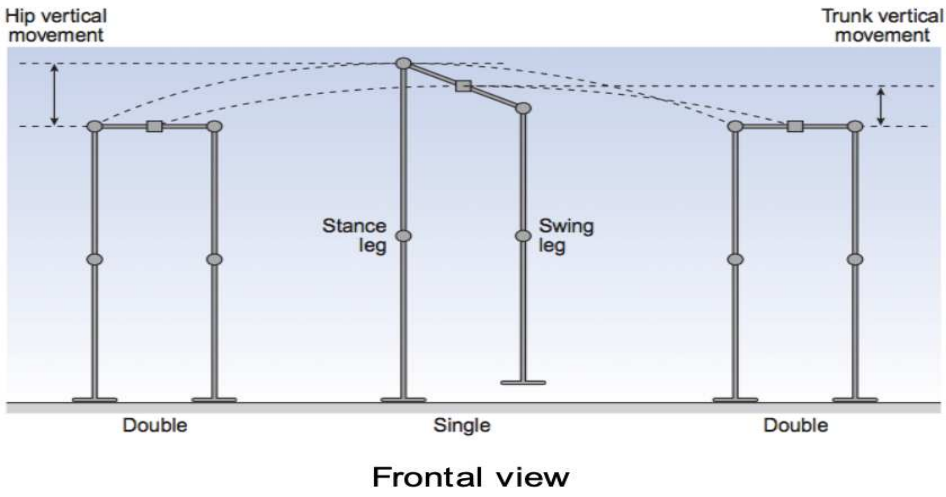

Figure 2. 8 *Pelvic tilt: the swinging leg drops during progression and the vertical excursion of the COG is limited*

2. *Knee flexion in stance phase*

The third determinant is the stance phase flexion of the knee. As the femur passes from flexion of into extension, if the knee remains extended and the femur aligned with the shank, the hip joint will rise vertically and then fall. However, flexion of the knee shortens the effective length of the leg during the mid stance phase, reducing the height of the center of gravity (***Figure 2. 10***) [20].

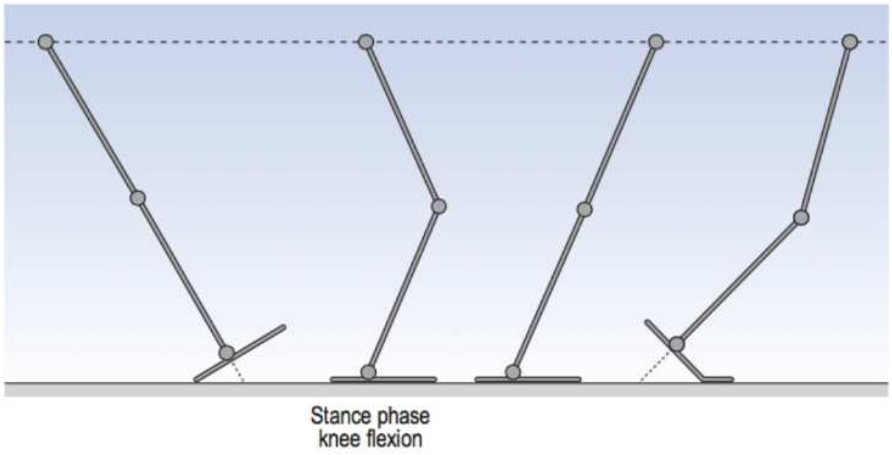

Figure 2. 9 *Knee flexion in stance shortens the length of the leg reducing the vertical excursion of the COG*

3. *Ankle mechanism*

During the initial contact the hip is at its maximum degree of flexion and the knee is totally extended. This joints configuration determines the lowest vertical position of the COG. The goal of the fourth determinant of gait is to keep the height of the COG as constant as possible, lengthening the leg with a dorsiflexor of the ankle during the initial contact (***Figure 2. 11***) [20].

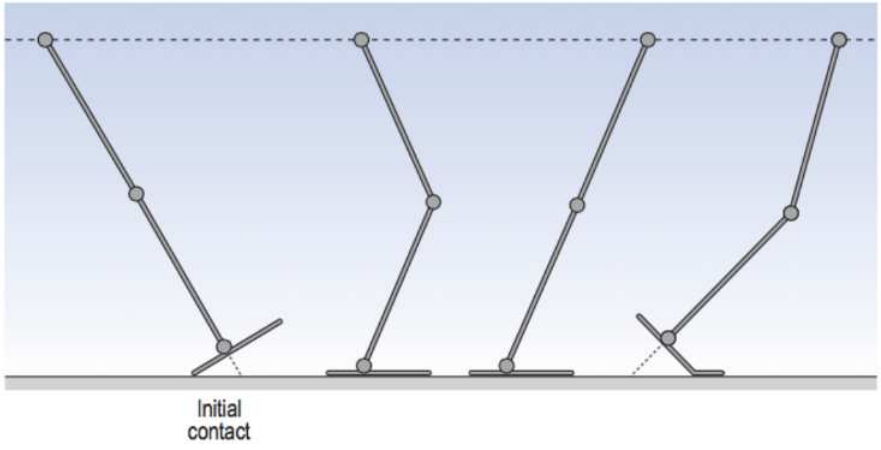

Figure 2. 10 *Ankle mechanism: it maintains the height of the COG constant during stance*

4. Foot mechanism

In the same way that the heel lengthens the leg at the start of the stance phase, the forefoot lengthens it at the end of stance, in the fifth determinant. The foot moves in plantar flexion while the knee begins to flex [20]. That will maintain the center of gravity in its beginning of progression with minimum displacement (***Figure 2. 12***).

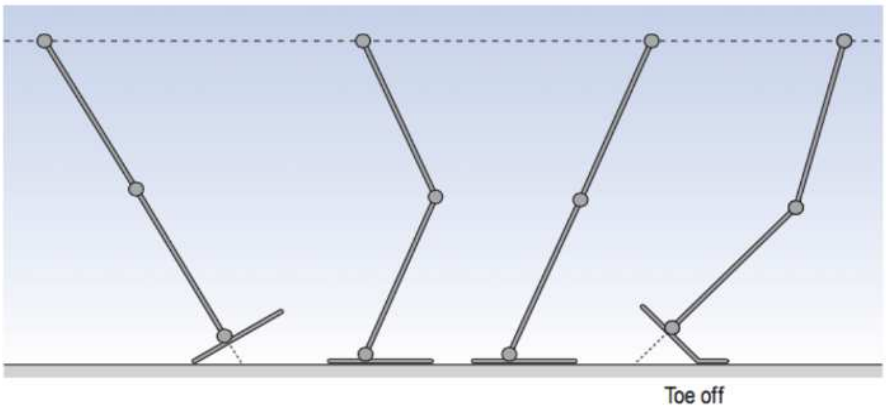

Figure 2. 11 *Foot mechanism: it works in synergy with the ankle mechanism which moves in plantar flexion as the knee flexes to maintain a reduced vertical COG excursion*

5. Lateral displacement of the body

The sixth determinant concerns lateral side-to-side oscillation that occurs within each step. It determines the motion of the COM in the horizontal plane. The center of mass shifts over to the supporting limb to provide further stability in stance phase. The degree of sway is determined by the width of the base of support. The main adaptation which allows the walking base to be narrow is a slight valgus angulation of the knee, which permits the tibia to be vertical while the femur inclines inwards, from a slightly adducted hip. If the feet are placed on the ground far apart (***Figure 2. 13 a***), large side-to-side movements of the center of gravity would be necessary to maintain balance, while having them closer together (***Figure 2. 13 b***) reduces the size of these movements. The reduction in lateral acceleration and deceleration leads to a reduction in the use of muscular energy [20].

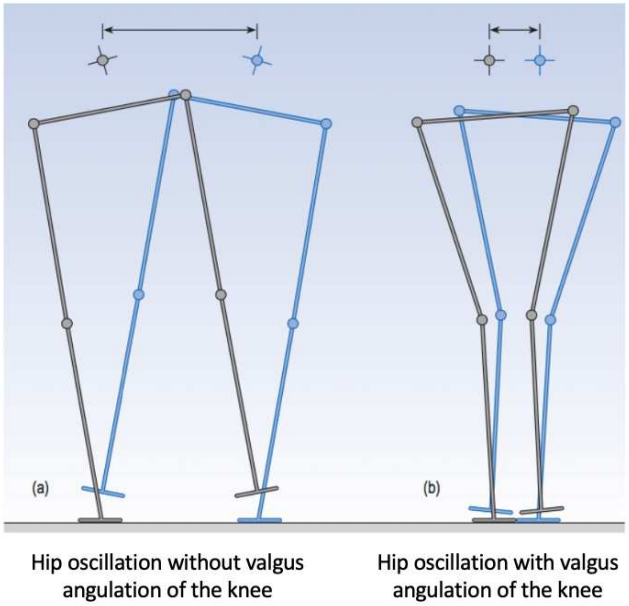

Figure 2. 12 *Lateral displacement of the body: the degree of sway is determined by the width of the base of support. (a) Large hip oscillations are necessary when the feet are placed far from each other. (b) Lower oscillations are needed with the feet close together.*

2.2.2 Selective Control

The progression and stability in support are controlled by muscles recruitment whose intensity and duration are selectively modulated to use the less possible energy [18]. During stance, muscles contract only when the alignment of body segments creates an antagonist moment that alters the stability of the limb under load and the trunk [18]. The intensity of the muscular responses to the different conditions of instability is proportional to the extent of the moments to be countered. As soon as alternative control is available, the muscles relax. There is a continuous exchange between external moments and the control mechanisms of the muscular action, inertia, and passive tension (of the ligaments) aimed at achieving stability and progression of the lower limbs during walking [18].

- Hip extensor muscles contract only during the limb loading and then relax allowing the moment generated by the rolling of the calcaneus and by the activity of quadriceps at the knee level to passively extend the hip [18].
- At the knee level the largest quadriceps activity is recorded during the loading response phase and at the beginning of the mid stance, when the body vector (the vector connecting the point of application of the ground reaction force and the centre of gravity of the head-neck-trunk-arms system where it is supposed the whole mass to be concentrated) passes behind the knee joint axis. As this axis passes in front of the joint axis, inducing an extension moment, the quadriceps relaxes, and the inertia completes the extension movement [18].

Muscle activity at the ankle joint persists from the load response until the onset of the pre-swing phase. Energy consumption is reduced by decreasing the number of contractions performed by the antagonist muscles. The modulation of the intensity of the activity of the plantar flexor muscles during the different phases of the gait represents a second mechanism to reduce the energy cost. The intensity is low during the mid stance and greater during the terminal stance when the weight is transferred on the forefoot [18].

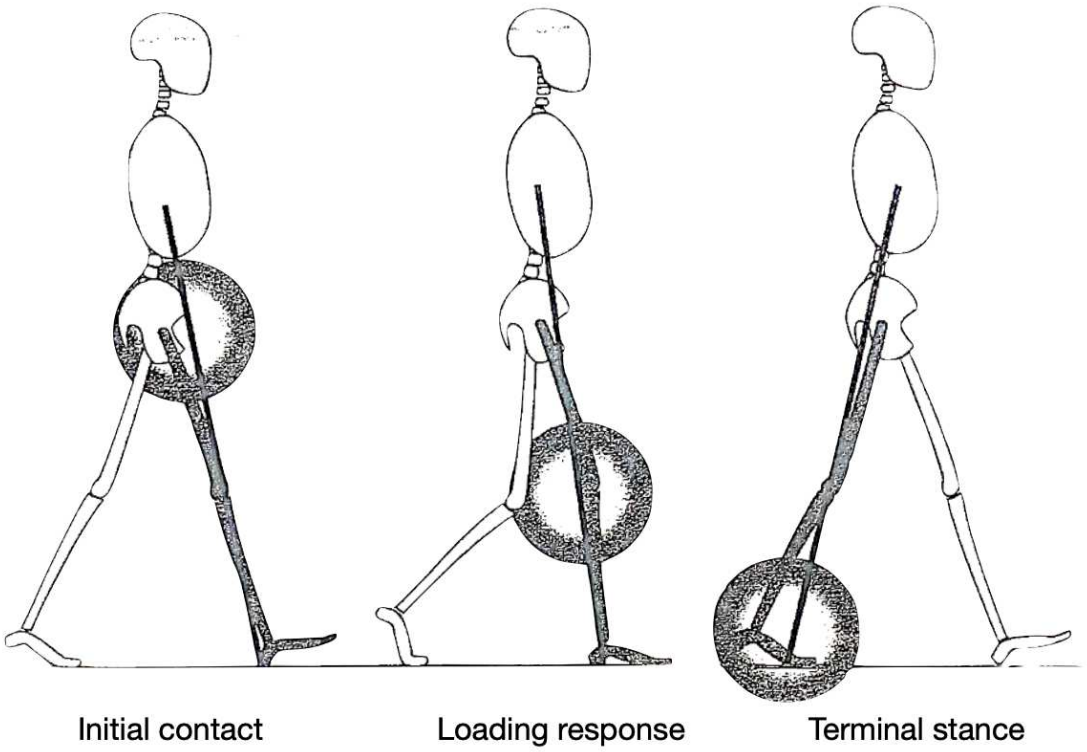

Figure 2. 13 *The black line represents the body vector while the dark circles identify the point with the greatest passive instability created by the body vector itself.*

2.3 Ankle Joint

The ankle joint is composed of the lower limb and the foot and forms the kinetic chain of the lower limb. It allows the lower extremity to interact with the ground, an important requirement for walking and other activities of daily life. The ankle joint is a synovial joint located in the lower limb, composed by the tibia and fibula (leg) and the talus (foot). The ankle joint is a synovial hinge joint connecting the distal ends of the tibia and fibula with the proximal end of the talus (***Figure 2. 15***). The medial malleolus is a bone that extends distally off the medial tibia. The most distal part of the fibula is called the lateral malleolus. Malleoli and ligaments stabilize the talus underneath the tibia.

Figure 2. 14 *Anatomy of the ankle and main bones that composed the joint*

The ankle joint complex is made up of the **talocalcaneal** (subtalar), **tibiotalar** (talocrural) and **transverse-tarsal** (talocalcaneonavicular) joint (***Figure 2. 16)*** [21]. The talocalcaneal mainly allows for the inversion and eversion of the ankle, while the tibiotalar primarily contributes to the plantar- and dorsiflexion motion of the foot. The transverse tarsal joint is considered as part of the same functional unit as the subtalar joint as they share a common axis of motion also contributing to eversion-inversion motion of the foot [21].

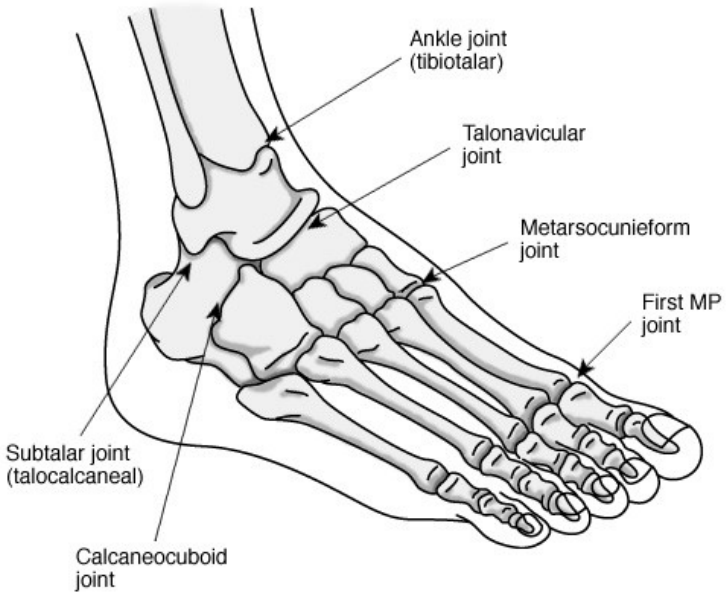

Figure 2. 15 *Major sub-articulations that form the ankle joint complex*

2.3.1 Ankle Joint Motion

The axis of rotation of the ankle joint complex in the sagittal plane occurs around the line passing through the medial and lateral malleoli. The coronal plane axis of rotation occurs around the intersecting point between the malleoli and the long axis of the tibia in the frontal plane. The transverse plane axis of rotation occurs around the long axis of the tibia intersecting the midline of foot. Motion of the ankle occurs primarily in the sagittal plane, with plantar- and dorsiflexion occurring predominantly at the tibiotalar joint [21]. During the gait cycle, the arcs of ankle motion are not large, it travels through four arcs of motion: it alternately plantar flexes and then dorsiflexes [18]. During the swing phase, the ankle only dorsiflexes contributing to the limb advancement. Several studies have indicated an overall range of motion (ROM) in the sagittal plane of between 65 and 75°, moving from 10 to 20° of dorsiflexion through to 40 e 55° of plantar flexion (***Figure 2. 17***) [18].

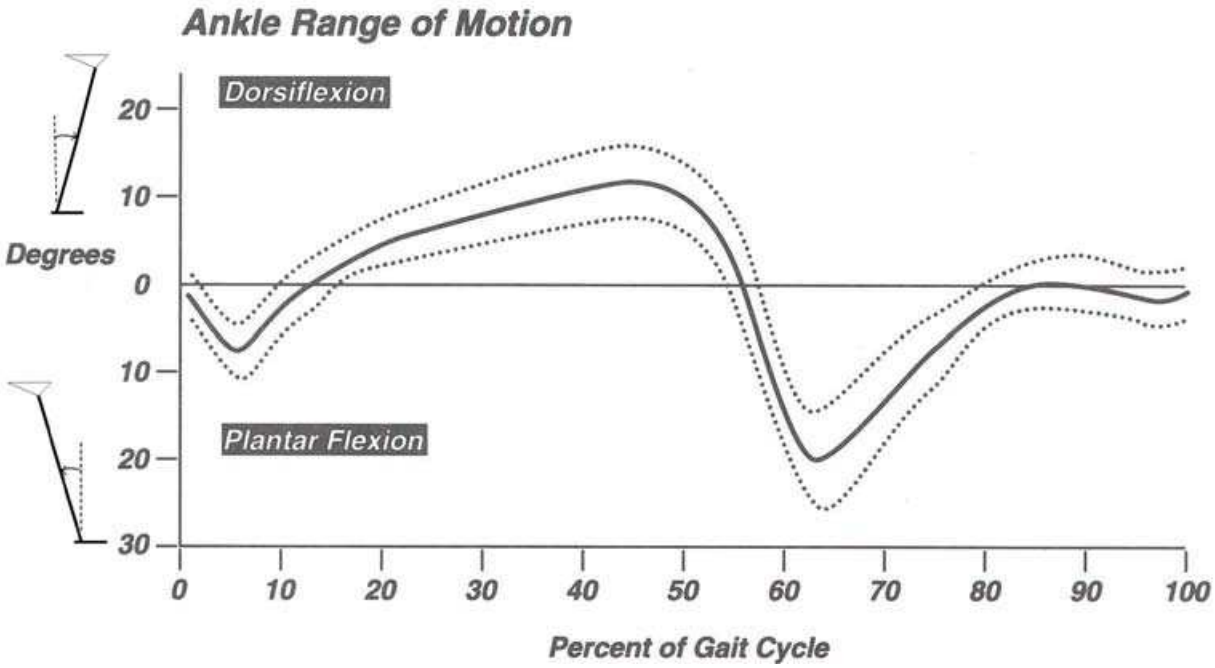

Figure 2. 16 *Ankle joint ROM: ankle plantarflexes after initial contact and rapidly dorsiflexes up to the middle of the terminal stance phase. At this point the ankle begins to plantarflex again, reaching a peak at the end of the stance phase. During swing the ankle dorsiflexes.*

Initial heel contact occurs with the ankle in a neutral position, at most with some degree of plantar flexion (3-5 °), followed by the first movement in plantar flexion during load response (0-10% of the gait cycle). Upon contact with the forefoot, the ankle changes direction of movement by dorsiflexing. The ankle returns to a neutral position around 20% of the gait cycle following a dorsal flexion arc for the entire duration of the intermediate stance and up to the first half of the terminal stance reaching a

peak of 10° at 48% of the gait cycle [18]. Then, there is a rapid ankle plantar flexion reaching the maximum angle of 30° at the end of the stance phase. At the beginning of the swing phase, after the toe off from the ground, the last movement in dorsiflexion begins. The neutral position is reached during mid swing phase and maintained until the next initial contact phase. The ankle joint motion is controlled by dorsiflexors and plantar flexors muscles. Usually there is a tendency in plantar flexion (3-5°) during terminal stance [18].

2.3.2 Muscle Control

Plantar flexors muscles are active in stance phase, while the dorsiflexors (pretibial muscles) are swing phase muscle, but there is an exception during the loading response phase where the dorsiflexor muscles participate to control the rate of ankle plantar flexion permitting the foot to be lowered to the ground. The internal moment of ankle muscles is directly proportional to their dimensions (transversal section) and lever arms [18]. The three main dorsal flexor muscles are located anterior to the ankle joint and correspond to the anterior tibialis, the extensor digitorum longus and the extensor hallucis longus (***Figure 2. 18***). The main muscle active in the dorsiflexion control of the ankle is the tibialis anterior which has the largest transversal section and generates the greatest internal moment values to stabilize the joint. The tibialis anterior muscle arises along the two-thirds of the lateral surface of the tibia and inserts into the first metatarsal bone and medial cuneiform bone of the foot [22].

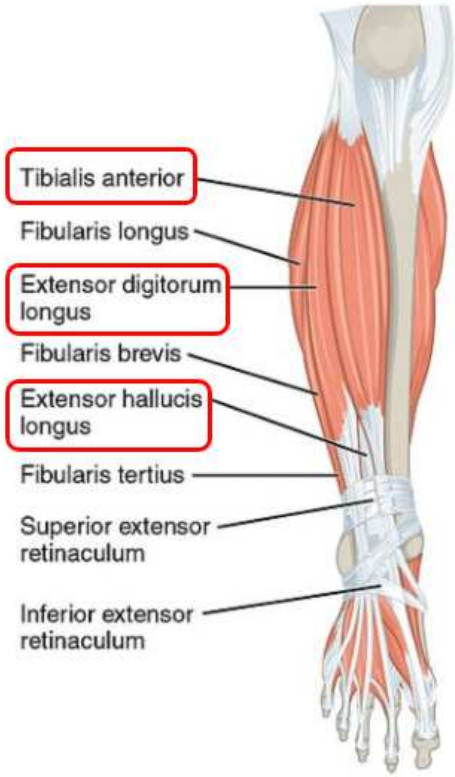

Figure 2. 17 *Main dorsiflexor muscles of the ankle joint. In red are highlighted the muscles belonging to this group.*

At the initial contact each dorsiflexor muscle is significantly active and contracts during the entire period of loading response. The second period of active dorsiflexion movement of the ankle occurs during the swing phase. The first muscle that starts contracting is the extensor hallucis longus which remain active during the entire pre swing phase. During the mid swing, the tibialis anterior and the extensor digitorum longus are activated with a rapid increase in the contraction of the tibialis. At the terminal swing it gradually increases in order to position the foot for the subsequent support [18].

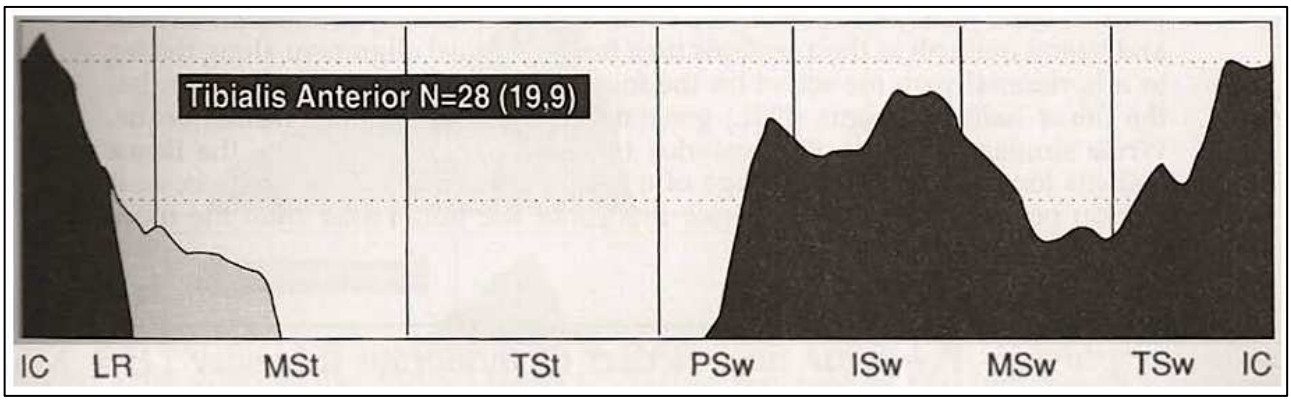

Figure 2. 18 *Activity of the tibialis anterior during a complete gait cycle.*

The seven muscles located behind the ankle joint act as plantar flexor muscles (***Figure 2. 20***). They contribute in a quantitatively different way to the control of the ankle: soleus and gastrocnemius provide 93% of the theoretical internal moment in plantar flexion, while the other five muscles (tibialis posterior, flexor hallucis longus, flexor digitorum longus, fibularis longus and fibularis brevis) provide only the remaining 7% [18]. Soleus and lateral and medial head of the gastrocnemius form the triceps surae muscle. The gastrocnemius lateral head arises from the lateral condyle of the femur and the medial head arises from the medial condyle. The soleus muscle arises from the soleal line on the dorsal surface of the tibia, from the medial margin of the tibia, from the head of the fibula, and from the posterior margin of the fibula. At the opposite side, soleus and gastrocnemius form a common tendon, the Achilles tendon, and inserts onto the posterior surface of the calcaneus [22].

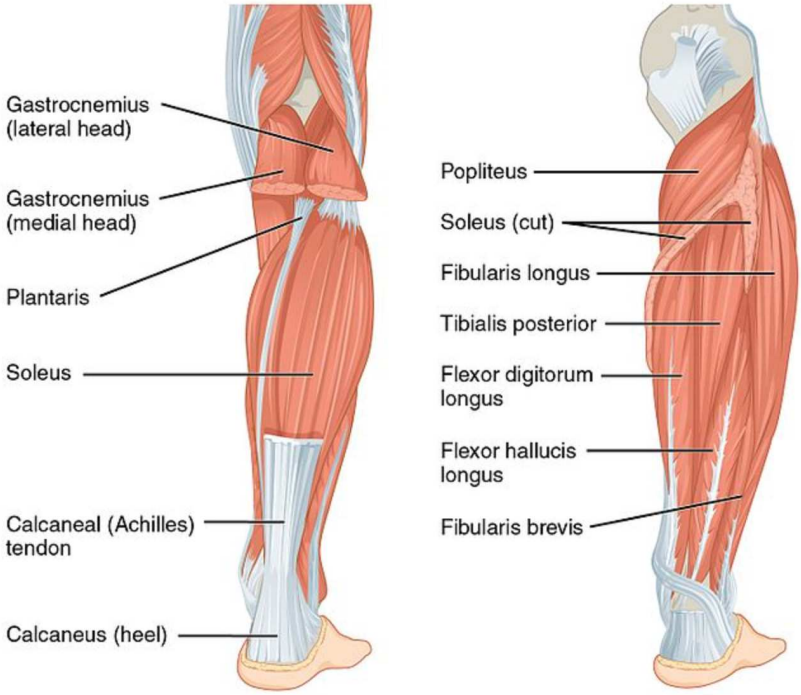

Figure 2. 19 *Main plantar flexor muscles of the ankle joint*

Soleus muscle begins to contract after the loading response phase and continues during the entire duration of the mid stance. At the terminal stance phase there is a rapid increase in the amplitude of contraction of this muscle. Subsequently the activity begins to decrease until its complete release during the pre swing phase. The medial head of the gastrocnemius is activated parallel to the soleus, while the activation of the lateral head can be delayed until the intermediate support. Contractions of the gastrocnemius rapidly follow the soleus but their increase during the mid stance phase is slower and less intense. During terminal stance the intensity increases, reaching a peak at 40% of the gait cycle and then rapidly decrease, until the release, after the beginning of the pre swing [18].

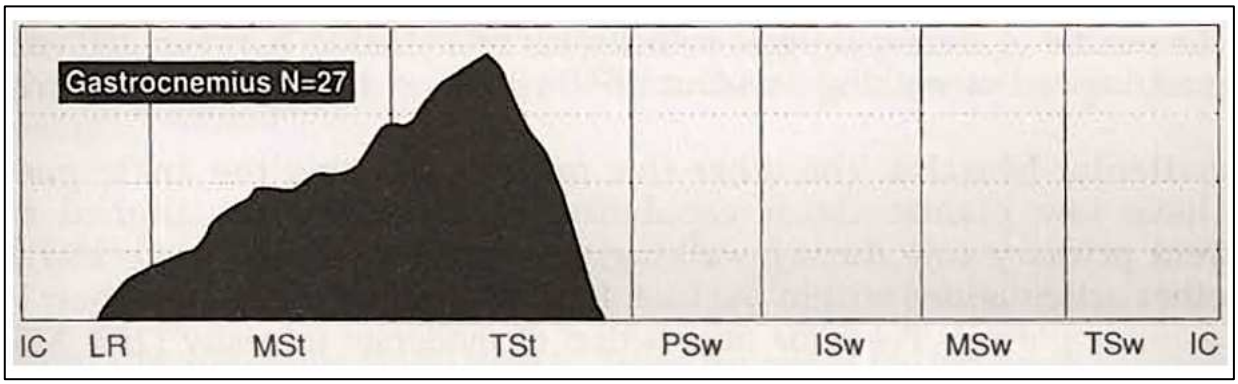

Figure 2. 20 *Activity of the gastrocnemius lateralis during a complete gait cycle.*

2.4 Knee Joint

The knee joint is a synovial joint that connects three bones: the femur, tibia and patella. The knee can be conceptualized as 2 joints: a **tibiofemoral** and a **patellofemoral** joint (***Figure 2. 22***). The tibiofemoral joint is the joint between the lateral and medial condyles of the distal end of the femur and the tibial plateau, both covered by a layer of hyaline cartilage. The articular surfaces of the tibiofemoral joint are generally incongruent, so compatibility is provided by the medial and lateral meniscus. The tibiofemoral joint allows transmission of body weight from the femur to the tibia while providing hinge-like, sagittal plane joint rotation along with a small degree of tibial axial rotation [23]. The patellofemoral joint is a saddle joint formed by the articulation of the patellar surface of femur and the posterior surface of patella. Several ligaments provide passive stability in all directions to the knee joint. In our daily activities, the knee carries a large portion of our body weight, allowing a wide range of motion for flexion–extension and internal–external rotation [24].

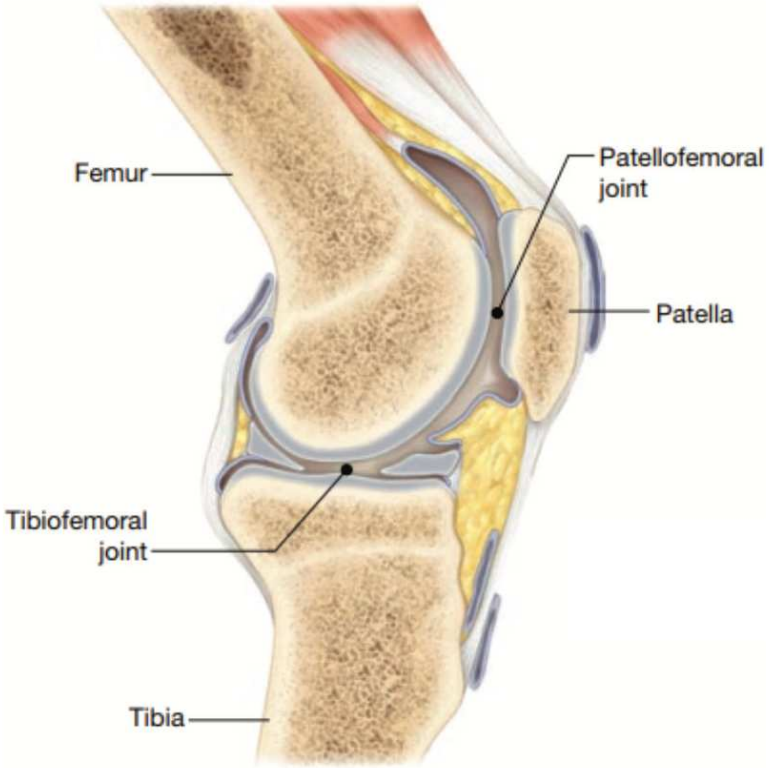

Figure 2. 21 *Major sub-articulations that form the knee joint complex and the relative bones*

2.4.1 Knee Joint Motion

The knee is characterized by a wide excursion of motion in the sagittal plane and reduced range of motion in frontal and transverse plane. The movements on the sagittal plane allow the progression during stance and the advancement of the lower limb during swing. During each step the knee flexes

and extends alternately, presenting two flexor peaks. When the knee is fully extended and the femur and tibia are aligned, the knee is in a neutral (0 °) position. For this reason, the knee never extends beyond this value (hyperextension) and the articular excursions always remain positive. At initial contact it is flexed about 5° and then flexes throughout the entire loading response phase reaching the peak of flexion at the onset of the single limb support. During the mid stance the knee begins to extend reaching the minimum value of 3° in the middle of the terminal stance. When the counter lateral limb touches the ground and the double support phase begins, the knee rapidly flexes again reaching the second peak of flexion (65°) at the end of the initial swing phase. Subsequently, it starts to extend again during the mid swing, obtaining the complete extension (3°). The final knee posture at the end of terminal swing reaches approximately 5° of flexion to prepare the limb for the next support (***Figure 2. 23***) [18].

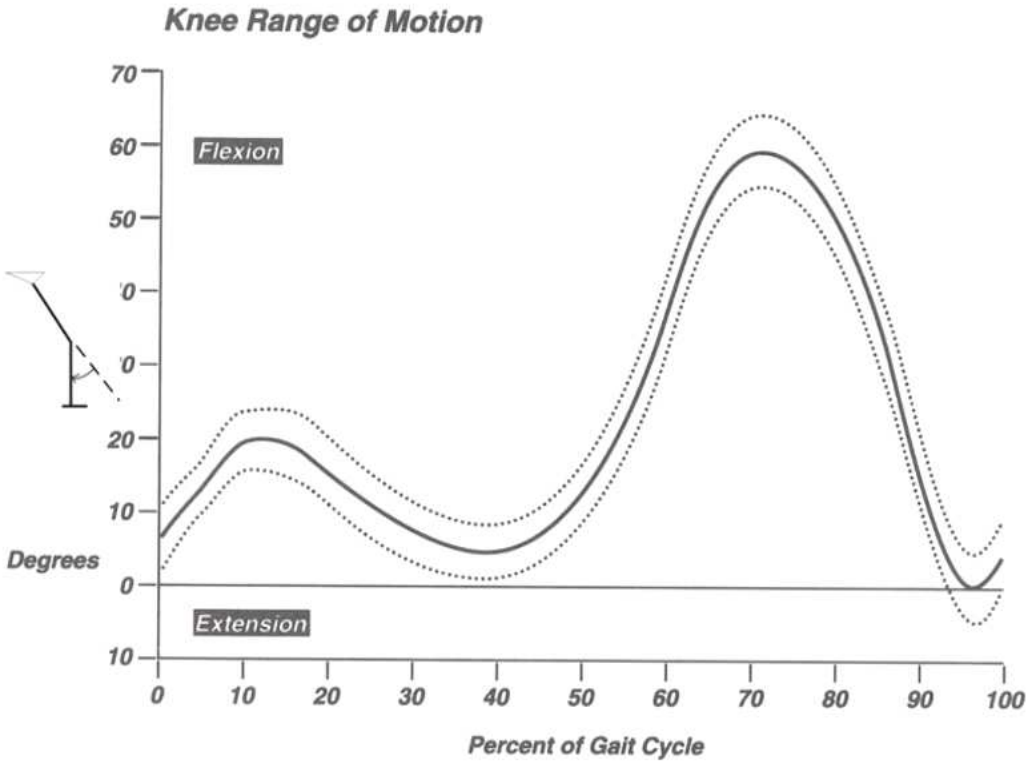

Figure 2. 22 *Knee joint ROM: the knee presents two flexion peak and never extended because the reference angle is considered as the angle formed by the knee during orthostatic position. Anatomical structures prevent the knee to hyperextend.*

2.4.2 Muscle Control

Control of stability and mobility during walking is attributed to the fourteen muscles that contribute to knee control. They contract at specific time intervals during the gait cycle and release to aid in energy conservation. The flexor muscles act to decrease the knee flexion rate and during the swing

phase the extensors and flexors both contribute to limb progression. Among the multiple muscles acting on the knee, six muscles don't act at another joints. These muscles are the four vasti heads of the quadriceps that extends the knee and two knee flexors, popliteus, and short head of the biceps femoris (***Figure 2. 24***). All the other muscles, except the gastrocnemius muscle which has a primary role as an ankle plantar flexor, also control hip motion [18]. The main knee extensor muscles are the quadriceps femoris that consists of four individual muscles, three of the heads originate from the femur (vastus intermedius, vastus medialis, and vastus lateralis), while the fourth head (rectus femoris) arises from the hip. These muscles differ in their origin but share a common quadriceps femoral tendon that inserts into the patella [22].

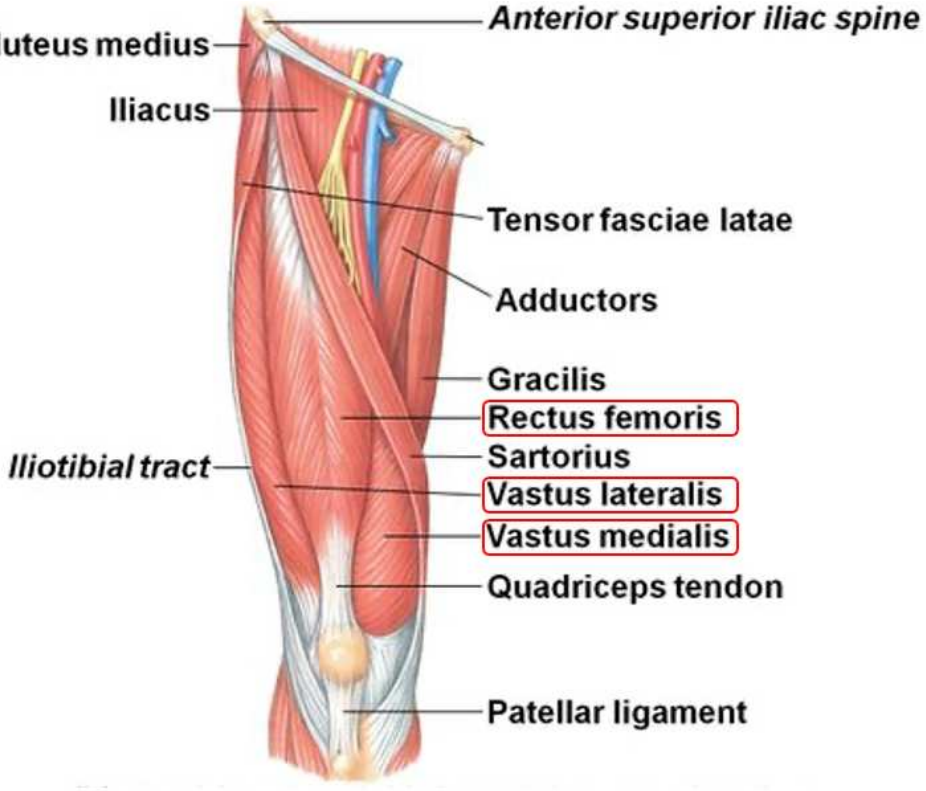

Figure 2. 23 *Main extensor muscles of the knee joint. The Vastus intermedius is located behind the rectus femoris and it is not visible. In red are highlighted the muscles belonging to this group.*

The vasti muscles contract during terminal swing reaching the maximum intensity during the loading response phase. At the onset of mid stance, the quadriceps reduces their activity and ceases at 15% of the gait cycle. The activity of rectus femoris is significantly different from those of vasti which has a short period of action between late pre swing and early initial swing [18].

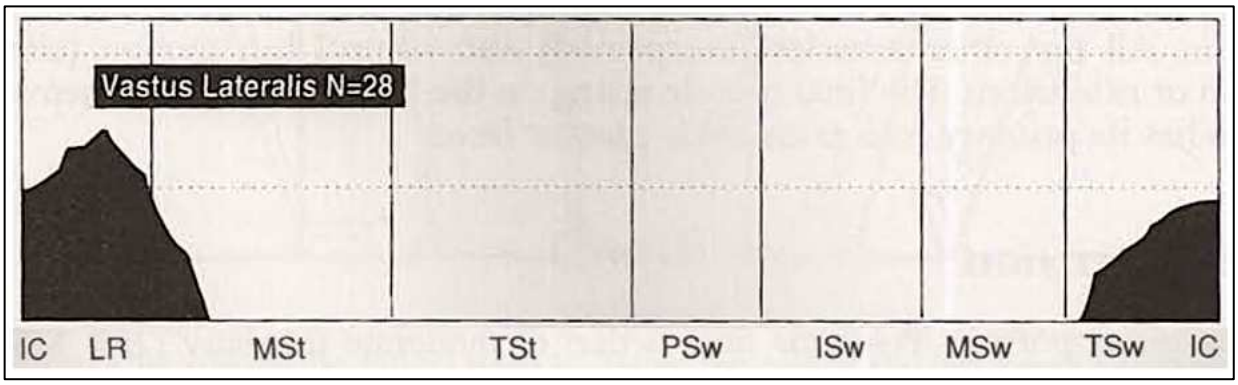

Figure 2. 24 *Activity of the vastus lateralis during a complete gait cycle.*

The knee flexors include the set of hamstrings, gracilis, sartorius, gastrocnemius, plantaris, and popliteus (***Figure 2. 26***). The semitendinosus, semimembranosus, and biceps femoris form the hamstring group. The popliteus muscle originates from the femur and the posterior horn of the lateral meniscus and inserts on the proximal tibia. Biceps femoris is the most lateral hamstring muscle located in the posterior thigh. This muscle has two heads: the long head of biceps femoris muscle originates from the medial facet (inferomedial impression) of ischial tuberosity, the short head arises from the lateral lip of the inferior third of the linea aspera and supracondylar ridge of femur [22].

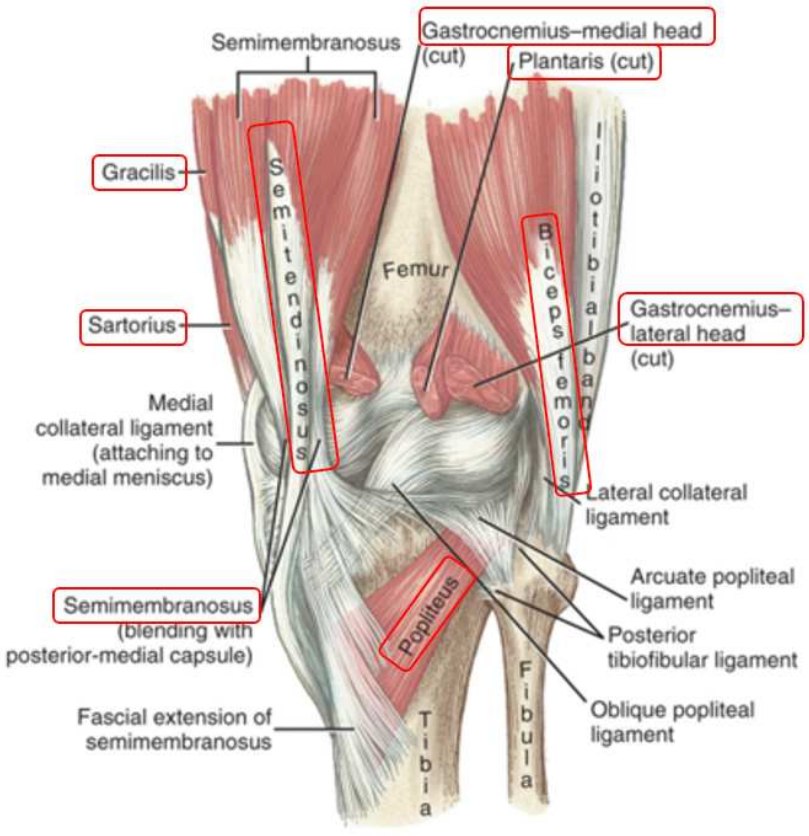

Figure 2. 25 *Main flexor muscles of the knee joint. In red are highlighted the muscles belonging to this group.*

Popliteus and the short head of the biceps femoris provide direct knee flexion. The popliteus acts throughout all the gait cycle. The biceps femoris is prevalently activated in initial and mid swing. The hamstring muscles are mainly hip extensor but also act as flexor at the knee. They contract during the final part of the mid swing phase and continues throughout the terminal swing, and at a lower level, also during the loading response. The gastrocnemius muscle is an additional stance phase muscle that principally act at the ankle but is also knee flexor. The gastrocnemius increases its intensity during the terminal stance phase before a rapid decline of action until its release at the onset of pre swing phase [18].

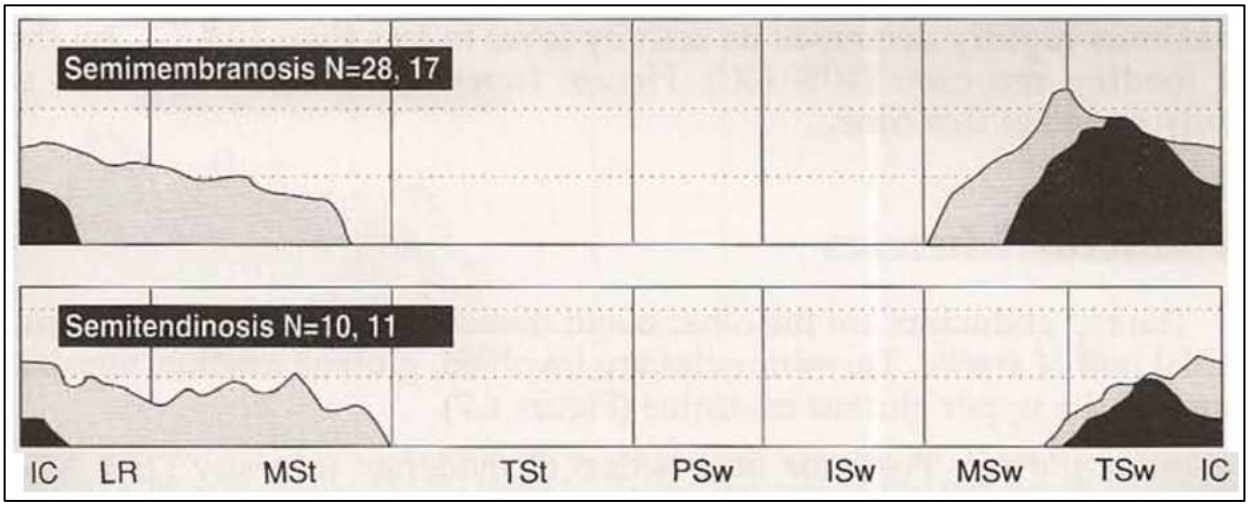

Figure 2. 26 *Activity of the hamstrings during a complete gait cycle. The upper graph reports the activity of the semimembranosis, the graph in the bottom reports the activity of the semitendinosis.*

2.5 Hip Joint

The hip is a true ball-and-socket joint surrounded by powerful and well-balanced muscles, enabling a wide range of motion in several physical planes (flexion-extension, abduction-adduction, and external-internal rotation) while also exhibiting remarkable stability. The cup-shaped **acetabulum** is formed by the innominate bone with contributions from the ilium (approximately 40% of the acetabulum), ischium (40%) and the pubis (20%). The hip joint is the articulation between the ellipsoid head of the femur and the hemispherical concavity of the acetabulum located on the lateral aspect of the hip bone. The femoral head is covered with a corresponding articular cartilage beyond the reaches of the acetabular brim to accommodate the full range of motion, except for a rough central depression, the fovea capitis (***Figure 2. 28***) [25].

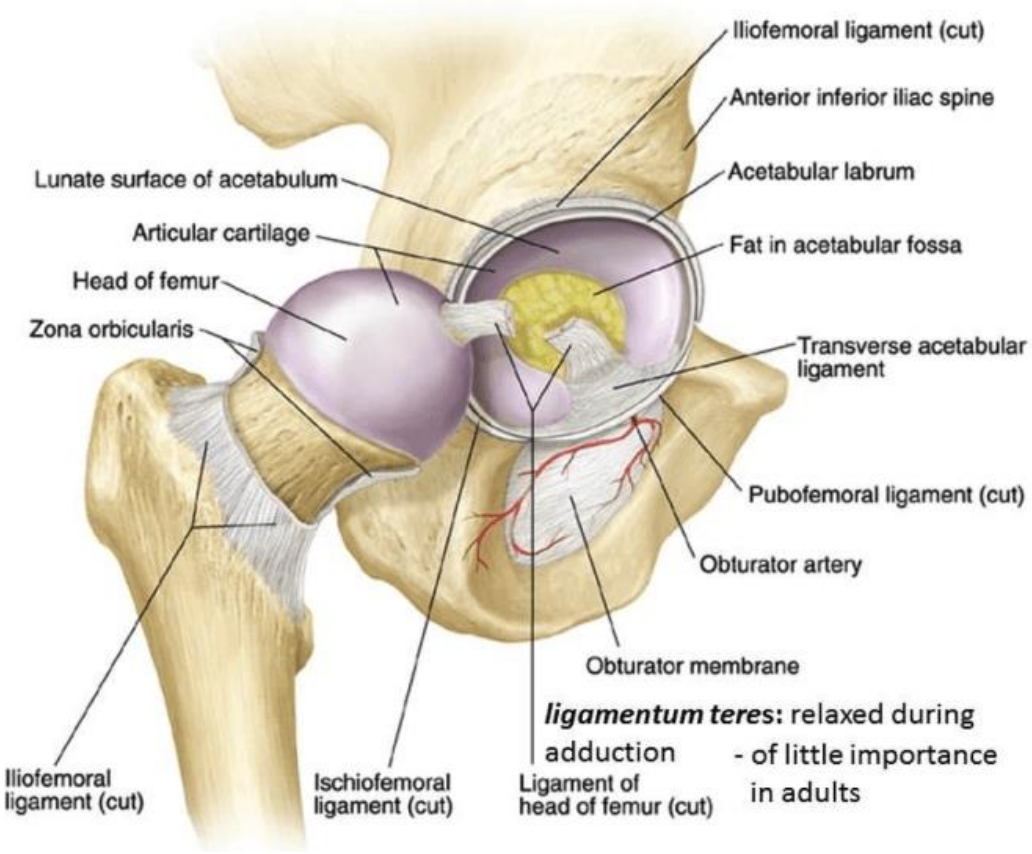

Figure 2. 27 *Hip joint anatomy*

2.5.1 Hip Joint Motion

The hip mainly performs two movements during locomotion: extension during stance and flexion in swing. Normally the hip range of motion is, in average, 40°. Considering as neutral position the one assumed when the thigh is vertical during orthostatic position, the degree of flexion of the thigh at initial contact is 20°. During mid stance, the hip progressively extends, and the thigh reaches neutral alignment at the terminal stance (38% of the gait cycle), reaching a peak of extension (10°) at 50% of the gait cycle. During the pre swing phase, the hip begins to flex again, assuming the neutral position at the end of the stance phase. Finally, the flexion movement continues throughout the first two swing phases [18]. The final 25° flexed position of the thigh is maintained during the terminal swing (***Figure 2. 29***).

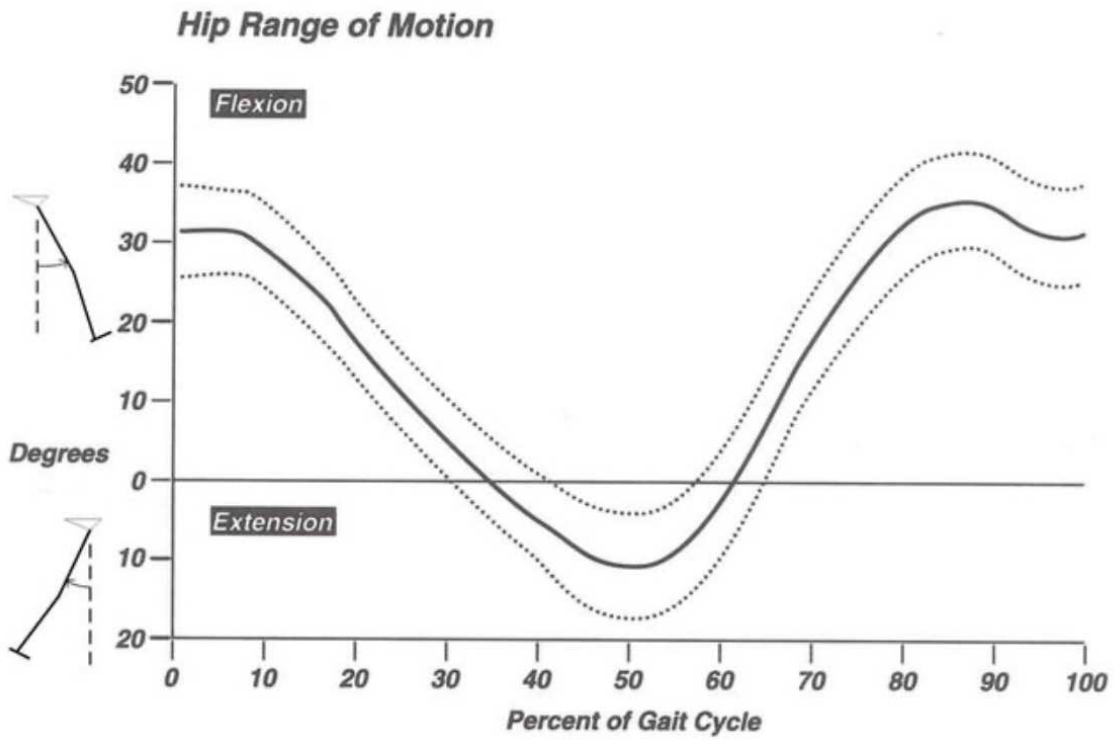

Figure 2. 28 *Hip joint ROM: the hip joint starts the gait in a flexion position. After the loading response phase, it begins to extend reaching a maximum at approximately the end of the stance phase. At this point the hip flexes up to the end of the swing phase.*

2.5.2 Muscle Control

During stance phase extensor and abductors muscles act to control the hip motion, while flexor muscles participate in controlling hip motion during swing. The adductors tend to participate during the transitions between swing and stance phases [18].

The primary hip extensors include the gluteus maximus, posterior head of the adductor magnus and the hamstrings (***Figure 2. 30***). The adductor magnus muscle is a massive triangular muscle that extends over the entire medial side of the thigh. It is a composite muscle consisting of two parts. The adductor portion arises from the outer surface of the inferior pubic ramus of the pubic bone and the ischial ramus. The hamstring portion originates from the inferolateral side of the ischial tuberosity. In the anatomic position, the posterior head of the adductor magnus has the greatest moment arm for extension [22]. The gluteus maximus muscle runs from the lateral aspect of the dorsal sacral surface, posterior part of the ilium and thoracolumbar fascia it inserts into the iliotibial tract and gluteal tuberosity on the femur [25]. The gluteus maximus and adductor magnus have the greatest cross-sectional areas of all the primary extensors. The hip extensor muscles, as a group, produce the greatest torque across the hip than any other muscle group [22].

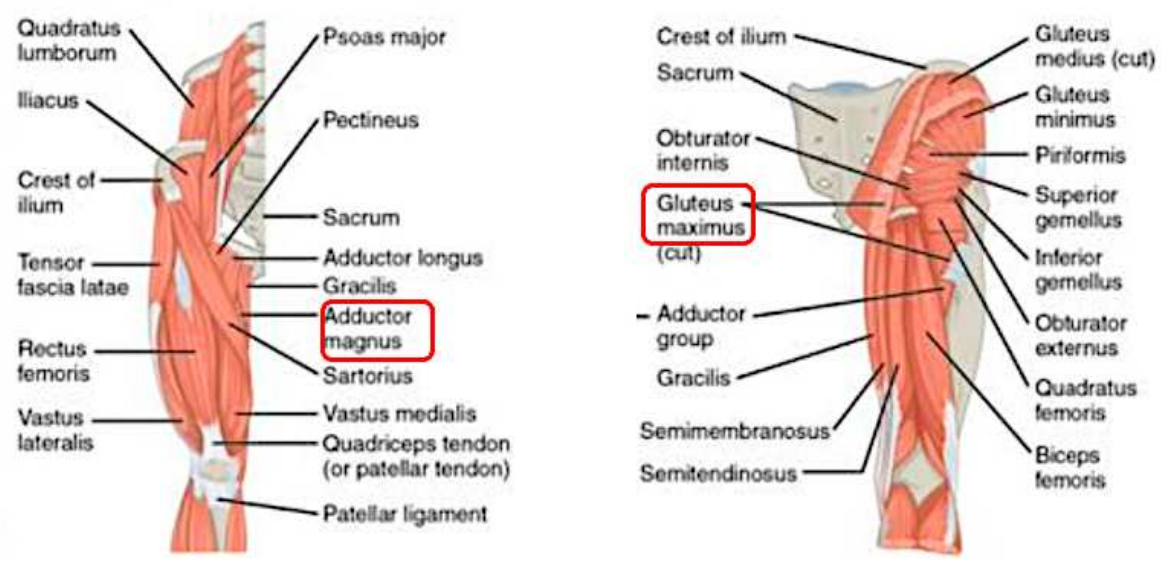

Figure 2. 29 *Main hip extensor muscles. In red are highlighted the muscles belonging to this group.*

The semitendinosus, semimembranosus, and biceps femoris start acting in the betrayal phase of the mid swing, reaching the peak strength during terminal swing. The three hamstring muscles cease their activity during the rest of gait cycle. The adductor magnus begins to contract, with progressive increase in intensity, at the end of the terminal swing, followed by a further increase at the initial contact. During loading response phase, it remains moderately active and finally relaxes. Lower gluteus maximus muscle activity increases at the end of terminal swing, with an increasing strength during loading response phase. Finally, it rapidly decreases at the end of loading response phase (10% of the gait cycle) [18].

The main hip flexor muscles are reported in ***Figure 2. 31***. The action of the flexor muscles strictly depends on the speed of walking and some subjects may not have a significant action [18]. The major flexor of the hip joint is **iliopsoas**. This comprises psoas major and minor, and iliacus. Psoas major arises from T12-L5 vertebral bodies and insets into the lesser trochanter. **Rectus femoris** arises from the anterior superior iliac spine and inserts into the tibial tuberosity by way of the patella ligament. It is joined at the level of the inguinal ligament to form the iliopsoas [25]. The adductor longus originates from the body of pubis inferior to pubic crest and lateral to pubic symphysis, while distally, it extends into the adductor canal.

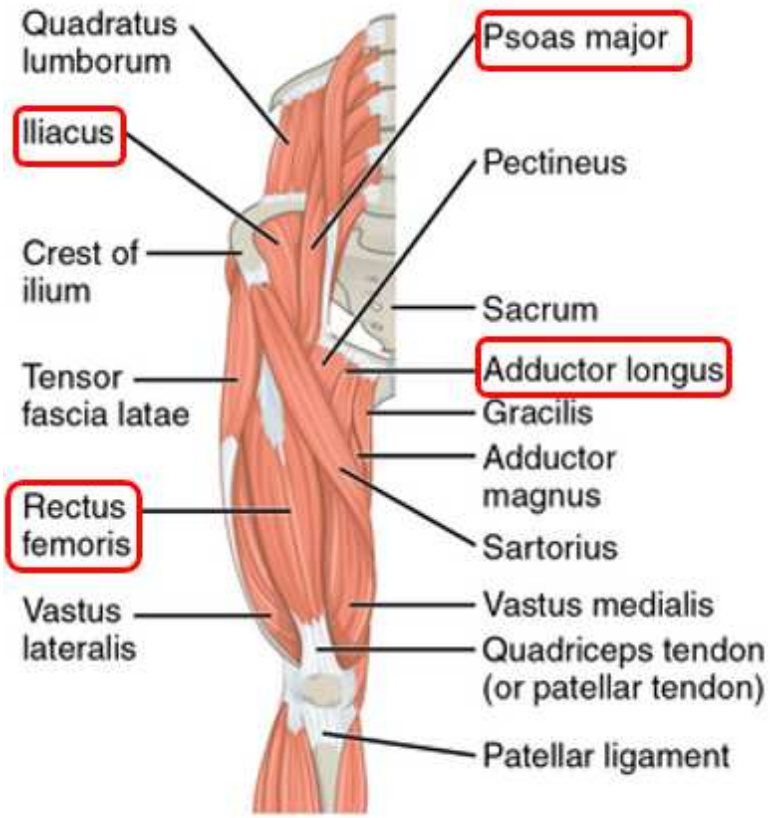

Figure 2. 30 *Main hip flexor muscles. In red are highlighted the muscles belonging to this group.*

The flexor muscles begin to contract in the final phase of terminal stance and continue until the beginning of the mid swing. The adductor longus is muscle that is activated first. Its activity begins during the pre swing and continues in the initial swing. The rectus femoris activates for a short period of time in pre swing and in the first initial swing. The iliac, sartorius, and gracilis muscles, on the other hand, have similar activation intervals during the initial swing [18].

CHAPTER 3: Surface Electromyography

Electromyography (EMG) is the study of muscle function through the inquiry of the electrical signal the muscles emanate [26]. The EMG signal is a biomedical signal that measures electrical currents generated in muscles during its contraction representing neuromuscular activities [27]. The musculoskeletal system comprises one of the body's major tissue/organ systems. The three main types of muscle tissue are **skeletal**, **cardiac**, and **smooth** muscle groups (***Figure 3. 1***). Skeletal muscle attaches to the bone by tendons, and together they produce all body movements [28].

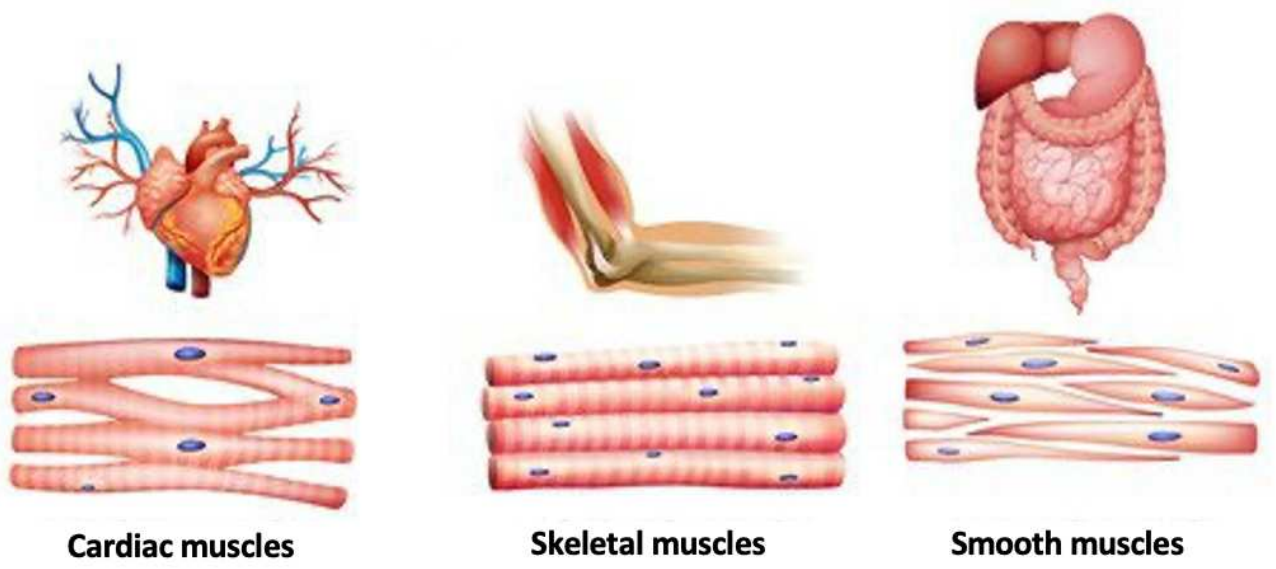

Figure 3. 1 *Three different type of muscle tissues: cardiac muscles (left), skeletal muscles (center) and smooth muscles (right)*

3.1 Skeletal Muscles

Skeletal muscles are composed by thousands of muscle fibers wrapped together by connective tissue sheaths. The individual bundles of muscle fibers in a skeletal muscle are known as fasciculi. The outermost connective tissue sheath surrounding the entire muscle is known as **epimysium**. The connective tissue sheath covering each fasciculus is known as **perimysium**, and the innermost sheath surrounding individual muscle fiber is known as **endomysium** [28]. Each individual muscle fiber is formed by myofibrils containing multiple myofilaments. Myofibrils are arranged in a unique striated pattern forming **sarcomeres** which are the fundamental contractile unit separated one from another by the Z-membranes. Sarcomeres are composed of three major myofilaments, or simply filaments, which are long chains of protein subunits: **myosin** (thick filament), **actin** (thin filament) and **titin**. Myosin and actin are contractile proteins. The **troponin complex** is a complex of three regulatory

proteins (troponin C, troponin I, and troponin T) that are attached to the protein **tropomyosin** and lies within the groove between actin filaments in muscle tissue.

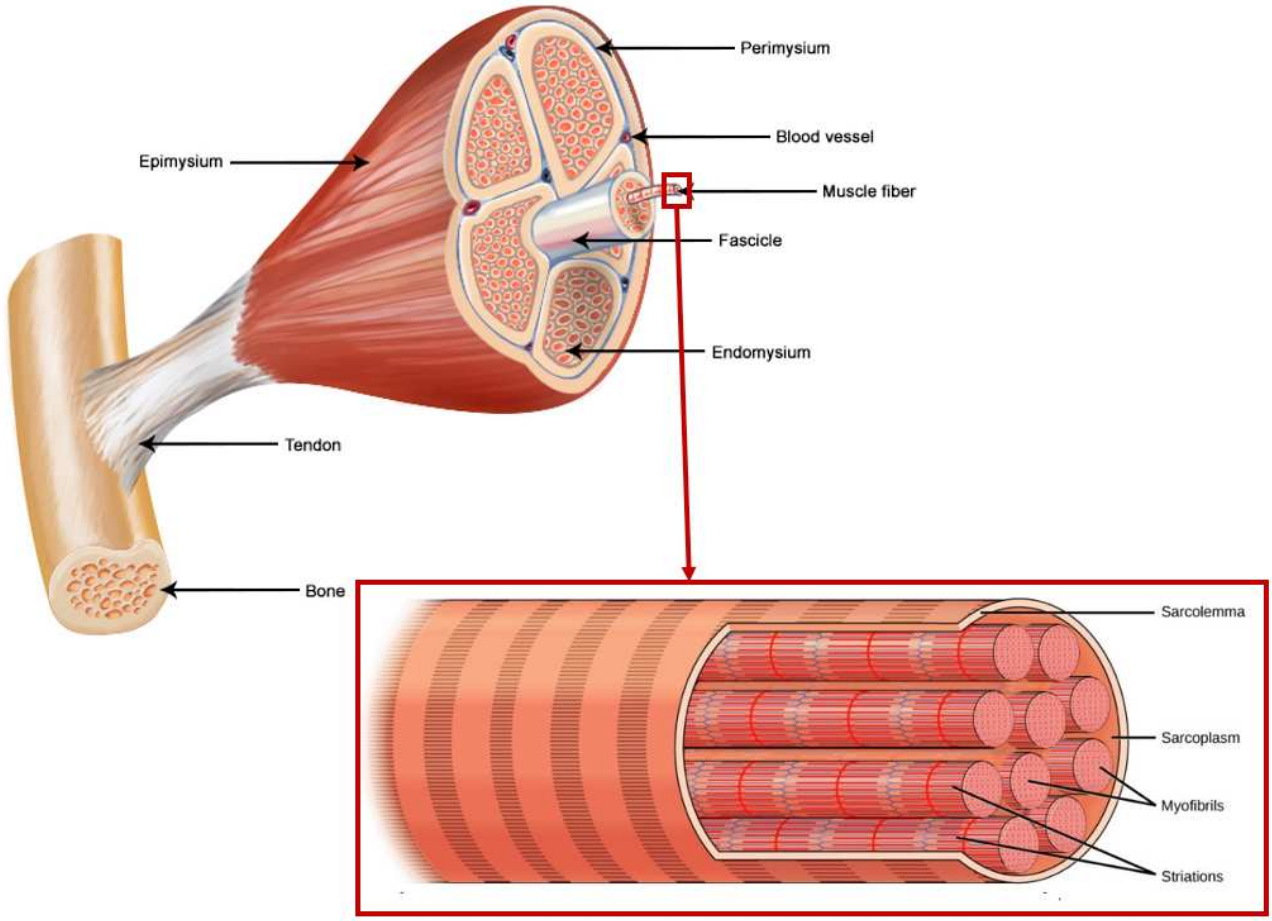

Figure 3. 2 *Cross section view of a muscle: it is formed by fascicles covered by the perimysium. Each fascicle is formed by multiple muscle fibers grouped together and covered by endomysium. Muscle fibers are formed by many myofibrils grouped by a membrane called sarcolemma.*

In a relaxed muscle, tropomyosin blocks the attachment site for the myosin crossbridge, thus preventing contraction. The highly extensible titin filaments connect the thick filaments to the membranes that are the terminal borders of the sarcomere. The myofibril extensibility is mainly attributable to the extensibility of titin filaments [29]. Titin acts like springs that keep the myosin filaments centered in the sarcomere and maintain the resting tension that allows a muscle to snap back if overextended. Within each sarcomere, dark bands alternate with light bands. These bands correspond to the presence or absence of myosin filaments.

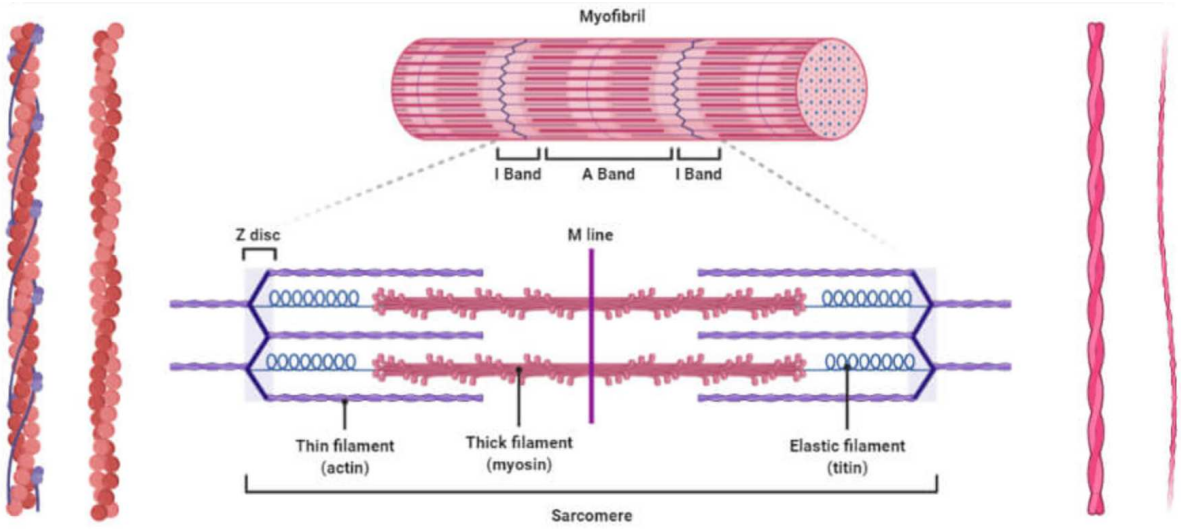

Figure 3. 3 *Sarcomere: it is formed by alternation of myosin and actin filaments. The sarcomere shows a repetition of light and dark area that identify different bands.*

The I bands contain only thin (actin) filaments, whereas the A bands contain thick (myosin) filaments. The myosin and actin filaments overlap in peripheral regions of the A band, whereas a middle region (called the H zone) contains only myosin [30]. The actin filaments are attached at to the Z disc, while myosin filaments are anchored at the M line in the middle of the sarcomere.

3.1.1 Excitation-Contraction coupling

The primary functions of the skeletal muscle take place via its intrinsic excitation-contraction coupling process. As the muscle is attached to the bone tendons, the contraction of the muscle leads to movement of that bone that allows for the performance of specific movements [28]. The excitation–contraction coupling in skeletal muscle refers to the Ca2+-mediated link between the membrane excitation and the mechanical contraction [31]. Propagation of action potentials to the motoneuron and subsequent depolarization results in the opening of voltage-gated calcium (Ca2+) channels of the presynaptic membrane[32]. Inward Ca2+ flow causes the release of acetylcholine (ACh) at the neuromuscular junction, which diffuses to the postsynaptic membrane at the muscle fiber, depolarizing it, and initiating the action potentials in the muscle fiber. The action potentials at the muscle cell membrane surrounding the myofibrils travel into the T-tubules, which are responsible for propagating the action potential from the surface to the interior of the muscle fiber[32]. The initiation and propagation of an action potential through the membranous system of the sarcolemma and the tubular network lead to the activation of the Ca2+-release units: tightly coupled dihydropyridine and ryanodine (RyR) receptors [31]. The RyR gating allows a rapid, massive, and highly regulated release of Ca2+ from the sarcoplasmic reticulum. The resulting increased intracellular Ca2+ attaches to

troponin C of the troponin complex on the thin filaments. The interaction between Ca2+ and troponin C exhibits cooperativity, which means that each Ca2+ that binds troponin C increases the affinity of troponin C binding for the next Ca2+ molecule, up to a total of four Ca2+ ions per troponin C. As a result of Ca2+ binding, the troponin complex undergoes a conformational change causing displacement of tropomyosin from the myosin-binding sites on the actin filament, which allows myosin heads of the thick filaments to bind [32].

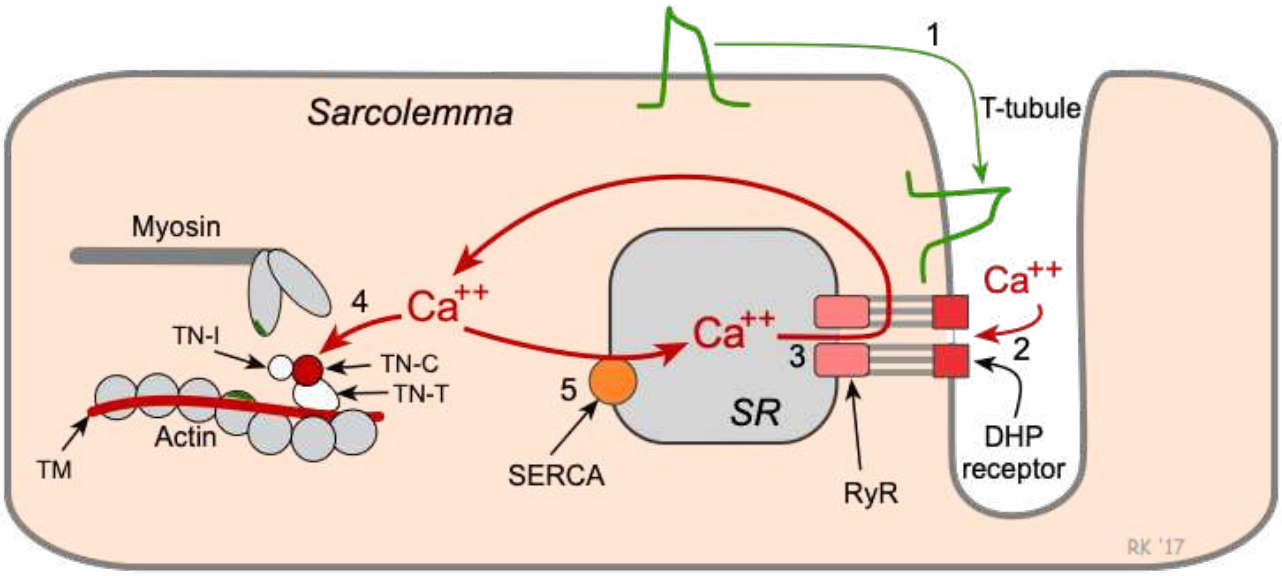

Figure 3. 4 *Excitation-contraction coupling mechanism: (1) the action potential arrives, and (2) calcium enter the cell. (3) RyR receptors trigger a large release of calcium from the sarcoplasmatic reticulum. (4) Calcium binds the troponin complex C and tropomyosin releases the myosin binding sites on the actin filament causing muscle contraction. (5) SERCA pump brings the calcium back into the sarcoplasmatic reticulum during muscle relaxation.*

3.1.2 Cross-Bridge Cycle

The cross-bridge cycle, an event that occurs during excitation-contraction coupling, refers to the mechanism by which the thick and thin filaments slide past one another to generate a muscle contraction (***Figure 3. 5***). At the beginning of the cycle, when myosin is tightly bound to actin, no adenosine triphosphate (ATP) is bound to myosin, a state known as rigor [32]. Next, myosin dissociates from actin and the myosin head becomes cocked toward the end of the sarcomere. The ATP bound to myosin becomes hydrolyzed to adenosine diphosphate (ADP) and one inorganic phosphate molecule, which both remain linked to myosin. In its cocked position, myosin then binds to a new site on the actin, creating a power stroke that pulls the actin filaments [32]. Each cross-bridge cycling event results in the myosin head progressing up the actin filament under the condition that Ca2+ remains bound to troponin C. Finally, ADP is released, and myosin returns to its original

state of rigor where it is bound to actin in the absence of ATP. After contraction, muscle relaxation occurs when Ca2+ reaccumulates in the sarcoplasmic reticulum via the active Ca2+ ATPase (SERCA) pump on the sarcoplasmic reticulum membrane [32]. This pump transports the intracellular Ca2+ into the sarcoplasmic reticulum, which maintains low intracellular Ca2+ with the tropomyosin that covers myosin binding sites on actin filaments.

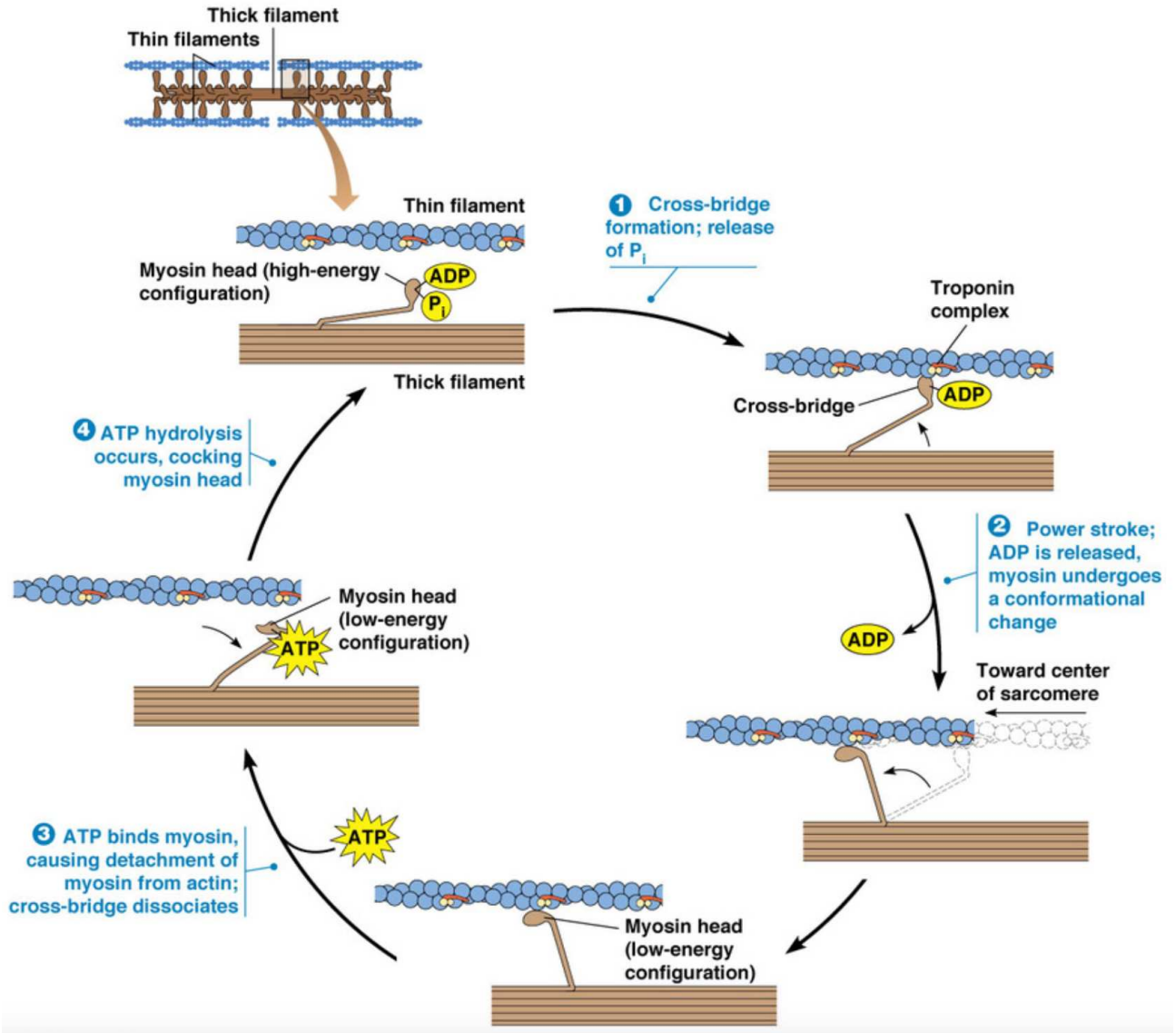

Figure 3. 5 *Cross-bridge cycle: Attached state: This step takes place when a cross-bridge is formed between actin and myosin. Power/working stroke step: When the stored energy is released, there is a conformational change in the myosin's head. This change leads to the pulling of actin filaments and therefore, sarcomere shortening. Detached state: This step includes the binding of the energy carrier molecule, the ATP. This change results in detachment of myosin and actin. High energy state: This step takes place when the ATP hydrolysis supplies energy to change the angle of the myosin head into cocking place for binding to the actin filament once again.*

3.2 Generation of Surface Electromyography (sEMG) Signal

The activation of an alpha-motor anterior horn cell (induced by the central nervous system or reflex) results in the conduction of the excitation along the motor nerve. Na+ ions inflow in the muscle fiber causes a membrane depolarization which is immediately restored by backward exchange of ions within the active ion pump mechanism, the repolarization [33]. During cellular depolarization, some positive ions transited inside the cell, due to the chemical gradient, move into the adjacent cell, raising the membrane potential and triggering a new depolarization. A depolarization front is therefore established towards adjacent cells not yet excited. The EMG signal is based upon action potentials at the muscle fiber membrane resulting from depolarization and repolarization processes[33]. The depolarization-repolarization cycle forms a depolarization wave (electrical dipole) which travels along the surface of a muscle fiber and that is recorded by surface electrodes.

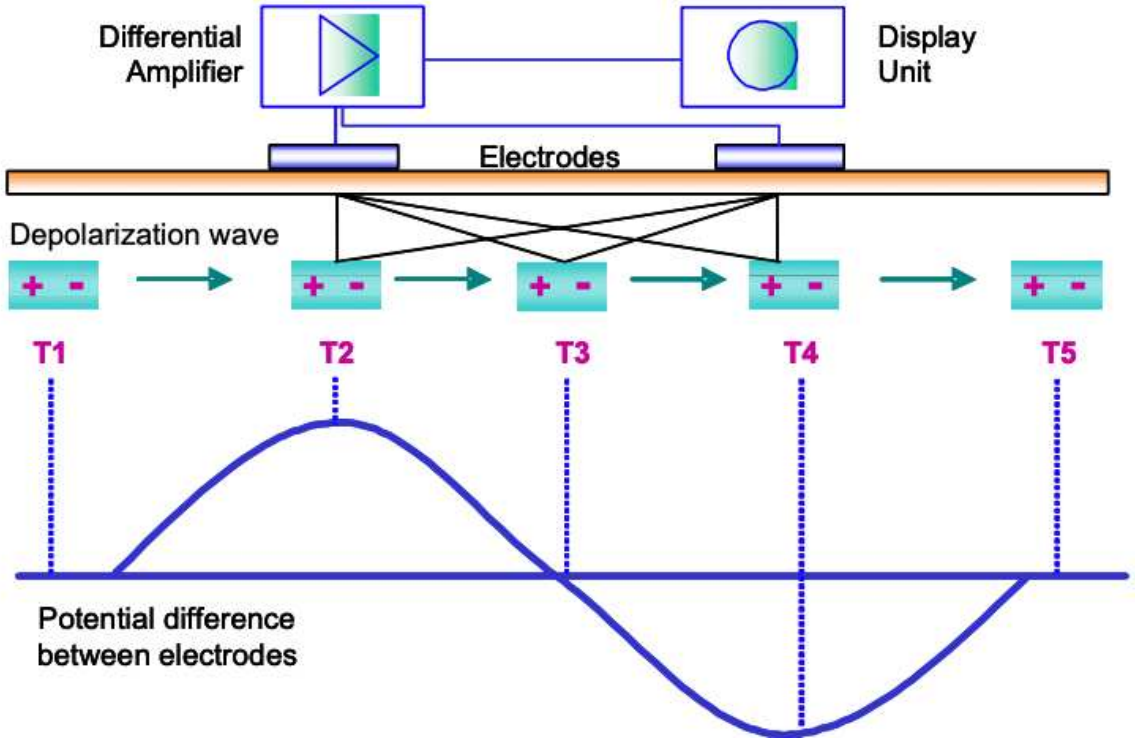

Figure 3. 6 *Bipolar electrode configuration.*

The sEMG measures require, in proximity of the site of the muscle, a pair of electrodes so that the recorded waveform is the difference of potential between the two electrodes. The first electrode in ***Figure 3. 6*** records a signal when the depolarization wavefront passes below it at time T2, while the second electrode is not able to record any voltage difference. At time T2, the signal has the highest amplitude recorded from the first electrode. When the depolarization wavefront passes in the middle point between the two electrodes, they both sense the same voltage difference, and the recorded signal

is null (time T3). Finally, the depolarization arrives below the second electrode that record the highest negative amplitude at time T4. This model explains why the monopolar action potential creates a bipolar signal within the differential amplification process. Because a motor unit consists of many muscle fibers, the electrode pair records the magnitude of all innervated fibers within this motor unit[33]. **A motor unit** is made up of a motor neuron and the skeletal muscle fibers innervated by that motor neuron's axonal terminals. Typically, they sum up to a **triphasic** Motor unit action potential (MUAP), which differs in form and size depending on the geometrical fiber orientation in ratio to the electrode site (***Figure 3. 7***) [33].

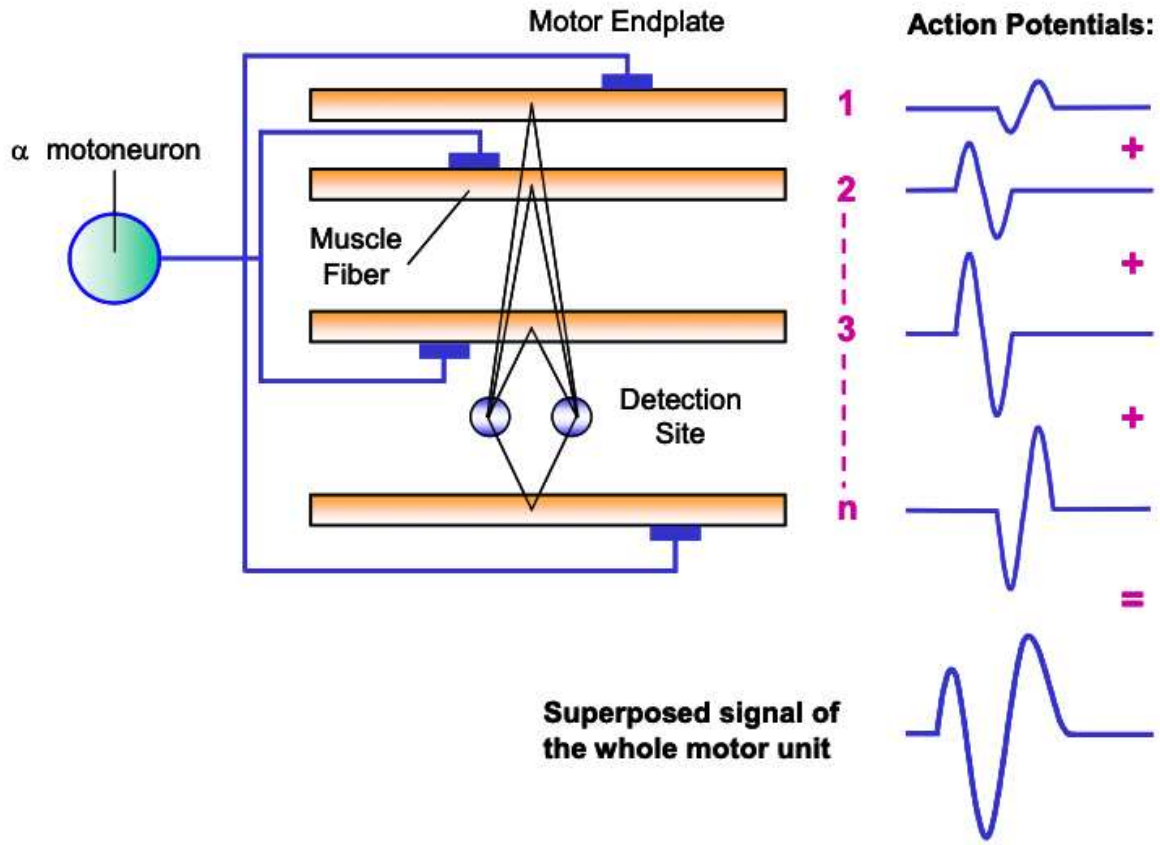

Figure 3. 7 *All the Motor Unit Action Potential are superposed. The resulting signal is characterized by positive and negative peaks.*

The two most important mechanisms influencing the magnitude and density of the observed signal are the Recruitment of MUAPs and their Firing Frequency. These are the main control strategies to adjust the contraction process and modulate the force output of the involved muscle. The EMG signal directly reflects the recruitment and firing characteristics of the detected motor units within the measured muscle (***Figure 3. 8***) [33].

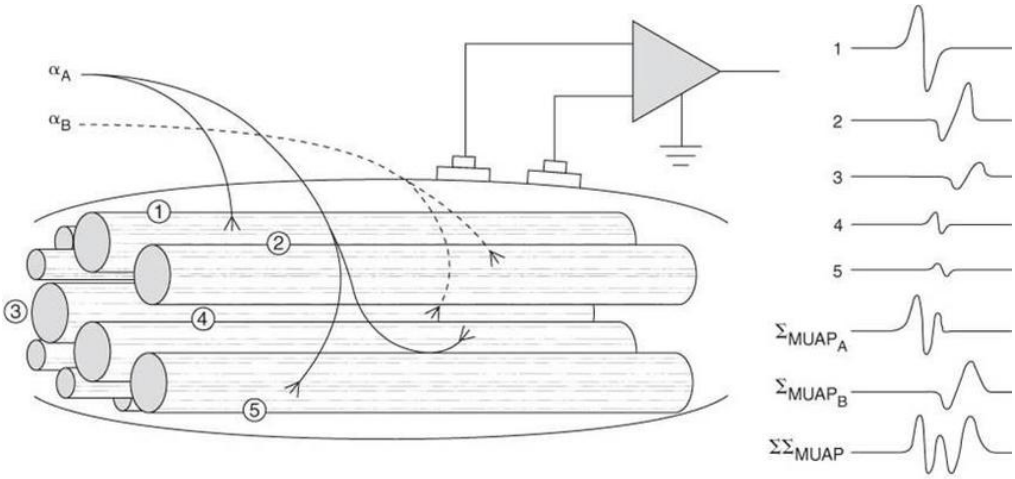

Figure 3. 8 *EMG record the summation of all the MUAP sensed by the electrodes*

The unfiltered and unprocessed signal recorded by the overlay of multiple MUAPs is called the **raw EMG signal**. When the muscle is relaxed electrodes prevalently record noise-free EMG baseline, that depend on factors like quality of the EMG amplifier, the environment noise and the quality of the given detection condition. Raw EMG spikes are of random shape, which means one raw recording burst cannot be precisely reproduced in exact shape. This is because the actual set of recruited motor units constantly changes within the matrix/diameter of available motor units. Typically, raw sEMG signal range between +/- 5000 mV and have a frequency content between 6- 500 Hz. the most frequency power ranges between 20 and 150 Hz [33].

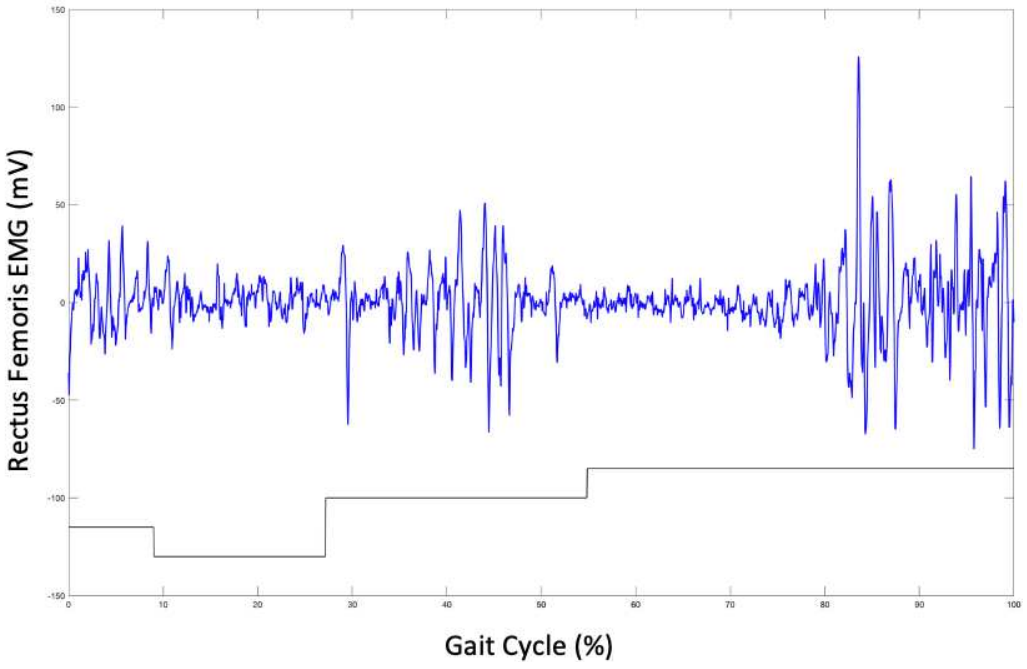

Figure 3. 9 *Raw sEMG signals of rectus femoris during a complete gait cycle. Sampling Frequency at 2000 Hz. Muscle Cross Talk and Power Line are overlapped on the EMG signal. The Amplitude is given in mV.*

EMG signal can be influenced by several external factors that can alters the shape and characteristics of the recording: physiological cross talk, changes in the geometry between muscle belly and electrode site, external noise and electrodes and amplifiers.

3.2.1 Surface Electrodes

Surface EMG electrodes provide a non-invasive technique for measurement and detection of EMG signal. They are usually inexpensive and easy to apply, but they require a minimum of patient skin preparation. Surface electrodes (***Figure 3. 10***) record signal in a lower frequency spectrum, with respect to needle electrodes, ranges from 20 to 500 Hz.

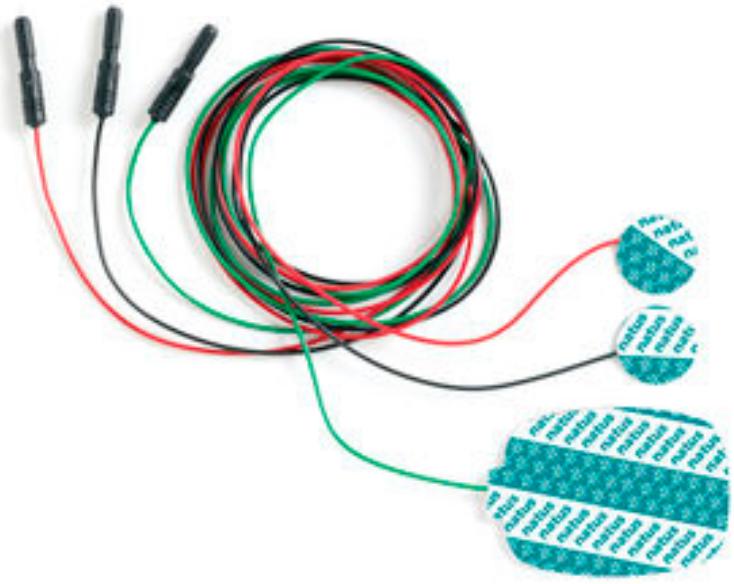

Figure 3. 10 *Surface electrodes*

3.2.2 Amplifiers

EMG amplifiers act as differential amplifiers (***Figure 3. 11***), and their main purpose is the ability to reject or eliminate artifacts and to eliminate the potentially much greater noise signal from power line sources. The signals are detected at two sites and electronic circuits subtracts the two signals and thus amplifies the difference. Any signal that is common to both detection sites will be removed (common mode signals) and signals that are different at the two sites will have a differential that will be amplified. Any signal that originates far from the detection sites (e.g., external noise) reach the electrodes with no phase shift, appearing as a common mode signal, whereas signals close to the detection surfaces will be different and consequently amplified [32].

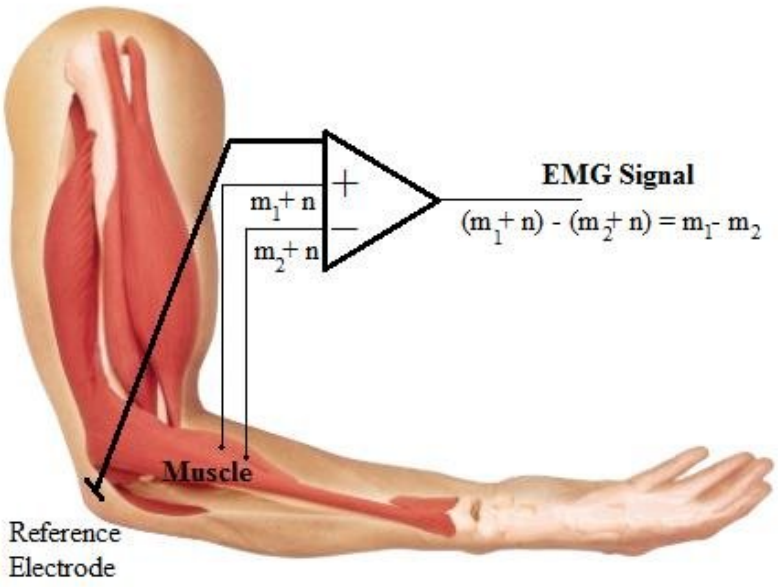

Figure 3. 11 *Differential amplifier eliminates common mode signals*

The main characteristics of a differential EMG amplifier [33] are:

- **Dynamic range and gain**: the gain is the ratio between the output voltage and the input voltage and usually ranges between 1'000 and 1'000'000 [34]
- **Common mode rejection ratio (CMRR)**: CMRR is calculated as the amplification of differential signals divided by the amplification of common mode signals, and it represents the accuracy of the differential amplifier in eliminate undesired common signals. A CMRR of 90 dB is generally sufficient to suppress extraneous electrical noises [34].
- **Input impedance**: The source impedance at the junction of the skin and detection surface should be as large as possible in order to prevent attenuation and distortion of the detected signal (ranging from kΩ to MΩ).
- **Frequency response**: The frequency response of the amplifier should adapt to the frequency spectrum of the EMG signal (10-500 Hz).

3.2.3 Analog-to-digital Resolution

Before a signal can be displayed and analyzed in the computer, it has to be converted from an analog to a digital signal (***Figure 3. 12***). The resolution of A/D measurement boards need to properly convert the expected amplitude range (e.g., +/- 5 Volts). 12-bit converters with a resolution of 4096 discrete levels (2^12=4096 levels =4095 intervals) are commonly used, but 16 bits or more are becoming increasingly popular [34].

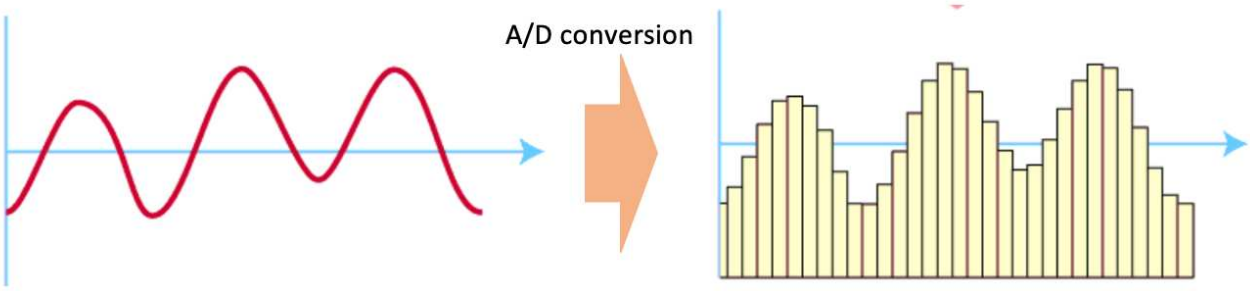

Figure 3. 12 *Analogue-to-digital resolution. The amplitude of an analogue signal is sampled using usually a 12-bit converter (4096 levels, with an increment of 0.00024)*

3.2.4 Analog-to-Digital Sampling Rate

The **Nyquist–Shannon sampling theorem** establishes a sufficient condition for a sample rate that permits a discrete sequence of samples to capture all the information from a continuous-time signal of finite bandwidth.

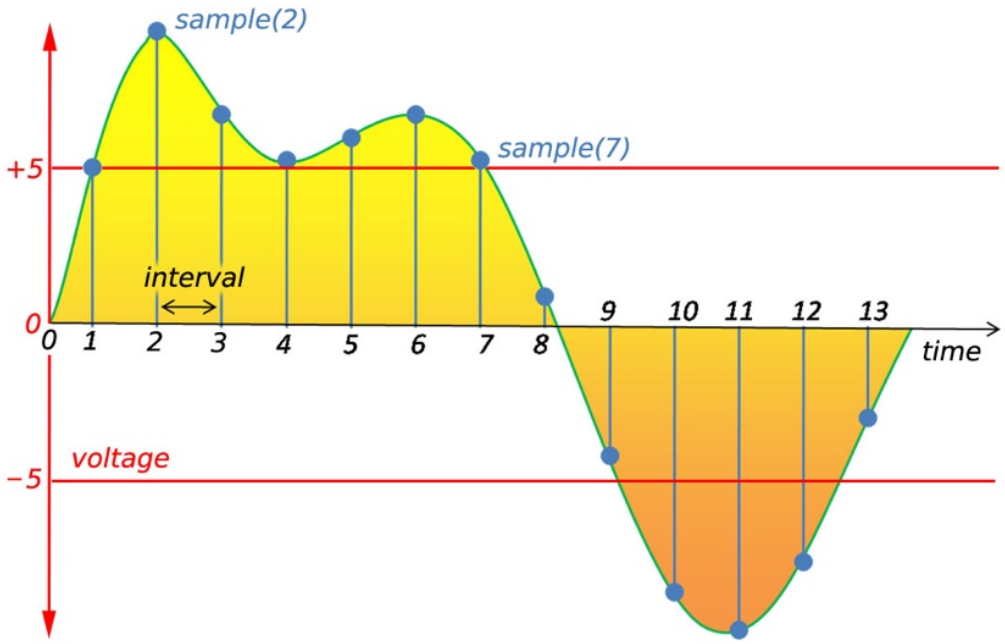

Figure 3. 13 *Analogue-to-digital sampling: each sample is recorded at a specific sampling period corresponding to the inverse of the sampling frequency.*

The minimum sampling frequency necessary to avoid aliasing is, at least, equal to twice the maximum frequency content of the recorded signal.

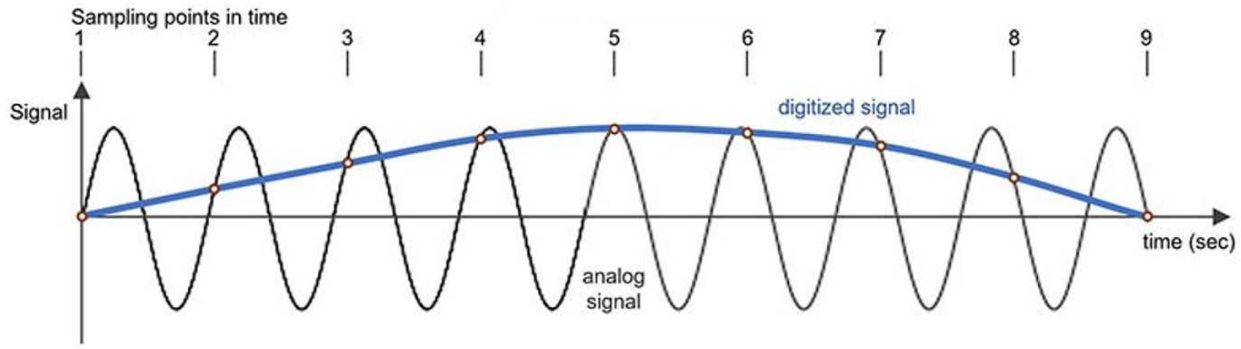

Figure 3. 14 *Aliasing: if the sampling frequency does not respect the Shannon theorem, the reconstructed signal will be different form the original one because high frequency components will be eliminated.*

3.2.5 Digital Filters

The analog system has the purpose of amplifying the sEMG while reducing the contributions of artifacts, noise, and power line interference, before the signal is converted in a sequence of binary numbers by the A/D converter. Additional attenuation of undesired contributions may be achieved by **digital processing** after the A/D conversion [35]. Low frequency artifact noise can be reduced by a high-pass filter with cut-off frequency in the range of 10–30 Hz and high frequency noise can be reduced with a low-pass filter with cut-off frequency in the range of 350–400 Hz [35].

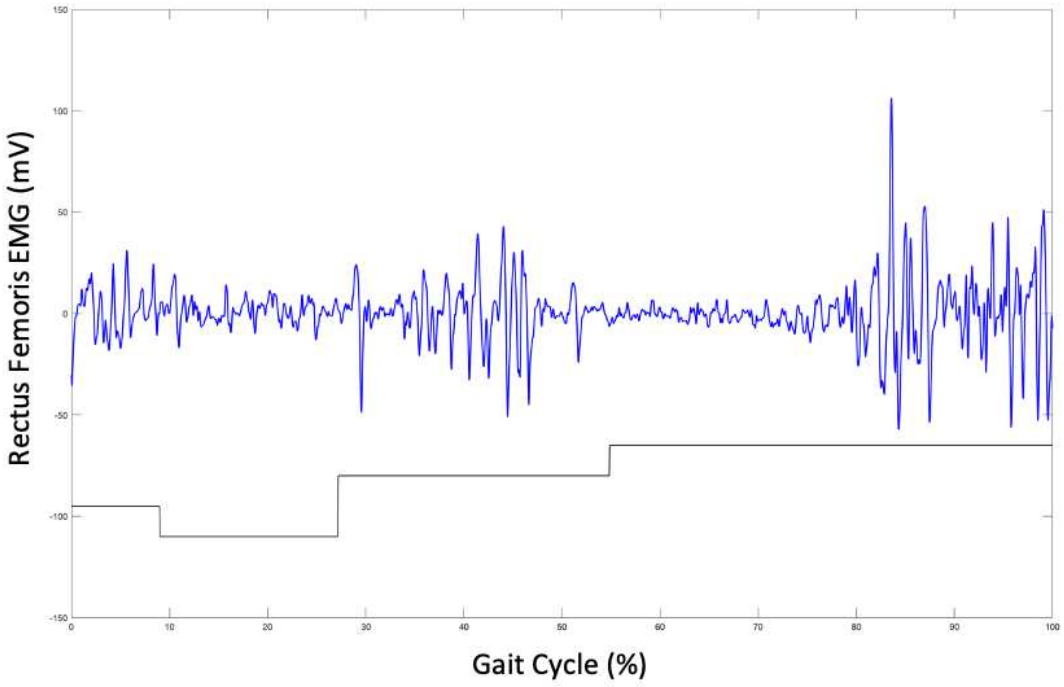

Figure 3. 15 *Denoised signal obtained using a band pass filter between 20 and 450 Hz.*

CHAPTER 4: Machine Learning

This chapter introduces the background of the various Machine Learning techniques, with a specific focus on the algorithms and models that are used in this study. In detail, Chapter 4 opens with a brief overview of the main concepts reported in the literature concerning artificial intelligence in general. Subsequently, the concept of machine learning will be presented in more detail, and then move on to the description of the two models adopted in this work.

4.1 Artificial Intelligence

A precise definition and meaning of Artificial Intelligence (AI) is still subject of discussions. Many authors try to give its own contribution to generally define AI. These definitions mainly fall into two classes that describe artificial intelligence as concerning:

- **Thought processes** and **reasoning**
- **Behaviour**

The definitions belonging to each of the two classes can be further distinguished based on the performance and the term of comparison used to measure them in:

- **Humanity**: measuring success in terms of fidelity to human performance
- **Rationality**: measuring success against an ideal performance

A human-centred approach must be in part an empirical science, involving observations and hypotheses about human behaviour. A rationalist approach involves a combination of mathematics and engineering [36].

Table 4. 1 *D Classes into which the various definitions of AI are divided*

Thinking Humanly	**Thinking Rationally**
"The exciting new effort to make computers think ... machines with minds, in the full and literal sense." (Haugeland, 1985 [37])	"The study of mental faculties through the use of computational models." (Charniak and McDermott, 1985 [38])
Acting Humanly	**Acting Rationally**
"The art of creating machines that per- form functions that require intelligence when performed by people." (Kurzweil, 1990 [39])	"Computational Intelligence is the study of the design of intelligent agents." (Poole et al., 1998 [40])

Informally, the term "artificial intelligence" is applied when a machine is capable of performing functions that humans associate with other human minds, such as learning and problem solving. Learning is a vital aspect of machines, therefore, machine learning is a subfield of AI [41]. Machine learning is constantly developing and a great effort in its advancement over the past few decades has led to higher expectations from machines. Deep learning is an attempt in this direction and has become part of AI as a sub-branch of machine learning (***Figure 4. 1***).

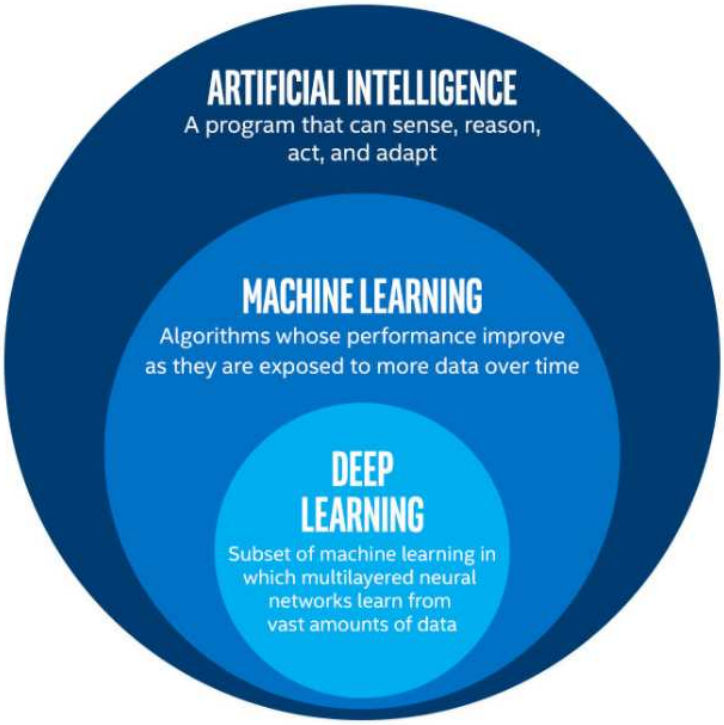

Figure 4. 1 *Artificial intelligence sub-groups*

4.2 Machine Learning

Machine learning is a branch of AI that focuses on using data and algorithms to mimic the way humans learn, gradually improving their accuracy. Through the use of statistical methods, algorithms are trained to make classifications or predictions on new data. There are three main categories of machine learning:

- **Supervised learning:** The main goal in supervised learning is to learn a model from labeled training data that allows us to make predictions about unseen or future data. Supervised refers to a set of training examples (*data inputs*) where the desired output signals (*labels*) are already known. Labeled training data is passed to a machine learning algorithm for fitting a predictive model that can generate predictions on new, unlabeled data inputs (***Figure 4. 2***) [42].

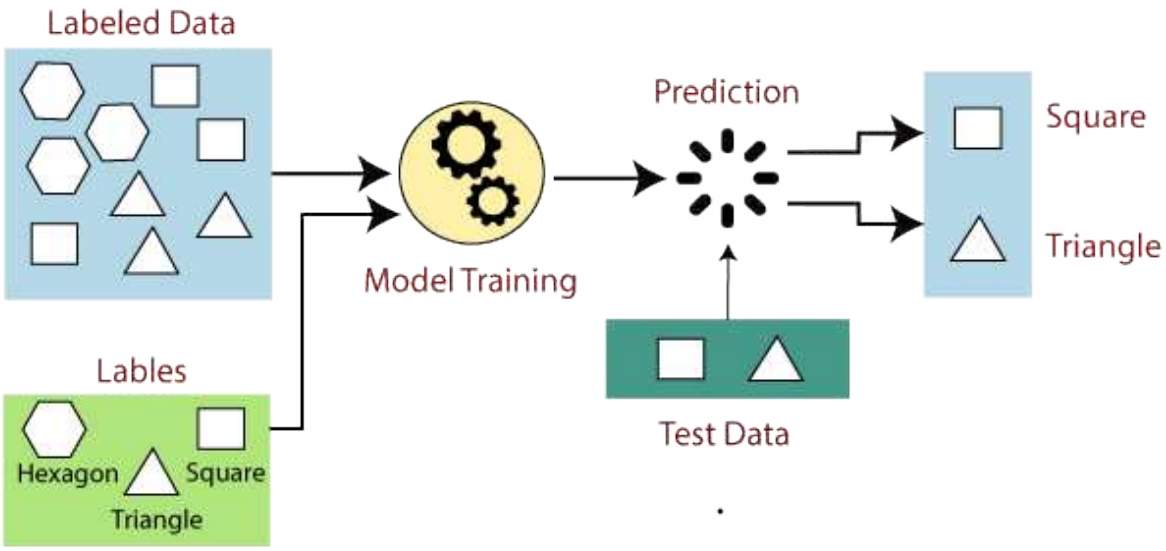

Figure 4. 2 *Supervised learning scheme for classification problems.*

A supervised learning task with discrete class labels is also called **classification** task. Classification is a subcategory of supervised learning where the goal is to predict the categorical class labels of new instances, based on past observations. Another type of supervised learning is **regression**, where the outcome signal is a continuous value. In regression analysis, starting from a number of predictor (**explanatory**) variables and a continuous response variable (**outcome**), the machine learning algorithm try to define a relationship between those variables to predict an outcome [42]. A schematic representation that explains the difference between classification and regression problems is reported in ***Figure 4. 3.***

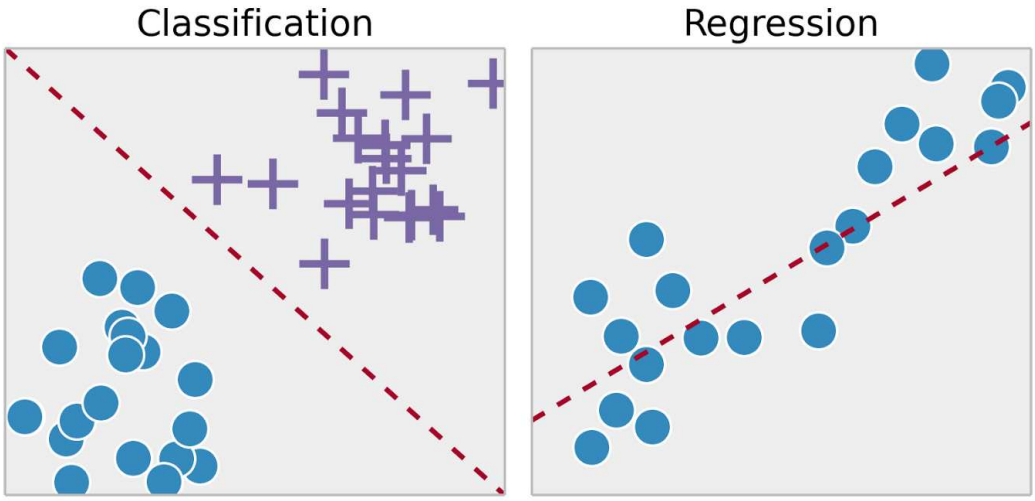

Figure 4. 3 *Schematic representation of classification and regression problems.*

- **Unsupervised learning:** In unsupervised learning, unlabeled data or data of unknown structure are used to build the model. Using unsupervised learning techniques meaningful information can be extracted without the guidance of a known outcome variable. **Clustering** is a technique that allows to organize information into meaningful subgroups (*clusters*) without having any prior knowledge of their group memberships (***Figure 4. 4***). Each cluster that arises during the analysis defines a group of objects that share a certain degree of similarity but are more dissimilar to objects in other clusters [42].

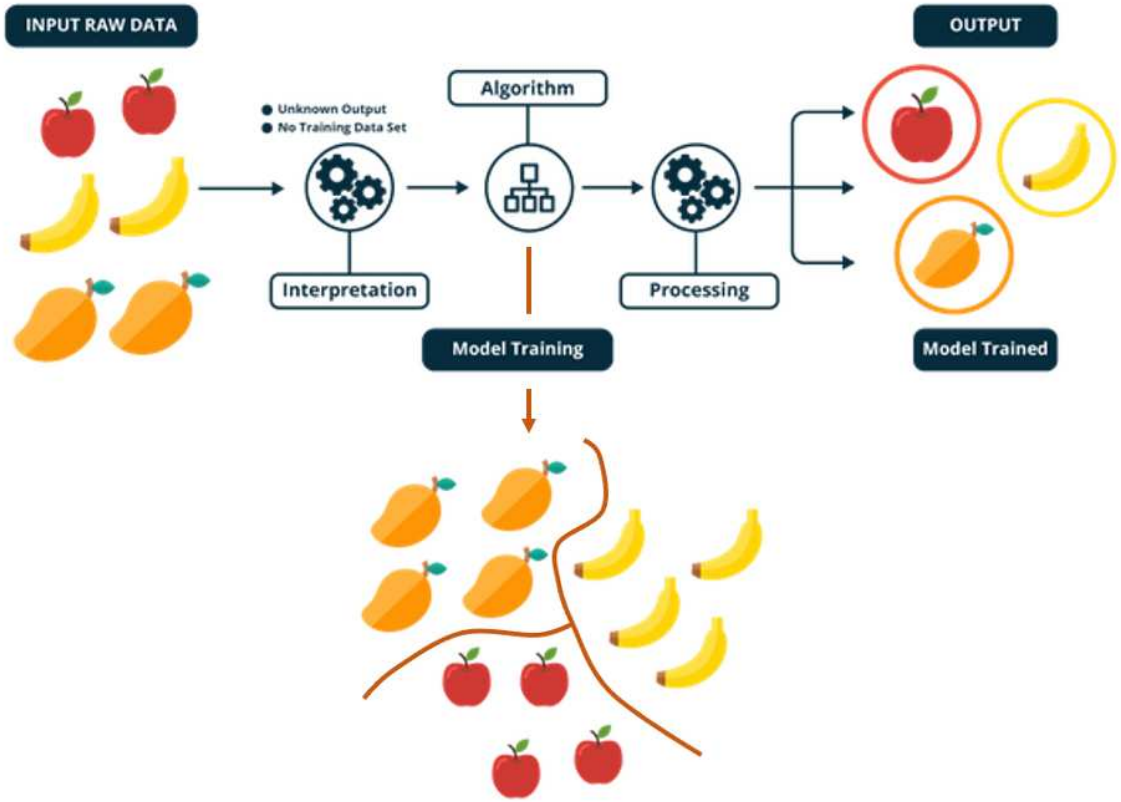

Figure 4. 4 *Unsupervised learning scheme.*

- **Reinforcement learning:** In reinforcement learning, the goal is to develop a system (*agent*) that improves its performance based on interactions with the environment. Since the information about the current state of the environment typically also includes a so-called **reward signal**. This feedback is not the correct *ground truth label* or value, but a measure of how well the action was measured by a reward function. Through its interaction with the environment, an agent can then use reinforcement learning to learn a series of actions that maximizes this reward via an exploratory trial-and-error approach or deliberative planning. Each state can be associated with a positive or negative reward, and a reward can be defined as accomplishing an overall goal (***Figure 4. 5***) [42].

Figure 4. 5 *Reinforcement learning scheme.*

4.3 Neural Network

Biological neurons are interconnected nerve cells in the brain that are involved in the processing and transmission of chemical and electrical signals. Multiple signals arriving at the dendrites are subsequently integrated into the cell body and, if the accumulated signal exceeds a certain threshold, an output signal passing through the axon is generated (***Figure 4. 6***). Frank Rosenblatt published the first concept of the perceptron learning rule based on the **McCulloch-Pitts neuron model** [43], proposing an algorithm that would automatically learn the optimal weight coefficients that would then be multiplied with the input features in order to make the decision of whether a neuron fires or not [42].

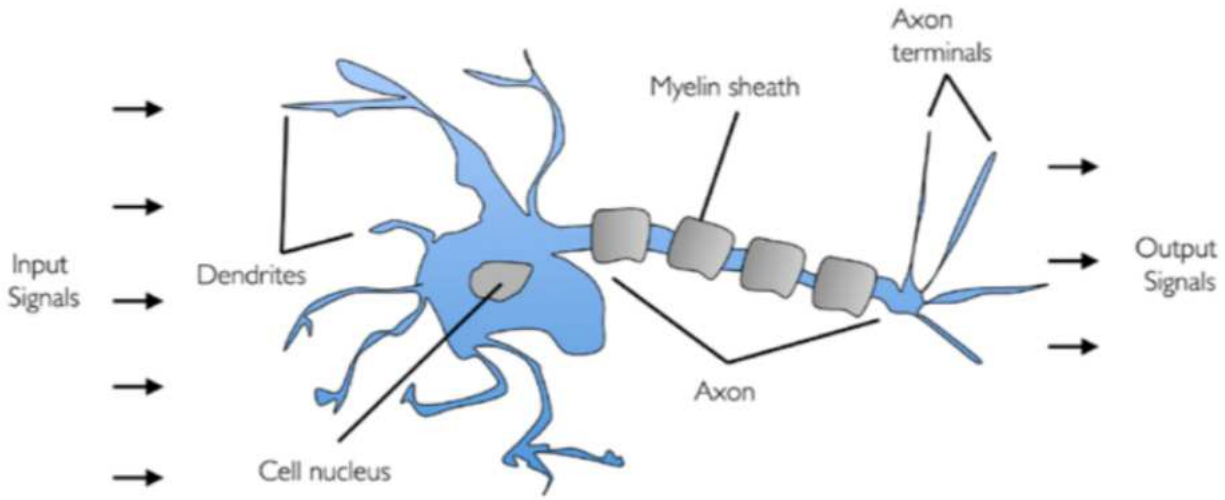

Figure 4. 6 *Biological Neuron. Each neuron is a cell that uses biochemical reactions to receive, process and transmit information.*

4.3.1 Perceptron

Perceptron is an algorithm developed for binary classification in supervised machine learning. Perceptron is a single function which can decide whether or not an input, represented by a feature vector, belongs to some specific class (1 - True, 0 - False). The **decision function**, $\boldsymbol{\phi(z)}$, can be applied to a linear combination of certain input values, x, and a corresponding weight vector, w.

$$z = w_1 x_1 + w_2 x_2 + \cdots + w_n x_n \tag{1}$$

Now, if the net input of a particular example, $x^{(i)}$, is greater than a defined threshold, θ, class 1 is predicted (class 0 otherwise). In the perceptron algorithm the decision function, $\phi(z)$, is a variant of a unit step function:

$$\phi(z) = \begin{cases} 1 & if\ z > \theta \\ 0 & otherwise \end{cases} \tag{2}$$

For simplicity, we can bring the threshold, e, to the left side of the equation and define a **weight-zero** as $w_0 = -\theta$ and $x_0 = 1$ so that we write z in a more compact form:

$$z = w_0 x_0 + w_1 x_1 + w_2 x_2 + \cdots + w_n x_n = w^T x \tag{3}$$

And:

$$\phi(z) = \begin{cases} 1 & if\ z > 0 \\ 0 & otherwise \end{cases} \tag{4}$$

In machine learning literature, the negative threshold, or weight, $w_0 = -\theta$, is usually called the bias unit. The net input, $z = w^T x$, is squashed into a binary output [42].

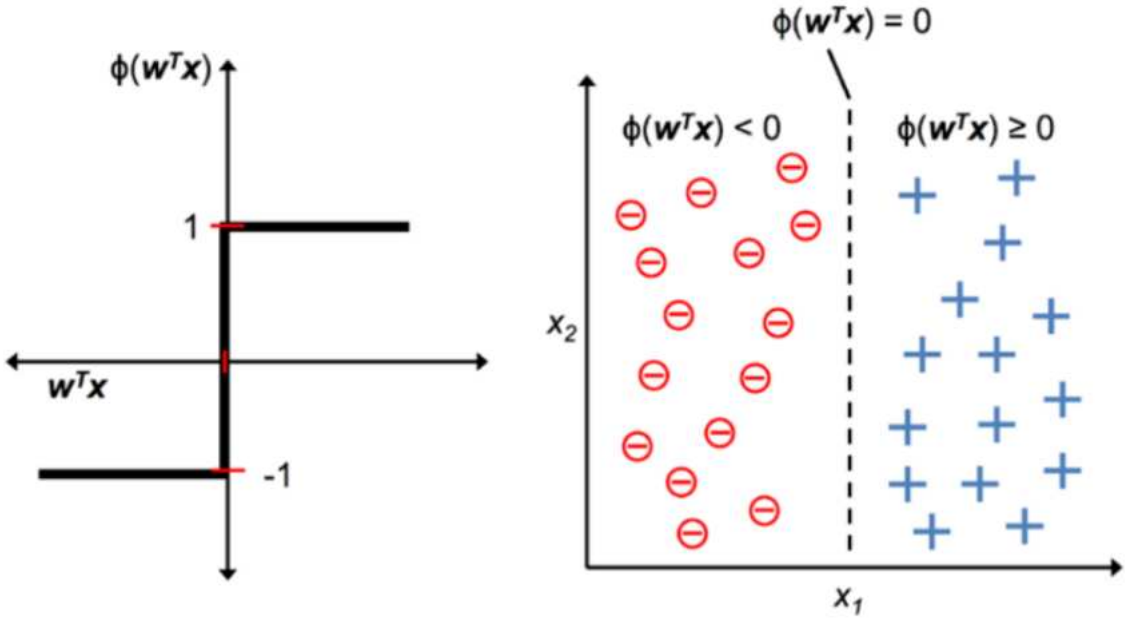

***Figure 4.** 7 Threshold function to separate two labeled classes.*

Thus, Rosenblatt's initial perceptron rule is simple, and the perceptron algorithm can be summarized by the following steps:

1. Initialize the weights to 0 or small random numbers.
2. For each training example:
    a. Compute the output value
    b. Update the weights

The output value is the class label predicted by the unit step function and the simultaneous update of each weight, w_j, in the weight vector, w.

$$w_j := w_j + \Delta w_j$$

(5)

The update value is calculated as:

$$\Delta w_j = \eta\left(y^{(i)} - \hat{y}^{(i)}\right)x_j{}^{(i)}$$

(6)

Where η is the **learning rate** (typically a constant between 0.0 and 1.0), $y^{(i)}$ is the true class label of the i^{th} training example, and $\hat{y}^{(i)}$ is the predicted class label. The weight update is proportional to the value of $x_j{}^{(i)}$ [42].

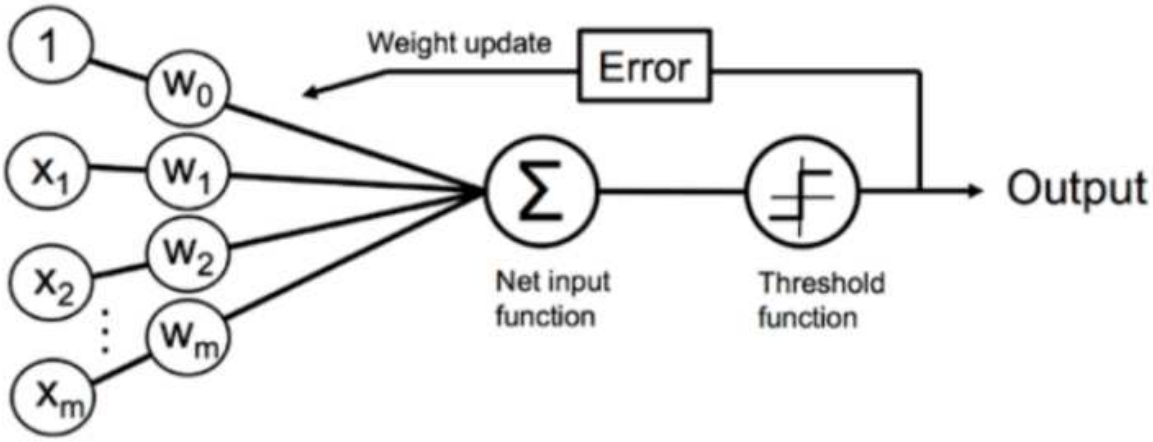

Figure 4. 8 *Neuron structure. The output of the neuron is given by the output of the threshold function that takes as input the weight associated to the input and the bias value associated to the neuron.*

4.3.2 Multilayer Perceptron

Multilayer perceptron (MLP) is a supplement of feed forward neural network. It consists of three types of layers: the **input layer**, **output layer** and **hidden layer** [44].

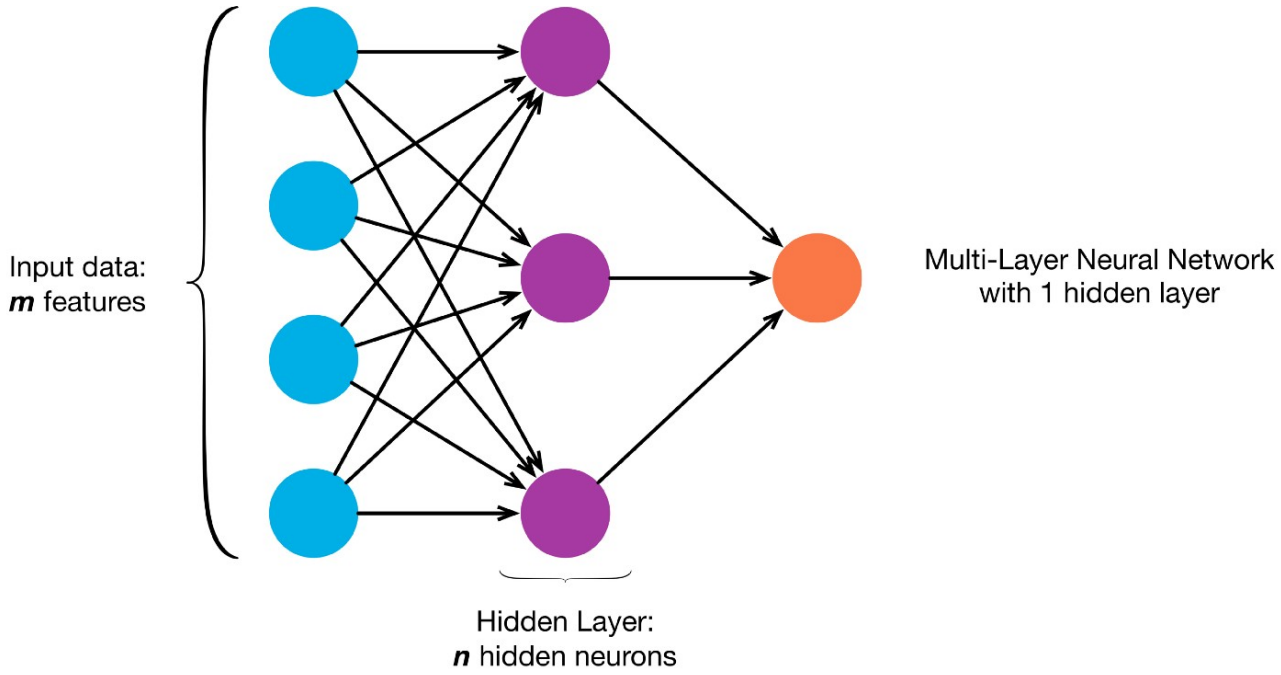

Figure 4. 9 *Generic Structure of a multilayer perceptron neural network. The first layer is formed by 4 neurons, each of which represents the input vector; the second layer is called hidden layer; the last layer is formed (in this case) by one neuron that represents the output vector (Predictions of the network).*

Each node in the input layer receives the input signal to be processed and fires according to the predefined local decision boundaries. Then the output of the first layer is passed to the second layer,

the results of which are passed to the final output layer consisting of one single neuron (***Figure 4. 9***). [44]. MLP is a fully connected hierarchical neural network where each neuron in a layer is connected to all neurons located in the previous layer and to all neurons in subsequent layers. Weights and biases need to be adjusted by providing a series of training examples in order to minimize errors produced in the output. Error minimization, seen as the difference between output value and actual value, is calculated using a specific **cost function** and **loss function** (the loss function is for a single training example, while the cost function is over the entire training set). This approach seems very intuitive, but it requires that a small change in weights (and/or biases) cause only a small change in the outputs. For this reason, a function, known as the **activation function**, is used to maps the resulting values from each perceptron to a value between 0 and 1. The activation function is a continuous function that compresses the input values into a continuous and small range of output values.

Typical activation functions used in machine learning architectures are:

- **Sigmoid function:** it maps the entire numeric range of output values to a small range from 0 to 1 (***Figure 4. 10***). The sigmoid function converts a real value into one that can be interpreted as a probability. The neuron can use the sigmoid for computing the non-linear function: $\sigma(z = w^T x)$

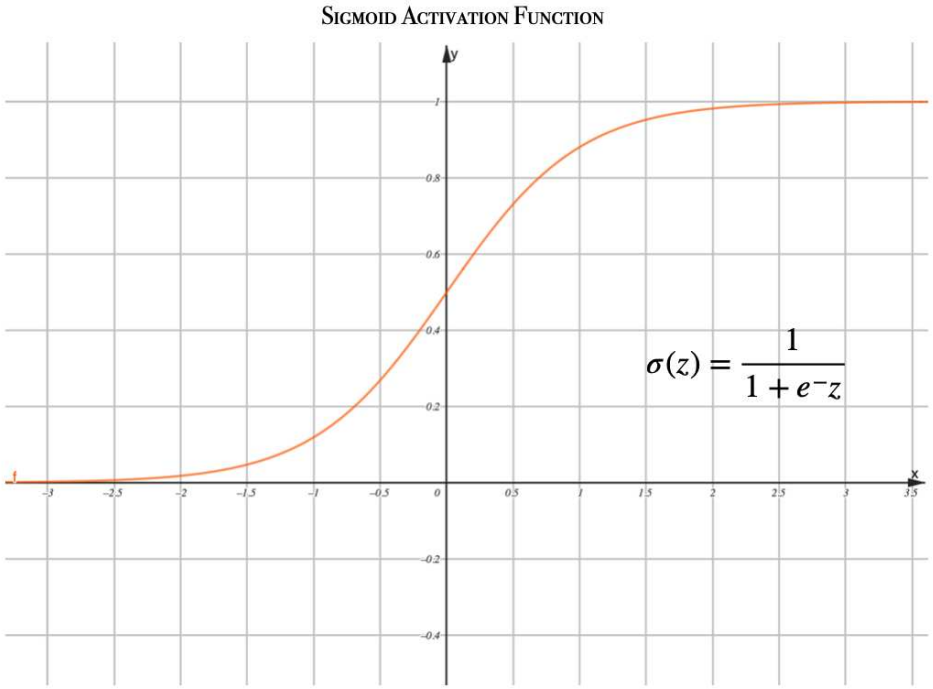

Figure 4. 10 *Sigmoid Function. Y axis function's output (0-1). X axis input vector z (sum of the products between weight (wi) and input (xi) and the bias value).*

- **Rectified Linear Unit (ReLU) function:** ReLU function is the most commonly used activation function. The function returns 0 if it receives any negative input, but for any positive value it returns that value back (***Figure 4. 11***).

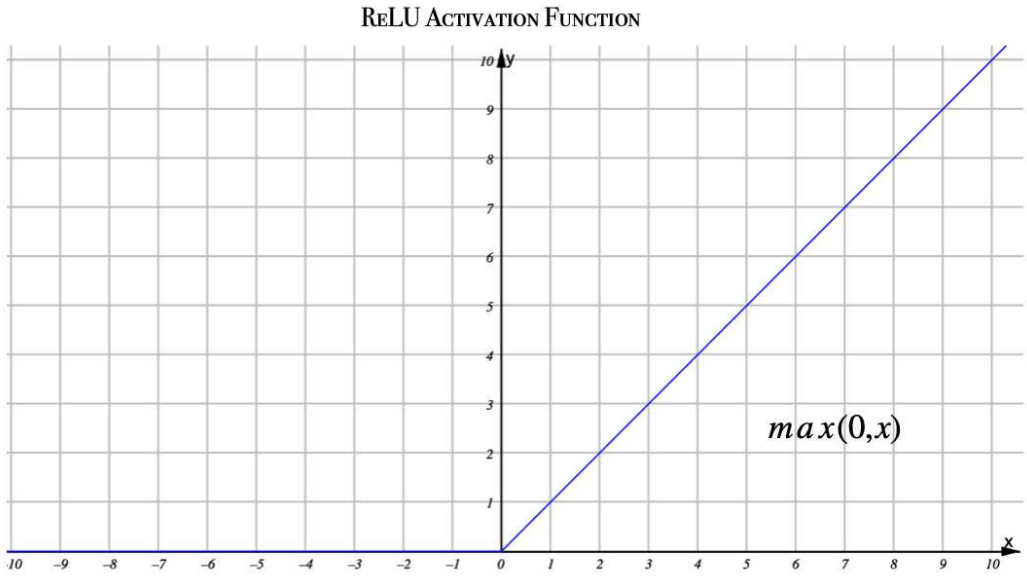

Figure 4. 11 *ReLU activation function. The output values are different from zero for positive values of the input vector.*

- **Tangent hyperbolic function (tanh):** The output of the tanh function ranges from -1 to 1 and it is a shifted and stretched version of the sigmoid. The main difference is the fact that the tanh function pushes the input values to 1 and -1 instead of 1 and 0 (***Figure 4. 12***).

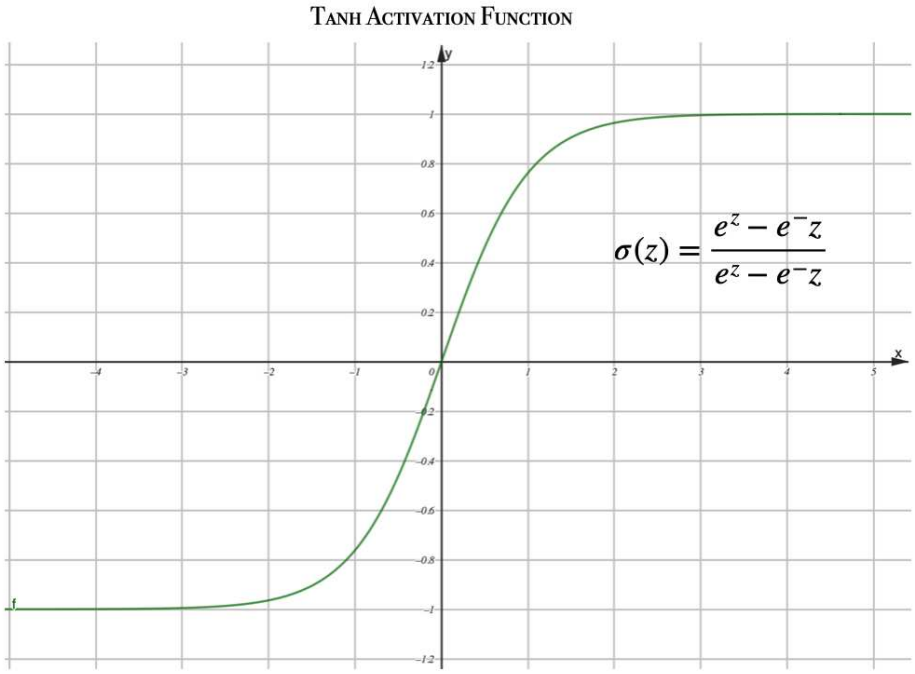

Figure 4. 12 *Tanh activation function. It ranges between -1 and 1.*

- **SoftMax**: it is a mathematical function that maps a vector of input values into a probability vector whose sum is equal to 1. Each value in the original vector is converted to a number between 0 and 1. SoftMax function is commonly used for **multi-class classification**.

$$softmax(z_j) = \frac{e^{z_j}}{\sum_{k=1}^{K} e^{z_k}} \qquad for\ j = 1, \dots, K \tag{7}$$

The output of the activation function is interpreted as the probability of a particular example in the training set belonging to class 1. Finally, the predicted probability can simply be converted into a binary outcome through a threshold function [42]:

$$\phi(z) = \begin{cases} 1 & if\ z > \theta \\ 0 & otherwise \end{cases} \tag{8}$$

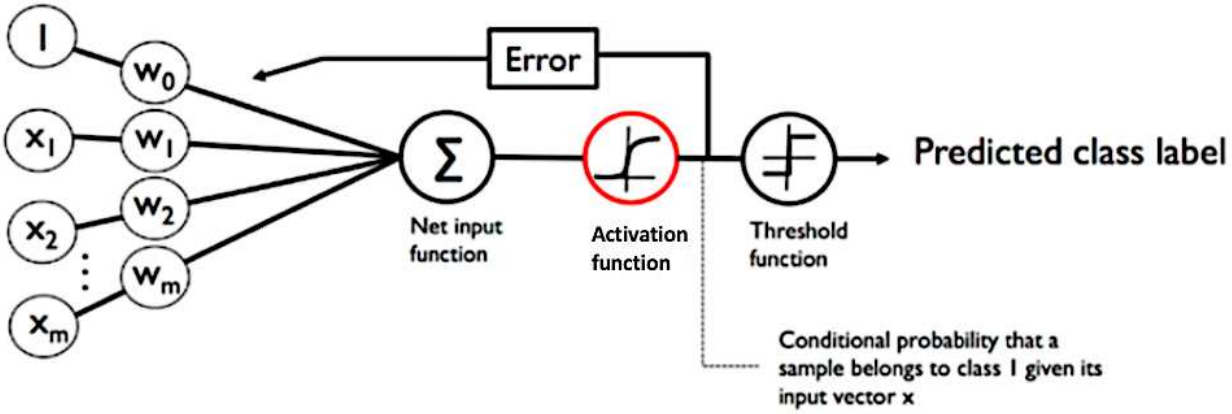

Figure 4. 13 *Neuron structure. The activation function is computed between the sum of all the input with the correspondent weight and bias and the threshold function. The error is computed between the output of the activation function and the actual value of the input.*

4.4 Support Vector Machines (SVM)

Support vector machine (SVM) is a supervised learning technique for classification and regression. While in the perceptron algorithm the goal was to minimize misclassification errors, in SVM the optimization objective is to maximize the margin. The margin is defined as the distance between the separating hyperplane (decision boundary) and the training examples closest to this hyperplane, which are the so-called **support vectors** (***Figure 4. 14***) [42].

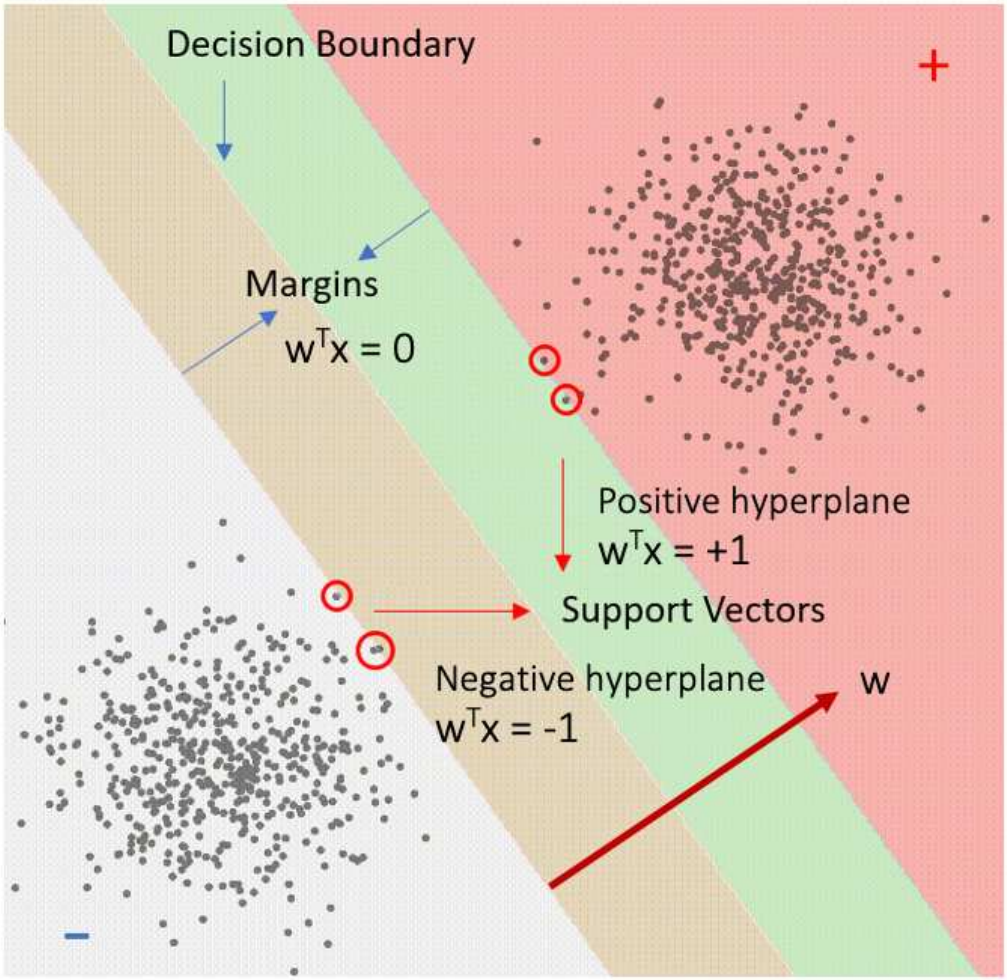

Figure 4. 14 *Support vector machine scheme: decision boundary and support vectors to classify positive from negative examples.*

Suppose w is the vector perpendicular to the hypothetical hyperplane that separates positive $(+)$ from negative $(-)$ examples and x is the unknown vector (the unknown sample to be classified). The vector product between w and x identifies the length of the projection of x on the vector w [42]. The **decision rule** is defined as:

$$w \cdot x \geq c \tag{9}$$

If this length is larger than a specific constant, $\boldsymbol{c}$, then vector $\boldsymbol{x}$ belongs to the set of positive examples (***Figure 4. 15***) [42]. Without loss of generality, the above equation can also be written as:

$$w \cdot x + b \geq 0 \qquad then\ x\ belong\ to\ (+) \tag{10}$$

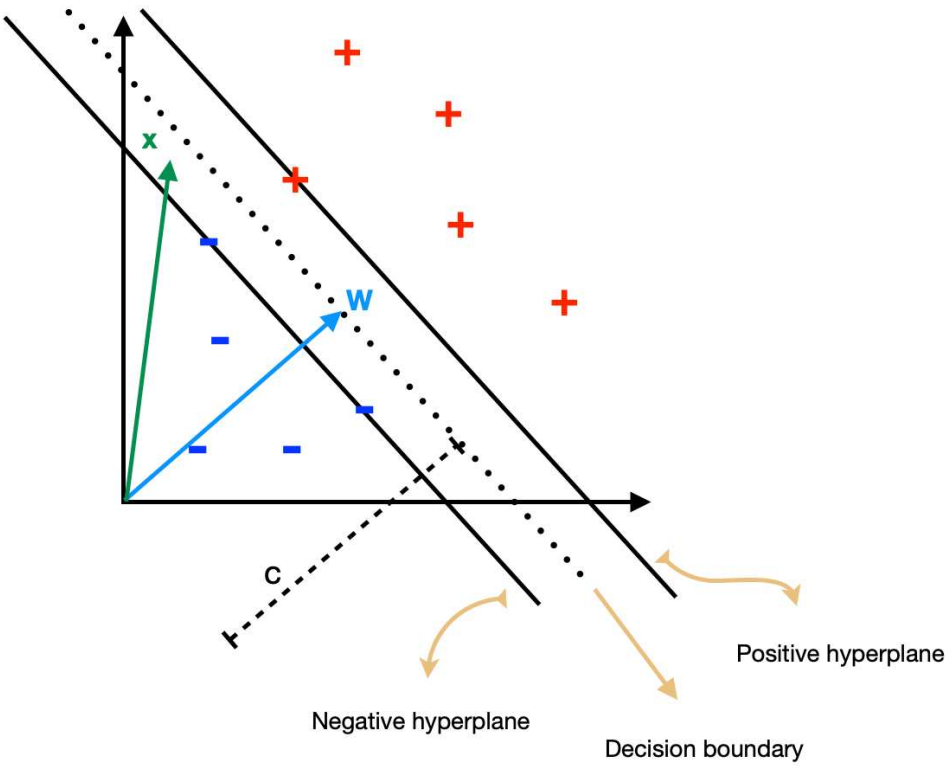

Figure 4. 15 *Decision boundary and positive and negative hyperplanes definitions. x is the unknown vector that represent the sample that must be classified as positive or negative. w is the vector perpendicular to the defined decision boundary.*

This condition defines the separation hyperplane. In addition, other constraints are introduced to find unique solutions for w and b, defining as positive examples (x_+) the samples in the training set within the space defined by the positive hyperplane and negative examples (x_-) the samples in the space defined by the negative hyperplane, as follows [42]:

$$w \cdot x_+ + b \geq 1 \tag{11}$$

$$w \cdot x_- + b \geq -1 \tag{12}$$

Both hyperplanes that divide positive from negative samples are parallel to the decision boundary. A variable y_i can be introduced at this point for mathematical convenience such that:

$$y_i = \begin{cases} 1 & for\ positive\ samples \\ -1 & for\ negative\ samples \end{cases} \tag{13}$$

The terms of the equation (11) and (12) become the same by multiplying both terms by y_i as follows:

$$y_i(w \cdot x_+ + b) \geq 1$$

(14)

And:

$$y_i(w \cdot x_+ + b) - 1 \geq 0$$

(15)

The equality sign of equation (15) defines the two hyperplanes. The width between the two lines can be calculated as the difference between the vector defined by the positive and negative samples lying on the two hyperplanes and projected on the unit vector of w [42].

$$(x_+ - x_-) \cdot \frac{w}{\|w\|} = [(1 - b) - (1 + b)] \cdot \frac{1}{\|w\|} = \frac{2}{\|w\|}$$

(16)

The left side of the preceding equation can then be interpreted as the distance between the positive and negative hyperplane, which is the so-called margin. The width between the two hyperplanes must be maximized:

$$max\left(\frac{2}{\|w\|}\right) = max\left(\frac{1}{\|w\|}\right) = min(\|w\|) = min(\|w\|^2)$$

(17)

The minimization of the norm of the vector w is a constrained problem because the equation (15) must be respected. Through Lagrange Multipliers, the constrained optimization problem become an unconstrained problem [42].

$$L(\alpha_i, w, b) = \frac{1}{2}\|w\|^2 - \sum \alpha_i[y_i(w \cdot x_i + b) - 1]$$

(18)

To find the maximum of the new equation, the first derivative of $L(\alpha_i, w, b)$ must be set equal to 0.

$$\frac{\partial L}{\partial w} = w - \sum \alpha_i y_i x_i = 0 \quad \Rightarrow \quad w = \sum \alpha_i y_i x_i$$

(19)

$$\frac{\partial L}{\partial b} = -\sum \alpha_i y_i = 0 \quad \Rightarrow \quad \sum \alpha_i y_i = 0$$

(20)

At this point equation (n°) can be rewritten using the results coming out from the previous equations as follow:

$$L(\alpha_i, w, b) = \frac{1}{2}\left(\sum \alpha_i y_i x_i\right)\left(\sum \alpha_j y_j x_j\right) - \sum \alpha_i y_i x_i \left(\sum \alpha_j y_j x_j\right) - \left(\sum \alpha_j y_j b\right) + \sum \alpha_i$$

(21)

$$L(\alpha_i, w, b) = \sum \alpha_i - \frac{1}{2}\sum_i \sum_j \alpha_i \alpha_j \, y_i \, y_j x_i x_j$$

(22)

Finally, the decision rule can then be re-written as [42]:

$$\sum \alpha_i y_i x_i \cdot x + b \geq 0 \qquad then\ x\ belong\ to\ (+)$$

(23)

4.4.1 Kernels

Another reason why SVMs enjoy high popularity in machine learning is that kernels can be used to solve nonlinear classification problems. To solve a nonlinear problem using an SVM, the training data can be transformed into a higher-dimensional feature space via a mapping function, ϕ, and a linear SVM model can be trained to classify the data in this new feature space. Then, the same mapping function, ϕ, is used to transform new, unseen data to be classified using the same linear SVM model. However, one problem with this mapping approach is that the construction of the new features is **computationally very expensive**, especially if we are dealing with high-dimensional data. The **kernel function** is defined as follow:

$$K(x_i, x_j) = \phi(x_i) \cdot \phi(x_j)$$

(24)

One of the most used kernels is the **radial basis function** (RBF), that can simply be called Gaussian Kernel [42].

CHAPTER 5: Materials and Methods

Electromyography is a widely accepted tool capable of providing an essential contribution to the characterization of the neuromuscular system. SEMG is strongly recommended for recording muscle signals during human locomotion because it is not invasive, does not expose patients to discomfort, and it can be easily applied to the patient skin. It is also able to record muscle activity from a significant portion of motor units that are representative of the entire muscle activity during specific tasks. It is proved that sEMG signals and muscle activity vary among different subjects, but a certain degree of variability exists also within the same person. Thus, it is important to analyse the variability associated with muscle activation during free walking to improve the interpretation of muscular signals in physiological and pathological conditions. In fact, the importance of examining the variability of the EMG was underlined to understand the difficulty of correctly analysing and interpreting muscle activity in order to identify the different gait phases through spatial/temporal parameters. [4,7,8].

5.1 Dataset

The present dataset is composed of five sEMG signals recorded from 2011 to 2018 during level-ground walking of 31 young able-bodied subjects (aged between 20 and 30 years) in the Movement Analysis Laboratory at Università Politecnica delle Marche, Ancona, Italy. Underweight, overweight, and obese people (18.5 Kg/m^2 < body mass index (BMI) < 25 Kg/m^2) and subjects affected by any pathological condition, joint pain, or undergone orthopedic surgery are not included in the present dataset. Basographic signals and electrogoniometers were acquired and synchronized with each muscle recordings. The signal acquisition takes about 5 minutes per subject, where the first 5 seconds, approximately, the subjects stand in an orthostatic position before starting to walk. The research was undertaken in compliance with the ethical principles of the Helsinki Declaration and was approved by an institutional expert committee. Participants signed informed consent prior to the beginning of the test [4,7,8].

5.2 Signal Acquisition

Muscular signals are acquired from the following five different muscles per leg: gastrocnemius lateralis (GL), tibialis anterior (TA), rectus femoris (RF), hamstrings (Ham), and vastus lateralis (VL). These signals were detected using single differential probes constituted by Ag/Ag-Cl disks of fixed geometry (manufacturer: Medical Technology, size: 7×27×19 mm; electrode diameter: 4 mm; inter-electrode distance: 8 mm, gain: 1000, high-pass filter: 10 Hz, input impedance > 1.5 GΩ, CMRR >

126 dB, input referred noise ≤ 1 μVrms), and with Ag/Ag-Cl disks of variable geometry (manufacturer: Medical Technology, minimum inter-electrode distance: 12 mm, gain: 1000, high-pass filter: 10 Hz, input impedance > 1.5 GΩ, CMRR > 126 dB, input referred noise ≤ 200 nVrms). After acquisition and amplification, sEMG signals were low pass filtered using analogue filters with a cut-off frequency of 450 Hz, implemented by the recording system [4] (***Figure 5. 1***).

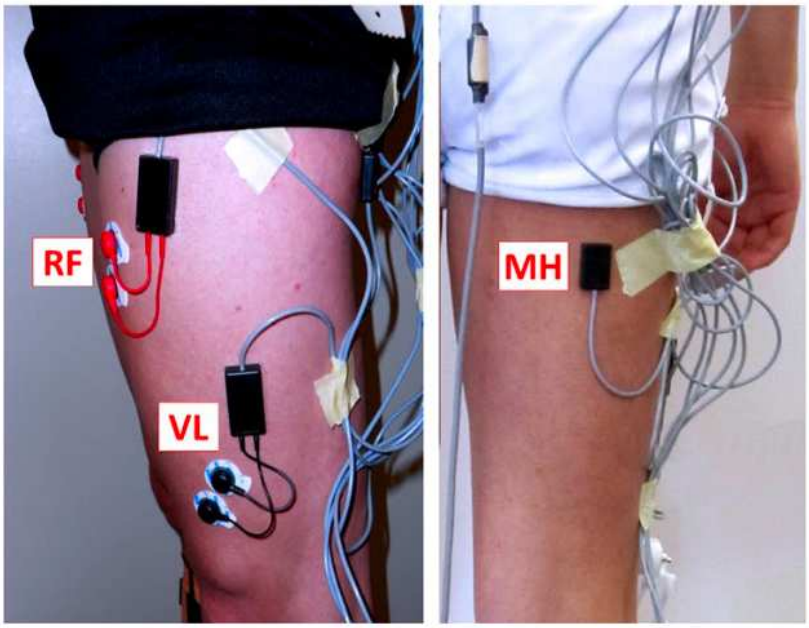

Figure 5. 1 *Five sEMG probes are applied over rectus femoris (RF), vastus lateralis (VL), medial hamstrings (MH) tibialis anterior (TA), and gastrocnemius lateralis (GL).*

Synchronized footswitch and electrogoniometric data are provided in order to achieve a spatial/temporal characterization of the corresponding sEMG signals. All signals are acquired with a sampling frequency of 2000 Hz and a digital resolution of 12 bit using a multichannel recording system Step32 developed by Medical Technology (Version PCI-32 ch2.0.1. DV, Italy). The basographic sensor consists of a rectangular membrane switch, with a size of (11×11×0.5) mm and an activation force of 3 N, placed at the end of a strip of flexible and insulating plastic material. On the opposite side there is a connector, necessary for connection to the preamplifier/decoder. The data, corresponding to each repetitive foot-floor contact during the walking of the subjects, are collected by basographic sensors. The footswitches are attached in 3 independent anatomical area under the feet of the subjects: the first switch sensor is applied under the heel (T), and the other two under the first (M) and the fifth (L) metatarsal heads and are connected through a wire to a computer [4,7,8] (***Figure 5. 2***).

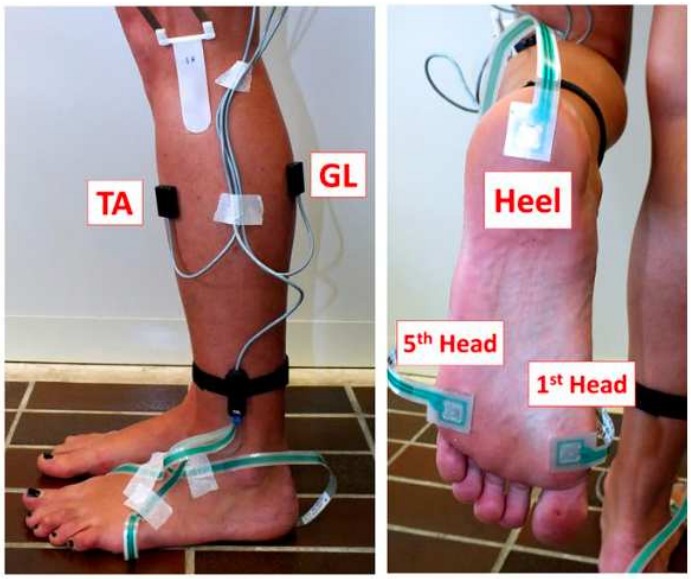

Figure 5. 2 *Footswitches are attached under the heel, the first (1st Head) and the fifth (5th Head) metatarsal heads.*

In the first experiment, the gait is simply divided in *stance* and *swing* phase. The stance phase is identified when at least one of the three footswitches placed under the foot is closed, while swing is uniquely identified when all the switches are open. For the second experiment, the sequence of gait was periodically divided into four sub-phases (Initial Stance, Mid Stance, Terminal Stance and Swing phase) according to the study of Luo et al. [9] (Initial Stance is assumed to be the Initial Stance phase identified by Luo et al.) and adapted to the current acquisition. The Initial Stance phase (PS) occurs when only the footswitch under the heel is closed. The Mid Stance phase (MS) occurs when the footswitch below the heel is closed, and at least one of the footswitches under the forefoot is also closed. The Mid Stance correspond, essentially, to the phase where the foot is completely in contact with the ground. The Terminal Stance phase (TS) occurs when the footswitch under the heel is open, and at least one of the footswitches under one of the two metatarsal head is closed. The Swing phase (S) occurs, finally, when all the footswitches are open (***Figure 5. 3***).

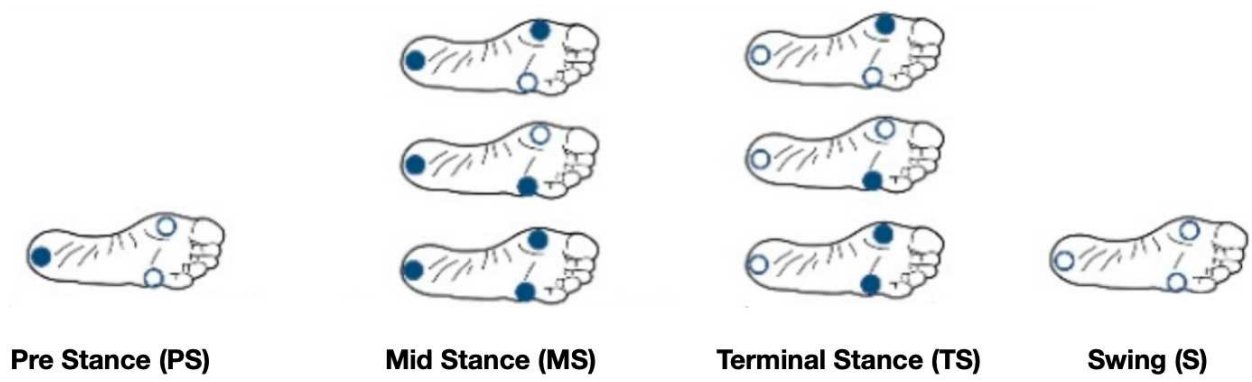

Figure 5. 3 *Gait phases identification through footswitches activation*

An electrogoniometer (accuracy: 0.5°) were attached to the lateral side of each lower limb to measure knee joint angles in the sagittal plane. All signals were collected while a subject walked barefoot at a self-selected comfortable pace following an eight-shaped path in the Motion Analysis Lab (Università Politecnica delle Marche, Ancona, Italy), for about 5 min. The path involves a natural deceleration, near the curve, and after the curve is overcome a natural acceleration along a linear path, until the next turn [4,7,8] (***Figure 5. 4***).

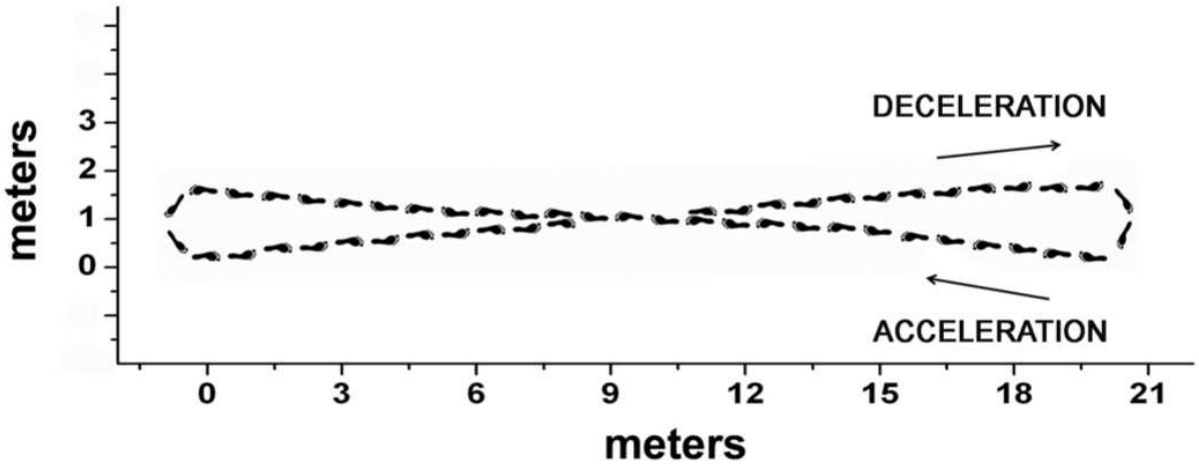

Figure 5. 4 *Schematic drawing of the eight-shaped path used in our experiments.*

5.3 Signal Pre-processing

First thing first, the basographic signals collected by the foot switches applied under the left foot were processed to identify the main gait sub-phases. The raw basographic signal $(baso_{left})$ is converted into an 8-level signal by computing the range as follow:

$$Range(V) = max(baso_{left}) - min(baso_{left}) \quad (25)$$

And dividing it by 8:

$$lsb = Range(V)/8 \quad (26)$$

The value of lsb defines the width of each of the eight intervals into which the raw signal has been divided. In ***Figure 5. 5*** is reported an example of 8-level division of the raw basographic signal.

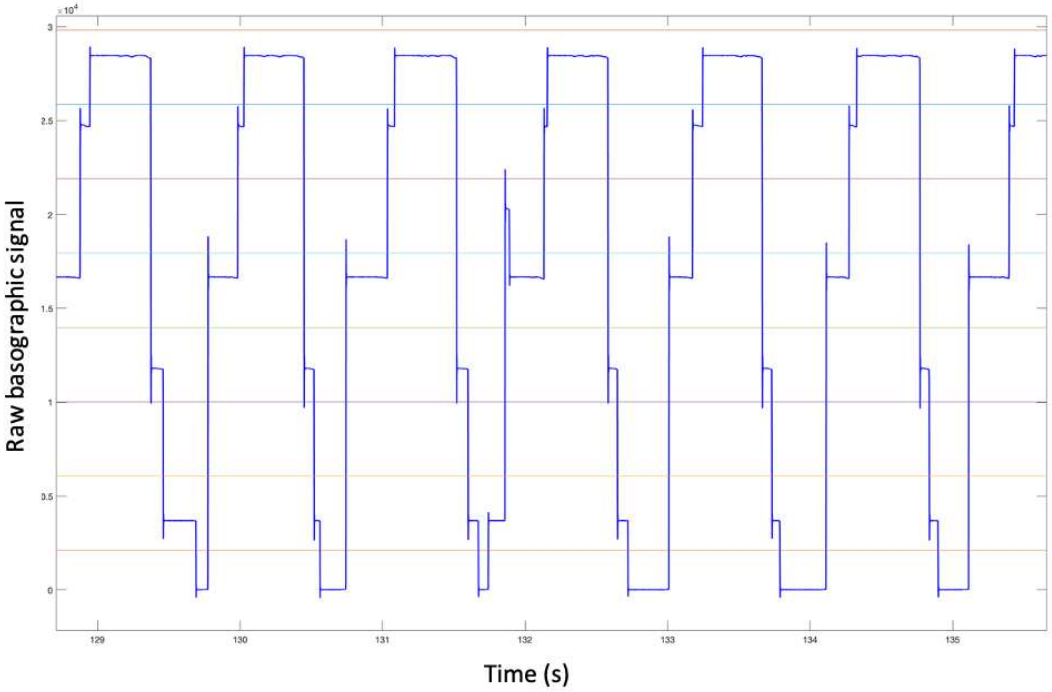

Figure 5. 5 *Raw basographic signal with the 8-quantization level*

Considering the first experiment that aims to classify 4 gait sub-phases, the basographic signal has been divided and coded into the 4 classes (Initial Stance, Mid Stance, Terminal Stance and Swing) according to which of the eight intervals the value of each sample of the raw basographic signal belongs to. If the sample of the raw basographic signal falls below the third level, the signal takes the value 0 and is coded as belonging to the mid stance phase. If, on the other hand, the sample falls between the third and fourth level, then it is coded with the value 1 and belongs to the Initial Stance phase, while if the sample is between the fourth and seventh level, the assigned code will be 2 and will belong to the terminal stance phase. Finally, if the sample has a higher value above level 7, the phase will be identified as swing and will be coded with the value 3. In ***Table 5. 1*** is reported encoding scheme followed in this study.

Table 5. 1 *Correspondence between classes and the 4 gait sub-phase*

Class 0	**Class 1**	**Class 2**	**Class 3**
Mid Stance	*Initial Stance*	*Terminal Stance*	*Swing*

The same procedure was adopted for the segmentation in stance and swing phase for the second experiment. If the sample of the raw basographic signal falls below the seventh level, the signal takes

the value 0 and is coded as belonging to the stance phase, otherwise it is coded with the value 1 and belongs to the swing phase (***Table 5. 2***).

Table 5. 2 *Correspondence between classes and the 2 gait sub-phase*

Class 0	Class 1
Stance	*Swing*

Results of the 4-phases and 2-phases segmentation of the basographici signal are reported in the following figure (***Figure 5. 6***).

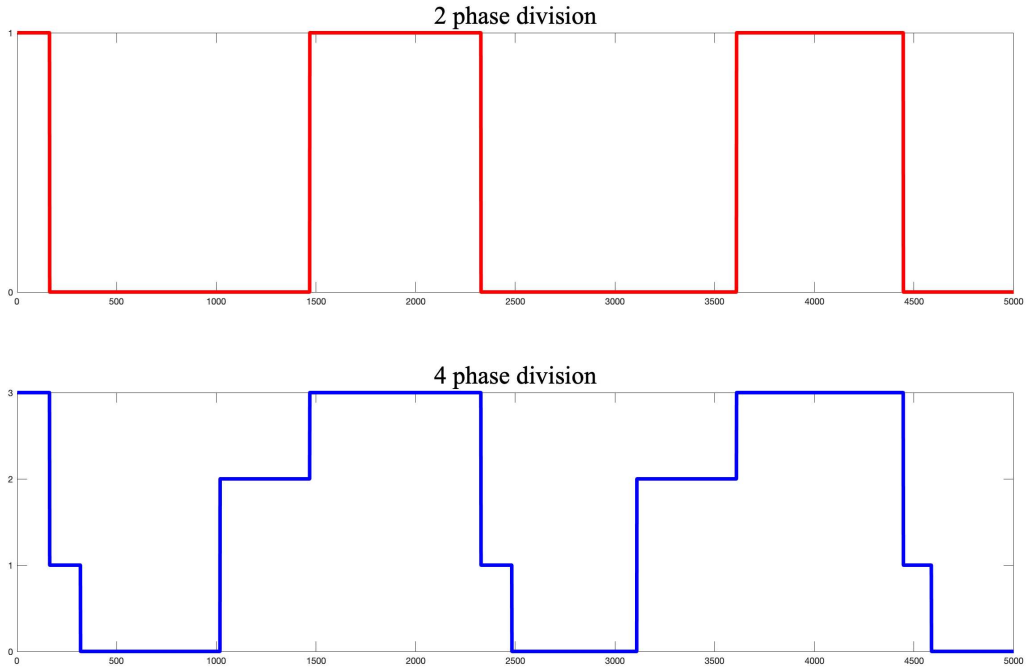

Figure 5. 6 *Division of the basographic signal in 4 (upper figure) and 2 phases (bottom figure).*

The information derived from the basographic signals were used as ground truth for training the neural network. sEMG signals were pre-processed before being provided as input to the supervised learning models to predict gait phases. After the acquisition, sEMG signals of each subjects have an amplitude ranging from 0 to 10 mV and a frequency content between 0 and 500 Hz. Pre-processing steps were applied to remove both motion artifacts and high frequency noise from each muscle signal by applying a low-pass finite impulse response (FIR) digital filter with a cut-off frequency of 450 Hz and a high-pass FIR digital filter with a cut-off frequency of 20 Hz, respectively. Zero-phase digital

filtering was performed to avoid phase shift (***Figure 5. 7***) [4-8]. Signal filtering were implemented using MATLAB_R2020b®.

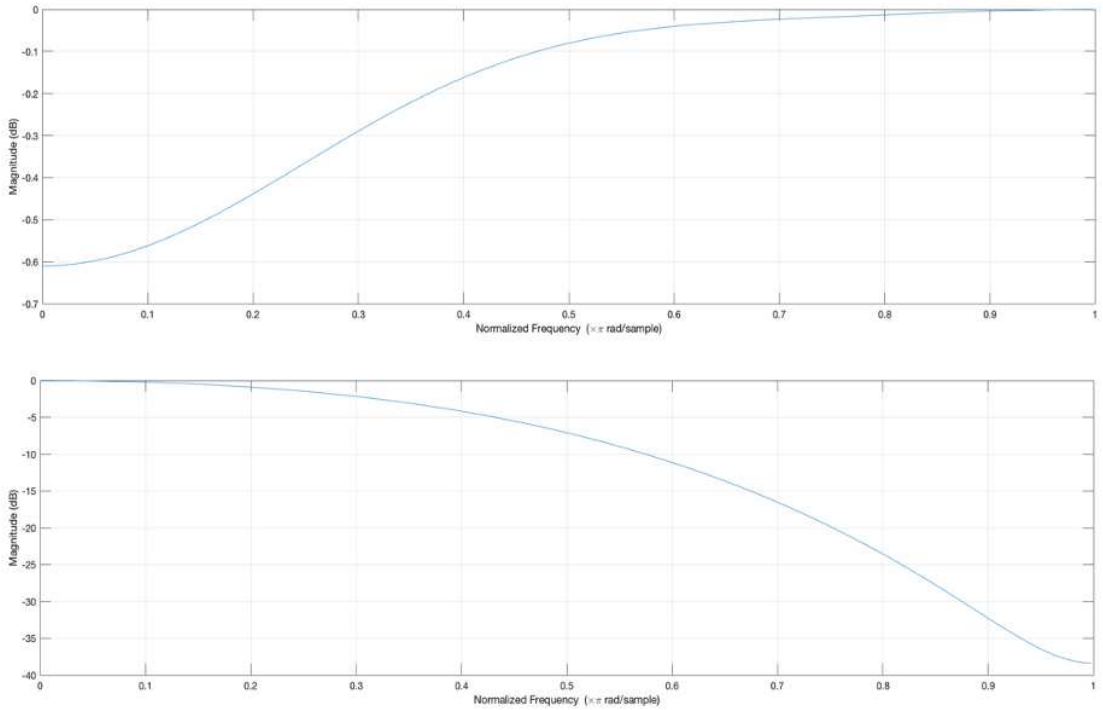

Figure 5. 7 *High-pass FIR digital filter with a cut-off frequency of 20 Hz (top); Low-pass FIR digital filter with a cut-off frequency of 450 Hz (bottom)*

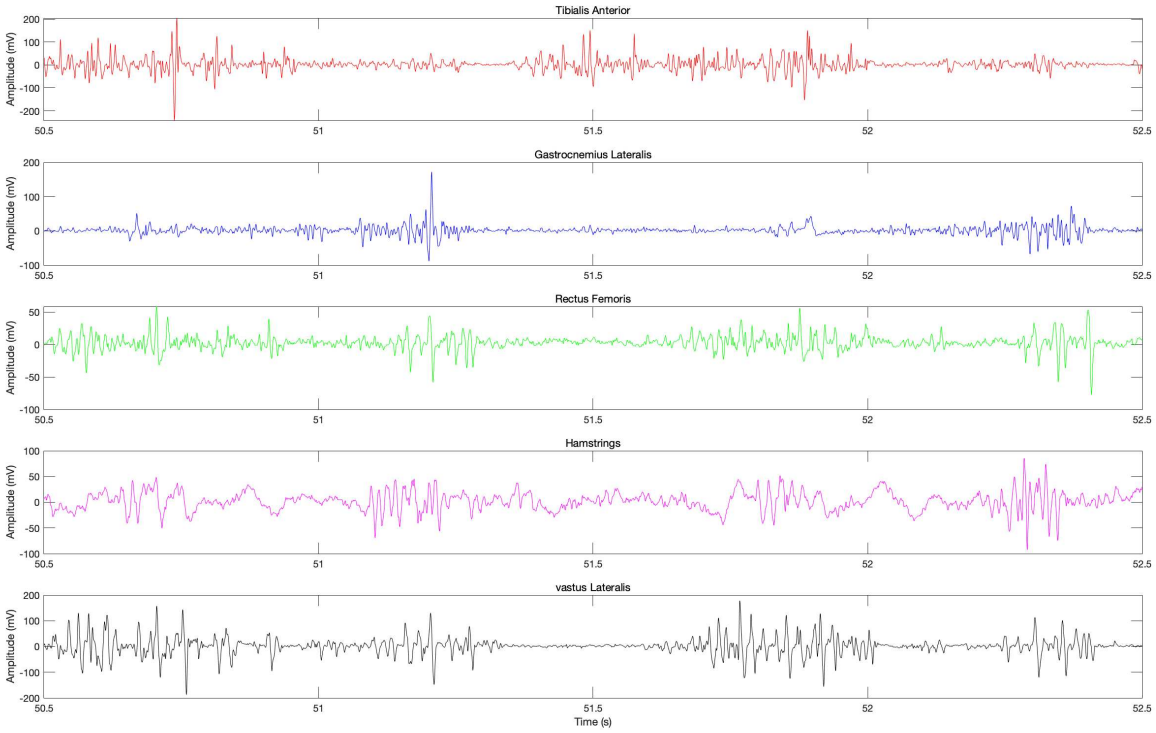

Figure 5. 8 *Filtered sEMG signals*

After filtering, all the signals were truncated to eliminate the initial part of the acquisition in which the subject remains in an orthostatic position before starting to walk along the predetermined path (***Figure 5. 9 upper***). The truncation preserved the first muscle activations as the subject begins to walk. The final part of each signal was eliminated, corresponding to the final part of the path during which the subject stops (***Figure 5. 9 bottom***).

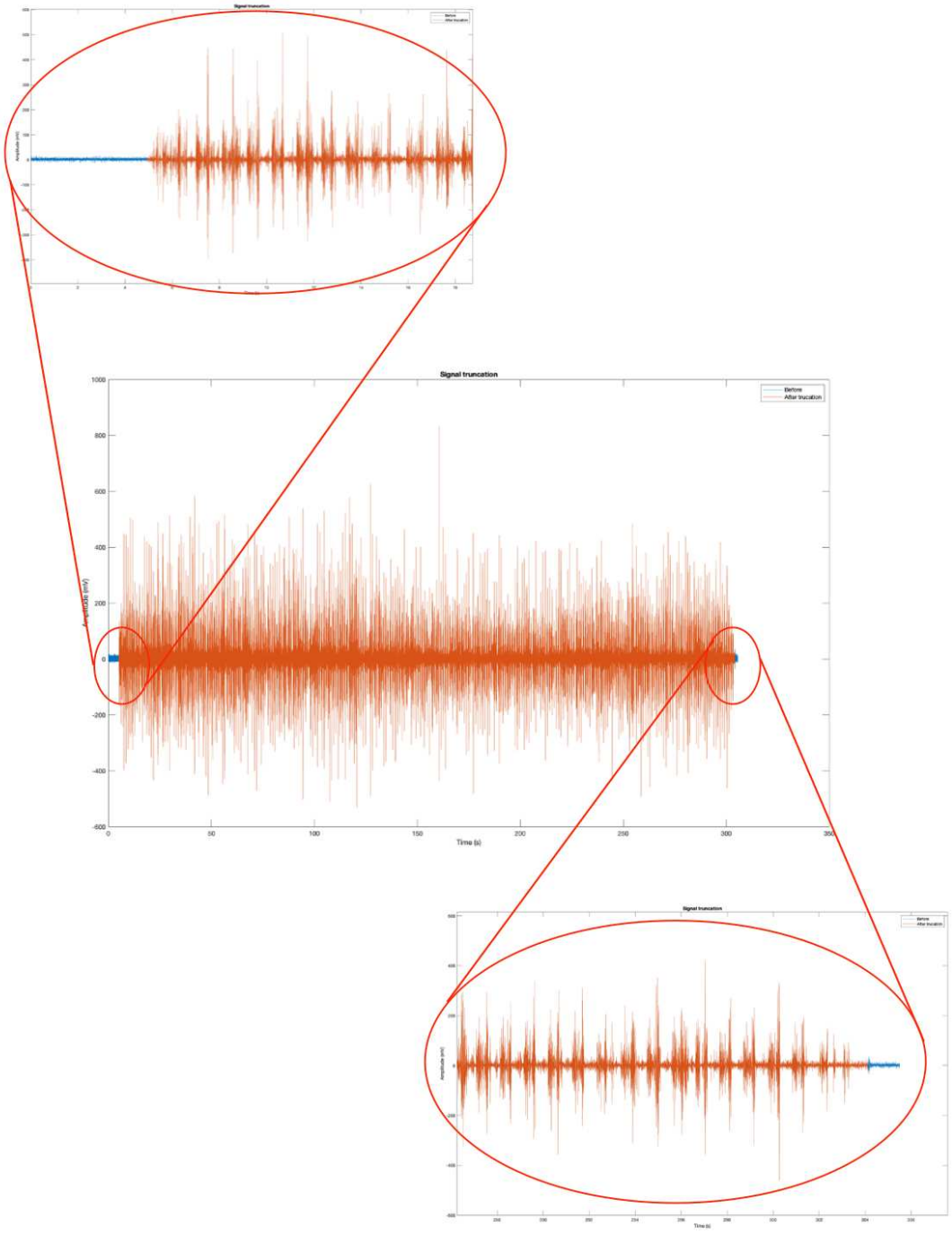

Figure 5. 9 *Signal truncation: truncated signal of the tibialis anterior in orange overleaped with the original signal in blue. Upper: initial signal truncation. Bottom: final signal truncation.*

For all sEMG signals of each subject the RMSS was extracted using sliding widows of 500 samples[8,14]. One sample of the RMSS contains redundant information of the subsequent 500 samples of the corresponding original sEMG signal.

$$RMSS = \sqrt{\frac{1}{N}\sum_{k=1}^{N}|x_k{}^2|}$$

(27)

The resulting signal length will have 500 samples shorter than the original truncated signal.
Finally, the RMSS signal was processed to compute the WSD signal proposed by Ziegler et al. [14], to prepare the vectors to train the multilayer perceptron neural network and the support vector machine classifier. First, given the RMSS muscle activities $a_{i,k}$ with $i = 1, \ldots, m$ and $k \in \{1, 2\}$, where i denotes the i^{th} muscle and k the k^{th} leg, the activation difference δ_i between the corresponding muscles of the two legs is calculated in the following way:

$$\delta_i = a_{i,1} - a_{i,2}$$

(28)

Using the maximum of the two activation values per muscle pair, $\widehat{a_\iota}$, the activity difference value is then normalized, resulting in:

$$\widehat{x_\iota} = \frac{\delta_i}{\widehat{a_\iota}} \qquad with \qquad \widehat{a_\iota} = \max_k a_{i,k}$$

(29)

x_i delivers values ranging from −1 to 1 even if none of the two corresponding muscles is contracting. Therefore, a weighting factor w_i based on a threshold value β>0 is defined, damping signals where both muscles show low activity. In this work β was set to 0.1.

$$w_i = \left|\tanh\left(\frac{\widehat{a_\iota}}{\beta}\right)\right|$$

(30)

In a final step and for every muscle pair, $\widehat{x_i}$ is weighted with this factor yielding the WSD feature x_i Ziegler et al. [14]. An example of the final WSD signal is reported in ***Figure 5. 10***.

$$x_i = \widehat{x_i} w_i \tag{31}$$

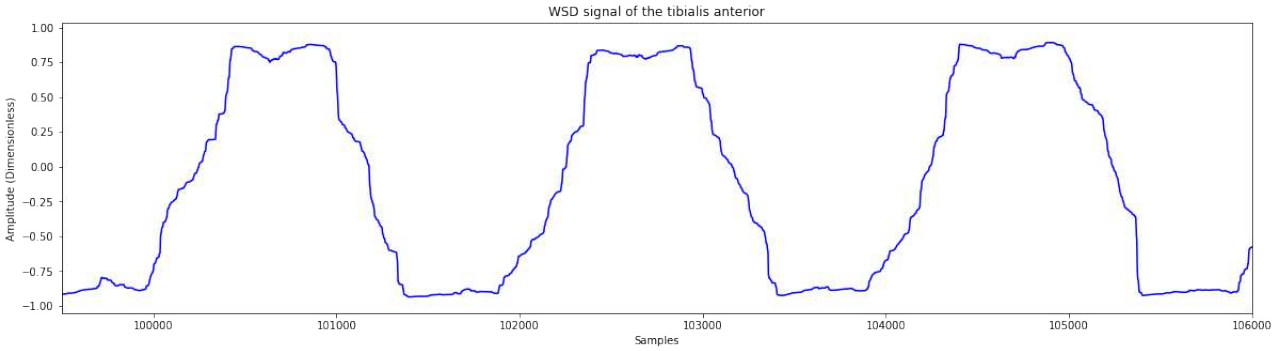

Figure 5. 10 *Weighted Signal difference (WSD) of the tibialis anterior*

5.4 Data Preparation

The five WSD signal extracted for each subject is used to train the support vector machine and multilayer perceptron models used in the proposed experiments to classify gait sub-phases and transition events between consecutive phases. The intra-subject approach is adopted in the present study because it was confirmed, by previous studies, that it better performs with respect to the inter-subject, leading to better performance in gait classification [7].

	WSD1	WSD2	WSD3	WSD4	WSD5
0	0.431174	-0.472111	0.462878	-0.059022	-0.599433
1	0.429603	-0.472506	0.469401	-0.057866	-0.595803
2	0.428738	-0.471746	0.474481	-0.058398	-0.592744
3	0.427975	-0.468751	0.477500	-0.059193	-0.590355
4	0.427663	-0.463990	0.479073	-0.059457	-0.588455
...	...	...	...	...	...
597837	-0.899537	-0.397224	0.541623	-0.668116	-0.716660

597838 rows × 5 columns

Figure 5. 11 *Initial Pandas Data Frame of the 5 WSD signal used to train and test the classifiers. WSD1 is the weighted signal difference of the tibialis anterior, WSD2 of the gastrocnemius lateralis, WSD3 of the rectus femoris, WSD4 of the hamstrings and WSD5 of the vastus lateralis.*

The WSD signals computed for each couple of muscle per leg are arranged in a (N x 5) data frame (N = number of samples of the signal, 5 signals) using Pandas library in Python (***Figure 5. 11***). The data frame is converted into a Numpy matrix in order to provide to the machine learning algorithm the requested input format. The entire dataset for each subject is split into a training set (80%) and a testing set (20%). The process is then repeated, each time changing the testing set to cover the entire dataset. A 5-fold cross validation strategy was performed and the initial dataset, is divided into 5 smaller datasets, 4 of which (80%) were used to train the model (learning samples) and the remaining fold (20%) to test it (unseen samples). At each of the five iteration the fold used to test the classifier is different (***Figure 5. 12***). The procedure was repeated for each of the 31 subject included in the study.

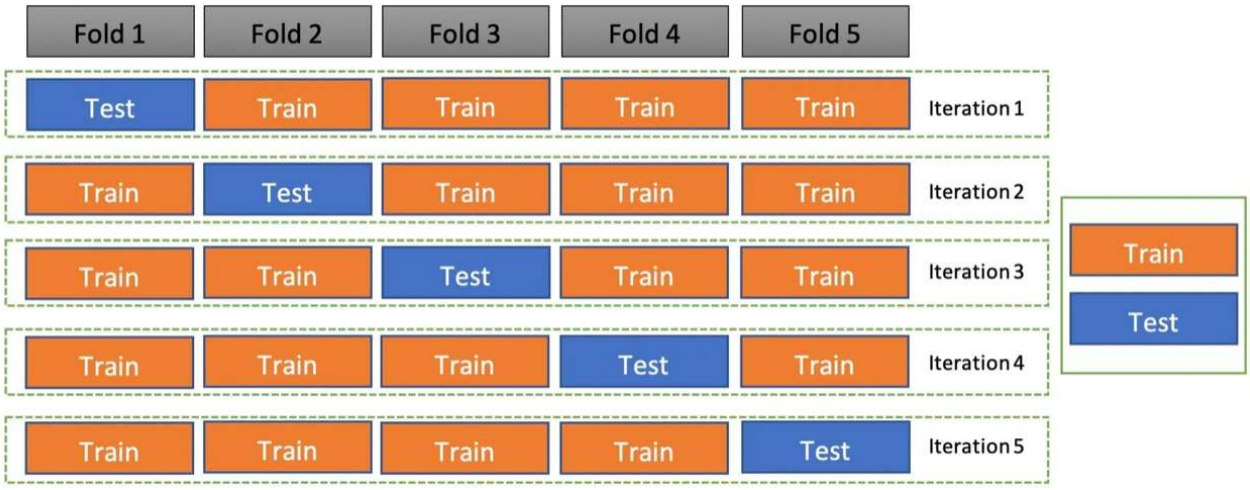

Figure 5. 12 *5-fold cross validation computed to train and test the classifier.*

Each row of the training dataset was used to iteratively train the classifier. Each of the 5 input vectors was provided to the classifier, sample-by-sample, with the corresponding label. The basographic signal was used as ground truth signal to form the label vector. Label vectors contain the values of the basogrphic signal, which was previously encoded using 4 different classes (class = 0 → Mid Stance, class = 1 → Initial Stance, class = 2 → Terminal Stance and class = 3 → Stance) for the 4-phases classification experiment and the 2 classes (class = 0 → Stance and class = 1 → Swing) for the 2-phases classification experiment, corresponding to each sample of each WSD signal. In the 4 phases classification using MLP, the categorical features digit with the value k ranges between 0 and 3, in which 0 represents Mid Stance phase, 1 the Initial Stance phase, 2 the Terminal Stance phase and 3 the Swing phase, were encoded into a binary vector with 4 positions, which always has 0 value,

except the k^{th} position where a 1 is assigned. This type of representation is called one-hot encoding and it is recommended for use with MLP implemented with Keras library in python.

5.5 Sub-phases Classification

The first experiment performed in this study consists in the 2 phases classification using both a MLP neural network and a SVM classifier. The two approaches are used to classify the 2 main gait phases, stance and swing. The results obtained from the 2 phases classification were compared with other methods already present in literature [4,7-9] using the same data preparation proposed by Ziegler et al. [14] in order to validate the two methods. Moreover, three new machine learning architecture are proposed which consists of two cascaded classifiers. The first classifier makes a prediction of the two main gait phases, stance and swing. Instead, the second classifier is trained only on WSD signal samples labeled as stance samples from the output of the first classifier. Before training the second classifier a suitable post-processing algorithm is applied to the output signal samples, in order to remove the non-physiological phases erroneously predicted by the binary model. The output of this model therefore provides a further prediction of the 3 stance sub-phases. The output of the two models is subsequently concatenated, considering the swing phase out of the first classifier and the three stance sub-phases out of the second. A first architecture consists of two cascaded MLP, a second is formed by a SVM for the binary classification and a MLP for the classification of the 3 stance sub-phases. A third model is also defined, composed by two cascaded SVM classifiers. The final prediction of these novel architectures provides a 4 phases classification of gait. Thus, two machine learning models, another SVM and MLP, for a 4 phases classification are proposed in order to test the performance of the cascaded models in predicting multiple gait events.

5.5.1 First Experiment: 2-phases Classification

The first machine learning model employed in the present study is a support vector machine. It was implemented using scikit-learn library in python. The SVM algorithm in scikit-learn requires two main parameters, C and γ, that represent respectively a regularization parameter (the strength of the regularization is inversely proportional to C and must be strictly positive) and the kernel coefficient. The kernel used in the experiment was the RBF kernel and the two parameters are set according to the study of Ziegler et al [14]. Ziegler et al. proposed a parameter tuning during the training phase of the SVM classifier to find the best pair of C and γ values that allows to reach the best prediction accuracy while using the same subject to train and test the classifier. The same couple of values are subsequently used to predict also unseen sample from other subjects. The couple of values for the two parameters ($C = 25.902$ and $\gamma = 0.018$) reaches the best accuracy of 94.04% when different

datasets are used to train and test the classifier. The aforementioned pair of values for the two parameters to be supplied to the SVM classifier has been shown to be the one able to better generalize and provide better accuracy between different subjects. Since in the proposed intra-subject experiment no parameter tuning was performed, the same set of parameters C and γ are used in order to reach the best prediction accuracy among all the subjects. The entire training dataset, together with the corresponding label vector, is provided repeatedly (for each cross-validation iteration) to the algorithm to train the classifier and define the hyperplane in the 5-dimensional space (input space dimension) that distinctly classifies the data points, maximizing the margins between different classes [42]. The algorithm was defined and trained in python by means of the SVM library function in scikit-learn. After training, the defined model is used to predict classes of the test samples. The function takes as input the entire test set (every iteration) and returns prediction for each sample of the feature vector. The function provides as output a vector of predictions with the same length of the test set. The predicted output of the SVM model is corrected using an appropriate post-processing algorithm in order to eliminate any non-physiological phase transitions (gait phases that are too long or too short). The final prediction is a signal corresponding to the predicted basographic signal (***Figure 5. 13***).

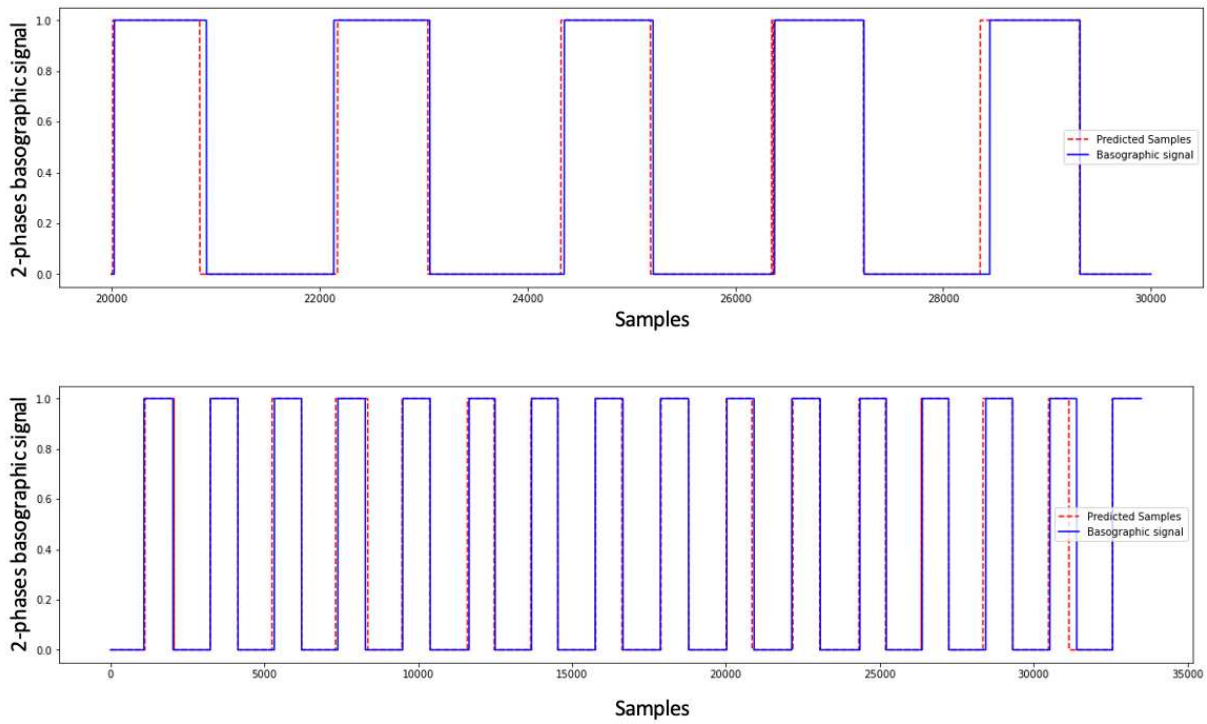

Figure 5. 13 *Example of the predictions of the MLP neural network for the last fold of the subject 22 in the study. The blue line is the basographic signal (labels) and the red dotted line is the vector of predictions.*

The second model adopted is a simple MLP neural architecture. The net is composed by 5 input neurons corresponding to the 5 WSD feature vectors provided as input, and a single hidden layer formed by 32 hidden units. The described architecture was demonstrated to be the best performing for the intra-subject approach [5]. The number of output neurons corresponds to the number of output classes (2 classes: Stance and Swing) that the net should predict from the WSD data. Keras libraries were used to define, compile and train the net for the classification of the 2 gait sub-phases. The ReLU activation function is defined between input and hidden layer, while the Sigmoid function is used between hidden and output layer. The Sigmoid function is used to reduce the k-dimensional vector of arbitrary values into a k-dimensional vector of real values in a range between 0 and 1. It collects the output returned from each unit in the previous hidden layer in 2 output neurons corresponding to the 2 gait sub-phases. The layout of the MLP architecture is shown in ***Figure 5. 14***.

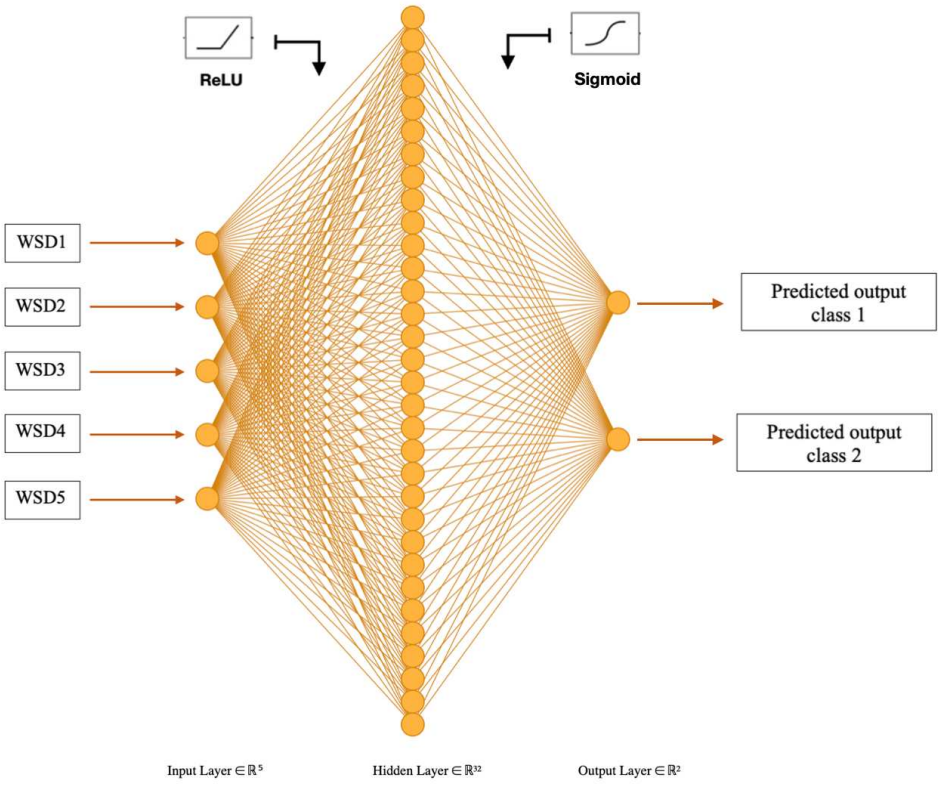

Figure 5. 14 MLP architecture for the 4-phases classification.

The compilation is the final step in creating a model and it configures it for training. The Neural network is compiled using keras API. Three additional functions are defined: loss function, optimizer and metrics. The loss function is used to compute the error between the actual output and the predicted output measuring the performance of the net in modelling training data. Weights and biases are adjusted in order to minimize the loss between target and output values. The **categorical cross entropy** function is generally used in multi-class classification problems, and also adopted for the

present model. In the present experiment the categorical cross entropy reduces to a simple binary cross entropy function. The optimizer algorithm finds the value of the parameters (weights) that minimize the loss function when mapping inputs to outputs. These optimization algorithms widely affect the accuracy of the model. The optimizer function defined for the model is **Adam**. Finally, **accuracy** is the metric function used to measure model performance. It is defined as the ratio of the correct predictions of the neural network to the total number of predictions. It is expressed as:

$$Accuracy = \frac{Number\ of\ correct\ predictions}{Total\ number\ of\ predictions} \tag{32}$$

Once the model is compiled, the MLP neural network is trained using the corresponding training data defined by the 5-fold cross validation strategy. Before training the net, other two hyperparameters must be defined: **batch size** and **epochs**. The batch size is a hyperparameter that defines the number of samples processed before updating the model parameters. At the end of each batch, the predictions are compared with output variables and the error is computed. The error is used by is used to improve the model accuracy. The training dataset can be divided into one or more batches. The number of epochs, instead, is a hyperparameter that defines the number times that the learning algorithm will process the entire training samples. An epoch is comprised of one or more batches. Batch size and epochs are set to 32 and 20, respectively. After the training process, weights and biases are defined and the model can be used to make predictions on previously unseen data samples.

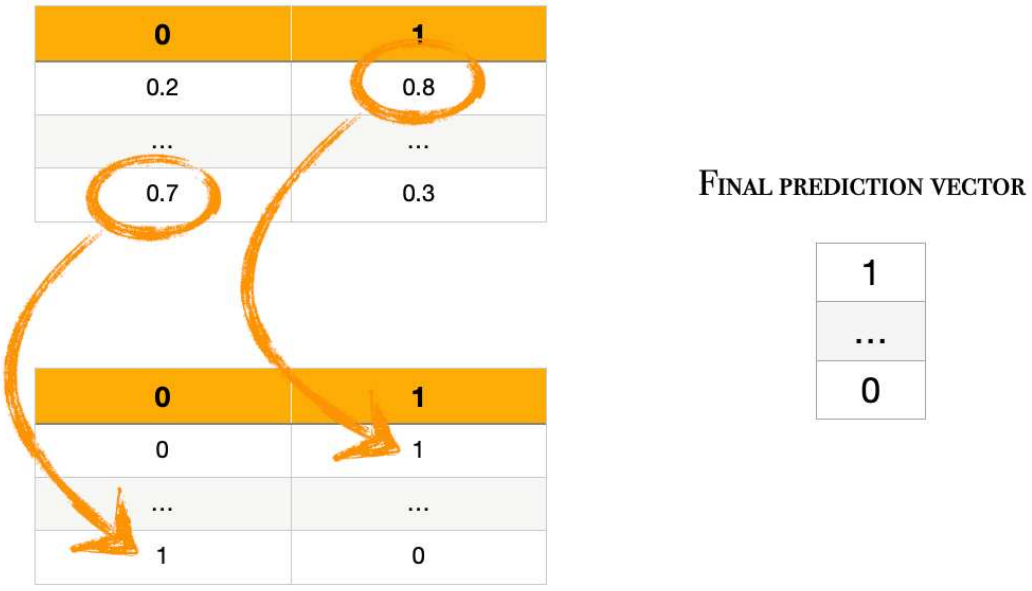

Figure 5. 15 *An example explaining the conversion of the prediction matrix into a categorical vector to obtain the final prediction vector that identifies the 2 gait sub-phase.*

The final output is a matrix of prediction with the same length of the label vector, corresponding to the output of the Sigmoid function. With the binary classification problem, the Sigmoid function return a value between 0 and 1 for each class. A prediction is a vector with 2 elements corresponding to each gait sub-phases (stance or swing). The element with the highest value is chosen as prediction and the label 1 is assigned, the other digit, in the remaining column, is set to 0. Then, in each raw of the prediction matrix, the positions of the label 1 were used to build a categorical vector assigning, based on the position of the label 1, either the value 0 or 1, corresponding to Stance and Swing phases, respectively. The same post-processing algorithm used for the binary SVM is used to correct non-physiological phases. An example is reported in ***Figure 5. 15***.

5.5.2 A Novel Multi-Classifier Architecture for Gait Identification

A novel multi-classifier architecture is proposed in the present study based on the considerations highlighted by the results obtained for the 2 and 4-phases classifications of the previous two experiments. The results obtained from the binary classification demonstrate a good ability of the two models to classify stance and swing phases and the relative transition events. The main problem of the 4-phases classifier is the poor accuracy of the models in predicting the Initial Stance phases, due to their very short duration. This problem also affects the ability to identify HS and CTO transition events. The idea behind this novel approach consists in exploiting the performance of the binary classifiers to predict the swing phases, with the corresponding gait events (HS and TO), and to build a second classifier to predict only stance sub-phases. The final prediction is reconstructed considering the swing samples coming out of the first binary model and implementing a second classifier, in cascade, which further subdivides the stance phases into its three sub-phases (Initial Stance, Mid Stance and Terminal Stance). A 5-fold cross validation strategy is adopted to validate the model performance. The entire dataset is iteratively divided into training and test sets and the WSD feature vectors belonging to the training dataset are provided to the first binary classifier. The predicted output is a vector with the same number of samples as the input vectors consisting of a series of 0 (stance) and 1 (swing) values. Subsequently, the WSD samples corresponding to the stance samples, predicted by the first model, are used to train the second classifier. Before training the second classifier, a suitable post-processing algorithm is used to eliminate non-physiological phases obtained from the prediction of the first binary model, in order to provide more reliable input data to the second model. Finally, the results of the two models are chronologically concatenated in order to reconstruct the final prediction. The first architecture consists in two cascaded MLP neural networks: the first binary MLP net is the same used in the second experiment, while the second MLP, for the classification of the stance phase, has the same architecture with the exception that the number of

output neurons correspond to the number of the 3 stance sub-phases. This architecture is referred to as MLP-MLP. Functions and hyperparameters used are the same defined in the experiment. The one-hot encoded representation of the 2-level basographic signal is used to label each sample the WSD vector used to feed the binary MLP classifier. The results of the first classifier are transformed in a categorical vector using the same algorithm described in ***Figure 5. 16***. Stance samples are then used to train the second MLP net to classify Initial Stance, Mid Stance and Terminal Stance phases. The one-hot encoded representation of the 4-level basographic signal is exploited to label each WSD samples. The final prediction vector is transformed again in a categorical vector. Finally, swing and stance sub-phases predictions are concatenated in chronological order to reconstruct the predicted gait sub-phases. In ***Figure 5. 16*** is reported a schematic representation of the first architecture.

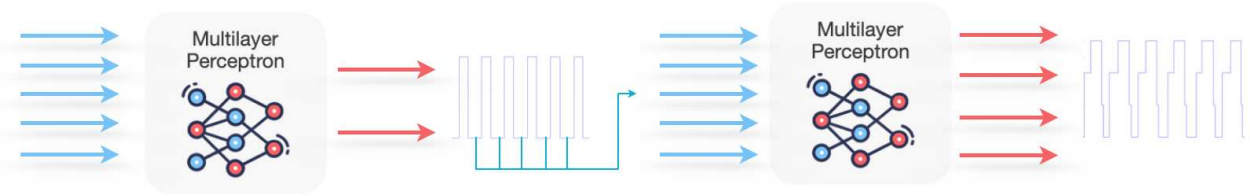

Figure 5. 16 *Schematic representation of the two cascaded MLP neural network proposed in the first architecture (MLP-MLP)..*

The second architecture is formed by a binary SVM classifier (kernel = 'RBF', $C = 25.902$ and $\gamma = 0.018$) and the same MLP classifier for the three stance sub-phases used in the previously defined approach. This architecture is referred to as SVM-MLP. The binary SVM model have slightly higher values of F1 score with respect to the binary MLP, resulting in higher number of true positive transition events detected. For this reason, the SVM classifier is used in the second approach to classify the 2 main gait phases. For the SVM model the hot-encoded representation of the 2-level basographic signal is not necessary and the resulting prediction vector is already formed by a sequence of 0 and 1 values. The same MLP neural network is then defined to classify the 3 stance sub-phases. In ***Figure 5. 17*** is represented the second architecture.

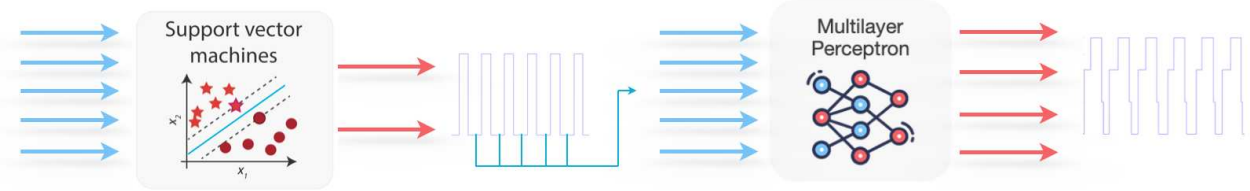

Figure 5. 17 *Schematic representation of second architecture formed by a SVM binary classifier and a MLP neural net (SVM-MLP).*

Furthermore, the ability to correctly predict all the 4 gait events is slightly higher for the SVM with respect to the MLP neural network. Thus, for completeness of the study, also a third architecture defined by two cascaded SVM classifiers, defined using the same set of parameters, are proposed to classify swing and the 3 stance sub-phases, respectively (***Figure 5. 18***). This architecture is referred to as SVM-SVM.

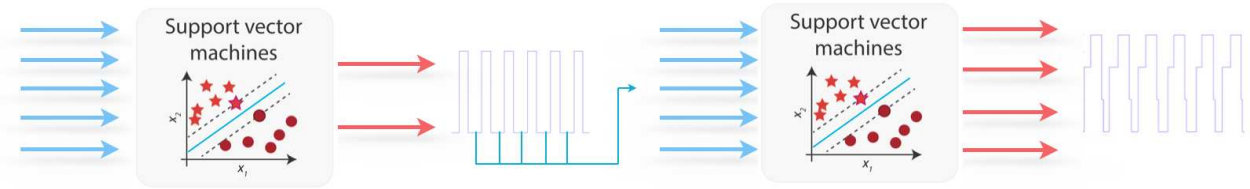

Figure 5. 18 *Schematic representation of the two cascaded SVM neural network proposed in the third architecture (SVM-SVM).*

To our knowledge, the machine learning architectures mentioned in the previous paragraph constitute a completely new approach not yet present in the literature. For this reason, these models have to be validated by comparing them with widely used methods for the identification of the different gait sub-phases and which generally represent the current state of the art. Two simple SVM and MLP models have been implemented, using the same parameters and functions used for the binary classification, which allow direct comparison, in terms of performance, with the proposed models. The classification accuracy for each class (and overall accuracy), as well as the performance achieved by the classifiers in identifying transition states, are assessed and compared to validate the models.

5.5.3 Performance evaluation

The 4-phases classification is used to validate and test the performances of the architectures proposed in this study. The SVM classifier is configured, as previously explained, using the same kernel function (RBF) and the same set of C and γ parameters ($C = 25.902$ and $\gamma = 0.018$). The model is trained using the 4-level basographic signal as label vector and the same 5-fold cross validation strategy. The prediction vector obtained from the algorithm has the same length of the corresponding test fold. Each value in this vector corresponds to the specific gait sub-phase: Initial Stance, Mid Stance, Terminal Stance and Swing. The MLP for the 4-phases classification has the same set of functions and hyperparameters used in the previous experiment, with the exception of the Softmax activation function employed between hidden and output layers, in place of the Sigmoid function. The loss function categorical cross entropy squeezes the k-dimensional vector of arbitrary values into a k-dimensional vector of real values in the probabilistic range (0,1). It collects the output returned from each unit in the previous hidden layer in 4 output neurons corresponding to the gait sub-phases. The neural network has one single hidden layer with 32 units. The number of input neurons is equal

to the number of WSD feature vector and the number of output neurons increases to 4. A schematic representation of the 4 phases MLP classifier is reported in ***Figure 5. 19***.

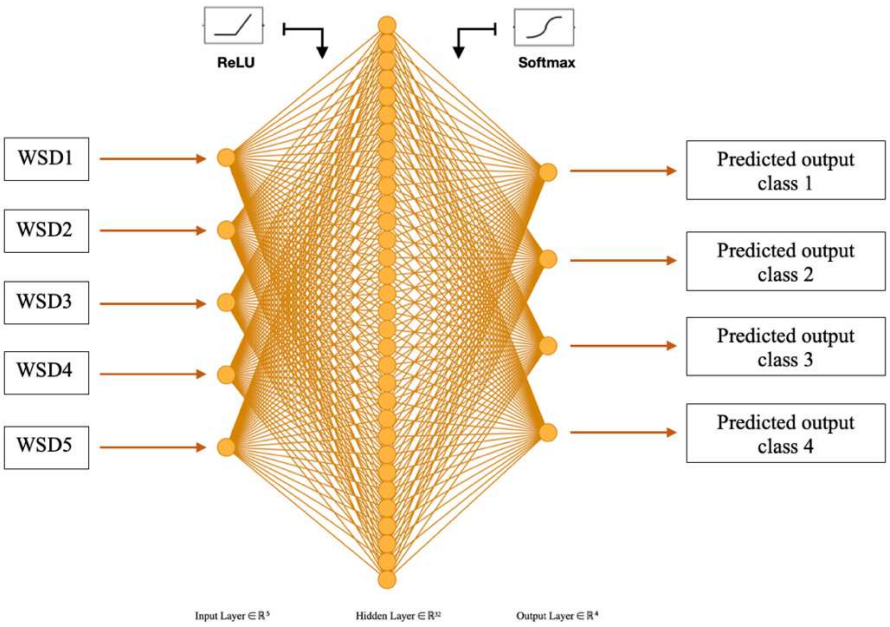

Figure 5. 19 *MLP architecture for the 4-phases classification.*

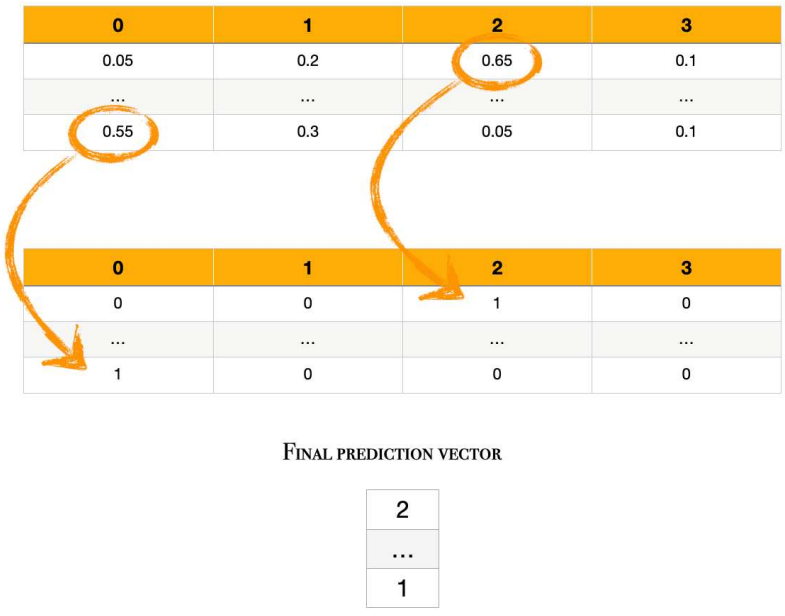

Figure 5. 20 *An example explaining the conversion of the prediction matrix into a categorical vector to obtain the final prediction vector that identifies each gait sub-phase class.*

Once the two models are trained, predictions are obtained by supplying the algorithm with each test fold defined by the cross-validation strategy. The final output of the MLP model, as in the 2-phase case, must be traced back to a categorical vector considering the position of the element with label 1

in the output prediction matrix, as explained in the ***Figure 5. 20***. In the case of SVM, on the other hand, the final vector of the predictions is already a categorical vector in which each value identifies the 4 phases (class 0 = Initial Stance, class 1 = Mid Stance, class 2 = Terminal Stance, class 3 = swing). In ***Figure 5. 21*** is reported an example of the predictions obtained from the SVM algorithm.

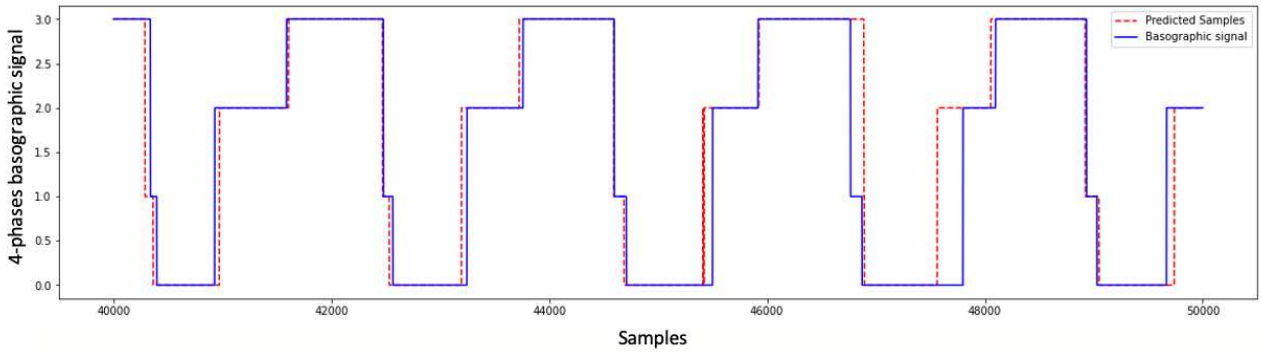

Figure 5. 21 *Predicted samples from the SVM for the 4-phases classification of the last fold of the subject 1. The blue line is the basographic signal (labels) and the red dotted line is the vector of predictions.*

5.6 Transition Events Detection

The prediction output of the two supervised learning architectures, in both experiments, are chronologically arranged and can be compared with the basographic signal assumed as ground truth. The overall prediction accuracy and class accuracies are computed in order to evaluate the goodness of the model in predicting gait sub-phases. Nevertheless, these measures have one major limitation because if the errors are concentrated near the point of transitions, unsatisfactory results will be obtained in terms of the error of the time prediction of gait transition events. Thus, an algorithm is proposed to detect the transitions between gait phases, for both basographic signal and prediction, in the 4-phases classification experiment: from class 3 to 1 (Heel Strike), from class 1 to class 0 (Counter lateral Toe Off), from class 0 to 2 (Heel Rise) and from class 2 to class 3 (Toe Off). The same modified algorithm is also proposed to detect transitions between stance and swing phases (Heel Strike and Toe Off). The ability of the models to correctly identify gait events are assessed using an algorithm widely used in literature [4,5,7,8,45,46]. A temporal tolerance T is set to 150 milliseconds (300 samples). Each identified transition in the predicted signal is considered as true positive (TP) event at time t_p if an event of the same type exists in the ground truth signal at time t_g such that:

$$|t_g - t_p| < T \tag{33}$$

Otherwise, the predicted event is considered as a false positive (FP). Finally, standard metrics (precision, recall and F1 score) and mean average error (MAE) are computed to evaluate model performance in detecting gait events.

Precision is defined as the ratio between the number of true positives events divided by the total number of predicted positive events. It is defined by the following equation:

$$Precision = \frac{TP}{TP + FP} \tag{34}$$

Recall is defined as the ratio between the number of true positives divided by the number of total actual positive events. It is defined by the following equation:

$$Recall = \frac{TP}{TP + FN} \tag{35}$$

A False negative (FN) event occurs when a transition is present in the ground truth signal but the correspondent event in the predicted signal is out of the tolerance range. F1-score is defined as the harmonic mean between precision and recall.

$$F1\ Score = \frac{2 \times (Precision \times Recall)}{Precision + Recall} \tag{36}$$

Furthermore, for all true positives, the mean average error (MAE) was computed measuring the temporal distance between the predicted event and the positive event in the ground truth. MAE is defined as the average time distance between the predicted event and the one, of the same type, in the basographic signal [4].

CHAPTER 6: Results

This chapter presents the results of the 4-sub-phase classification achieved using a novel approach that consists in two classifiers implemented in cascade. The first classifier provides an identification of the two main gait phases, stance and swing, and the second classifier split the predicted stance into 3 further sub-phases. In the first part of this chapter, the results of a comparative analysis are reported, in terms of the performances of two binary classifiers taken from the literature. Results are compared also with further studies widely acknowledged in the literature. A 5-fold cross validation strategy is adopted to evaluate the performance of the models.

6.1 Binary Classifiers

The two binary models involved in this study are a SVM classifier and a MLP neural network, described in the previous chapter. Both models have been trained providing as input the samples of the five WSD signals obtained as described in chapter 5. 3. Each sample of the five input vectors is supplied to the classifier together with the corresponding label (stance = 0, swing = 1). Once the classifier has been trained, the test fold, organized in chronological order, is fed to the model to predict the class of each individual sample. The predictions coming out of each classifier form a vector of the same length as the test fold and already arranged with the same chronological order. The mean classification accuracy (± Standard Deviation, SD) for each fold of each subject included in the study, after post-processing correction, are reported in ***Table 6. 1***. Results include class accuracy (±SD) for each gait phase and the overall prediction accuracy (± SD).

Table 6. 1 *Stance and swing classification accuracy (±SD) of the two binary model. Accuracies are referred to the mean values among each fold of all the 31 subjects involved in the study.*

Model	***Stance Accuracy (±SD)***	***Swing Accuracy (±SD)***	***Overall Accuracy (±SD)***
SVM	94.62% ± 3.21%	93.39% ± 3.39%	94.04% ± 2.61%
MLP	94.55% ± 3.02%	93.60% ± 3.38%	94.13% ± 2.48%

The two models are able to predict the two main gait phases with an accuracy higher than 93% for both classes. However, the MLP architecture has slightly higher prediction ability (94.21%), with respect to SVM (94.09%), but lower than 0.13% (negligible). In addition, the accuracy for the stance and swing classes are also higher for MLP (94.71% ± 2.95% for stance and 93.55% ± 3.36%) model than SVM (94.63% ± 3.27% for stance and 93.47% ± 3.18%). Nevertheless, prediction accuracies

are similar between the two proposed approach and no significant differences exist among them. The variability, in terms of standard deviation, remains always under 3.5%, despite the large size of the dataset. The results will be reported for each of the 5 test fold used during the cross-validation and for each of the 31 subjects involved in the study. The results are also comparable with those found in literature, even if the two models are very simple machine learning architectures, defined without any parametric tuning (SVM) or high structural complexity (MLP). The mean prediction accuracy among all the values reported by other works, that adopt the same intra-subject approach, is 97.02%, against 94.21% mean overall prediction accuracy reached by the present study. ***Table 6. 2*** reports same brief review of the mean prediction accuracy results achieved by other related works.

Table 6. 2 *Values of prediction accuracy among related works in literature. For the intra-subject approaches, values refer to mean prediction accuracy values. For intra-subject approaches the values refer to the prediction accuracy tested on unseen subjects. In every case the best prediction value is reported, if more than one architecture is tested.*

Authors	***Adopted Approach***	***Mean Classification Accuracy (%)***	***Standard Deviation (%)***
Morbidoni et al. [5]	Intra-Subject	97.00%	1.00%
Morbidoni et al. [4]	Inter-Subject	93.41%	2.3%
Di Nardo et al. [7]	Intra-Subject	96.10%	1.9
Di Nardo et al. [8]	Inter-Subject	93.40%	2.3%
Morbidoni et al. [6]	Intra-Subject	95.18%	1.58%
Nazmi et al. [10]	Inter-Subject	77.00%	-
Nazmi et al. [12]	Inter-Subject	77.00%	-
Ziegler et al. [14]	Inter-Subject	96.09%	-
Ghalyan et al. [2]	Intra-Subject	99.8%	-

The accuracy metric determines the ability of the model to correctly classify gait phases. However, this measure has one major limitation that occurs when prediction errors are concentrated in proximity of phase transitions, leading to unsatisfactory results in terms of time localization of the gait event. Transition events detection is performed using a time tolerance of 150 ms. MAE and F1-Scores are computed to evaluate the performance of the two models in predicting HS and TO events. Mean values of MAE and F1-Score for each subject in the study are reported in ***Table 6. 3***. The SVM classifier reports higher values of F1-Score (89.34% for HS and 88.63% for TO) with respect to the MLP neural network, highlighting a greater ability of the SVM to correctly identify transitions

between gait phases, avoiding false positive events. The average number of true positive events detected by this latter architecture (45.07 for HS and 44.81 for TO) is similar to the number of true positives detected by the MLP (45.25 for HS and 44.97 for TO). However, the number of false positive in average is much lower for SVM (10.72 for HS and 10.95 for TO), rather than for MLP (20.66 for HS and 20.94 for TO). Lower number of false positive predictions determines the higher values of the F1-Score metric.

Table 6. 3 *MAE and F1-Score metrics of the HS and TO events for both the machine learning models*

Model		***HS***	***TO***
SVM	*MAE*	22.43 ± 9.52 ms	29.18 ± 10.88 ms
	F1-Score	97.03% ± 4.11%	96.28% ± 5.58%
MLP	*MAE*	22.49 ± 9.70 ms	29.06 ± 10.25 ms
	F1-Score	96.98% ± 4.17%	95.98% ± 5.44%

Considering both the architectures a tendency to better identify HS events is visible, associated with lower values of MAE. These results suggest a greater ease of the two machine learning algorithms to determine the instant of transition between the swing phase and the stance phase. The variability remains under 10% using SVM architecture, differently from MLP characterized by a standard deviation higher than 10% for both HS and TO. For the SVM model the average value of MAE, among all the subjects, is 20.82 ± 7.01 ms for HS event and 28.24 ± 10.09 ms for TO. However, MLP has better MAE performance, 19.74 ± 6.21 ms for HS and 26.69 ± 8.62 ms for TO, that determines greater ability of the model to correctly localize, in time, true positive events. Time difference (TD) between the actual transition event and the predicted event is computed for all the true positives detected in the test set. The sign of the average TD value highlights the tendency of the two model to localize, in time, the predicted event before (positive) or after (negative) the actual event. SVM has an average TD value equal to -0.92 ms for HS and -1.37 ms for TO, while MLP has an average TD of -0.67 ms for HS and -0.66 ms for TO, with a tendency to postpone the prediction of the transition between the 2 gait phases.

6.2 Proposed approach: Multi-Classifier Architecture

The promising results obtained from the binary classification of gait phases have been exploited to define an innovative approach which, according to our knowledge, has never been tested before in the literature. The predicted samples belonging to the stance phase out of the first binary classifier

are used to determine three stance sub-phases: Initial Stance, Mid Stance and Terminal Stance, with the relative transition events (CTO, HR). The first architecture implemented in the present study was composed by two cascaded MLP neural networks (MLP-MLP). The mean classification accuracies for each class among all the subjects are reported in ***Figure 6. 1***. The values correspond to the average of all folds for all the 31 subjects involved.

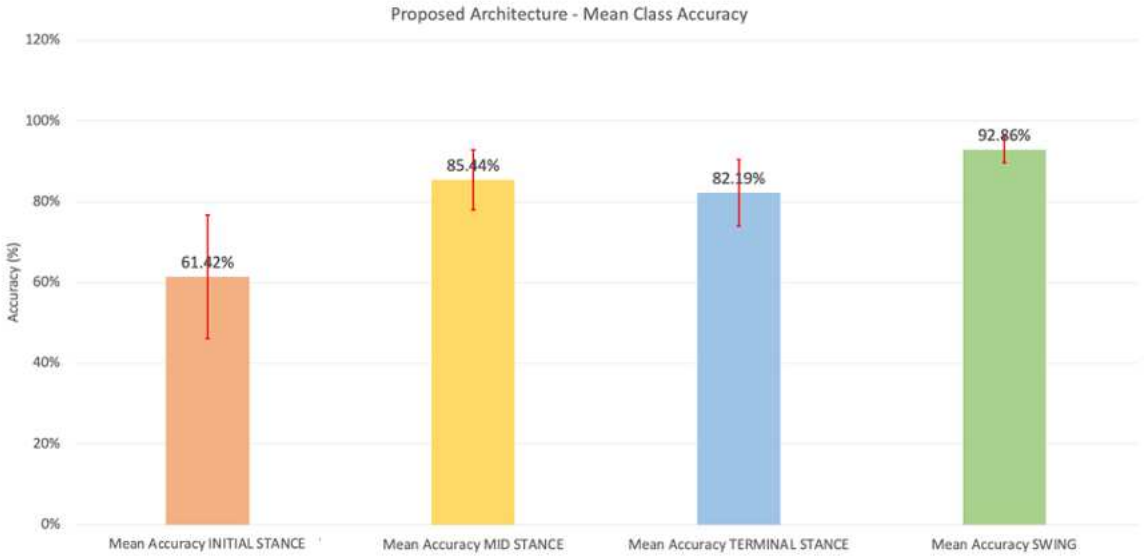

Figure 6. 1 *Average classification accuracy per class for the MLP-MLP architecture consisting of 2 MLP networks implemented in cascade.*

The Initial Stance phase reaches the worst accuracy, 61.42%, due to its very short duration. This phase also exhibits the highest value also in terms of variability (± 15.28%, SD). The Mid Stance phase is identified with an accuracy of 85.44%, with respect to the total number of samples belonging to this class. It also has a relatively low standard deviation (± 7.44%) which indicates a low rate of variability. The last stance phase, Terminal Stance, is also quite accurately predicted, reaching a value of 82.19% ± 8.24%. Finally, the Swing phase, derived from the binary MLP classifier, is predicted with an accuracy of 92.86% ± 3.21%. The mean overall accuracy reached by this first architecture is 86.71% ± 3.31%. Moving to the prediction outcomes of the second architecture (SVM-MLP), formed by the binary SVM classifier, used to predict the two main gait phases and a second 3 stance sub-phases MLP classifier, the classification results are reported in ***Figure 6. 2***. The Initial Stance phases accuracy worsen with respect to the previous architecture to a value of 60.84% ± 15.45%. Both classification accuracy and variability decrease but values remain comparable with the first approach. The Mid Stance phase shows an accuracy value of 85.46%, with a tiny improvement in prediction and variability (± 7.41%, SD). The Terminal Stance phase also is better predicted reaching a value of

86.63% ± 8.49%. Finally, the Swing phase shows a little worsening in accuracy, 92.74%, but it was predictable by looking at the results of the binary classifiers. The mean overall accuracy reached by the present architecture is 86.70% ± 3.38%.

Figure 6. 2 *Average classification accuracy per class for the second proposed architecture consisting of 2 cascaded classifiers, a binary SVM model and a MLP for the classification of the 3 stance sub-phases (SVM-MLP).*

A third architecture is introduced, composed by 2 cascaded SVM classifiers to identify the 4 gait sub-phases (SVM-SVM). The accuracy results per each of the 4 classes are reported in ***Figure 6. 3***.

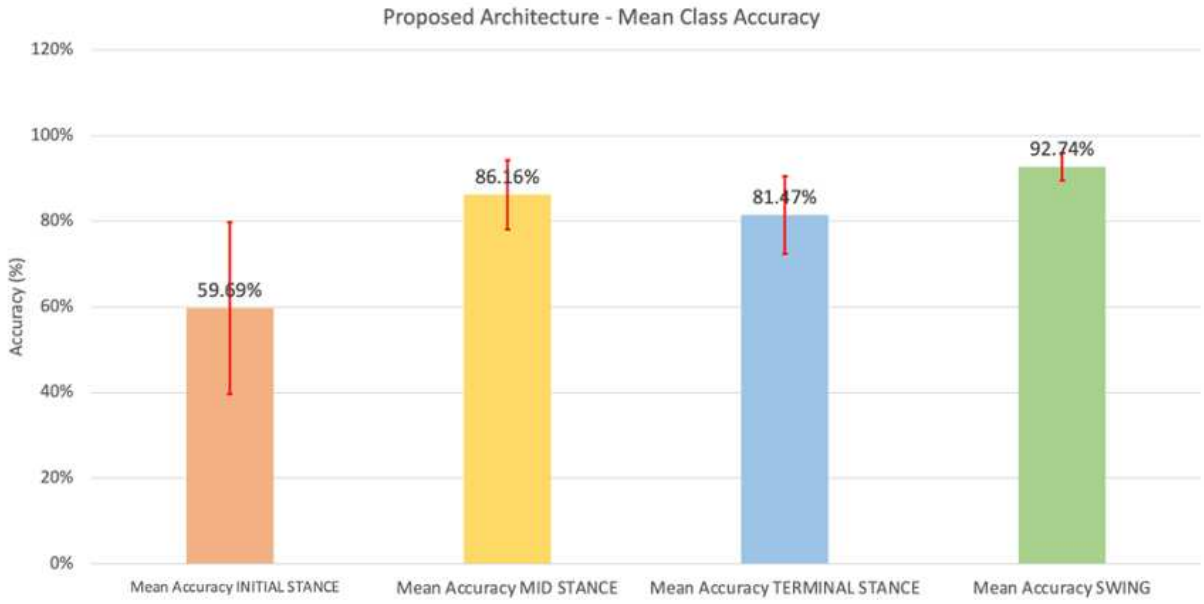

Figure 6. 3 *Average classification accuracy per class for the third proposed architecture consisting of 2 cascaded SVM classifiers (SVM-SVM).*

As expected, the swing phase is predicted with same accuracy and variability (92.74% ± 3.19%) of the previous architecture because the same binary classifier is used. The other 3 stance sub-phases, i.e. Initial Stance, Mid Stance and Terminal stance, are predicted with 59.69%, 86.16% and 81.47%, respectively. The performance of the model is estimated as the overall accuracy of the prediction which turns out to be equal to 86.64% ± 3.28%. The mid stance phase in this case is the one reported the best accuracy among all the three architectures (86.16% vs. 85.46% and 85.44%), while the Initial Stance phase is the worst predicted. However, all the accuracy values among all the three architectures shows comparable values and significant difference are visible. The three architectures perform similarly in terms of class and overall prediction accuracy. The Kruskal-Wallis test suggests that no significant statistical differences exist among the three architectures. The Kruskal-Wallis one-way analysis of variance test is an analogue of ANOVA that can be used when the assumption of normality cannot be met. The normality of the three distributions has been evaluated using the Lilliefors test. The null-hypothesis of the test, for which the data comes from a normal distribution, has been rejected in at least one of the three distributions. Thus, the Kruskal-Wallis test has been performed. The accuracy values computed for each fold of all the subjects in the study represent the three distributions evaluated by the non-parametric test. For the Initial Stance phase, the computed p-value ($p = 0.91 > 0.01$) suggests that no differences exist between the median values of the three distributions. The p-value is computed also for the Mid Stance phase ($p = 0.21 > 0.01$), Terminal Stance phase ($p = 0.49 > 0.01$) and Swing phase ($p = 0.93 > 0.01$) and no statistical differences are highlighted. The performance of the three models to detect transition events are evaluated through MAE and F1-Score. Comparison results between the three architectures are reported in ***Table 6. 4***.

Table 6. 4 *Comparison results between the three proposed architectures in terms of MAE and F1-Score, describing the performance to identify gait events.*

Model	***Metric***	***HS***	***CTO***	***HR***	***TO***	***Mean Values***
MLP - MLP	*MAE*	18.60 ms	25.99 ms	37.97 ms	29.14 ms	27.93 ms
	F1-Score	92.10%	79.44%	85.31%	95.82%	88.17%
SVM - MLP	*MAE*	18.49 ms	26.06 ms	37.96 ms	29.26 ms	27.94 ms
	F1-Score	91.53%	79.61%	85.68%	96.08%	88.23%
SVM - SVM	*MAE*	18.73 ms	27.67 ms	40.45 ms	29.26 ms	29.03 ms
	F1-Score	89.93%	88.10%	91.61%	96.08%	91.43%

The firs architecture has a MAE of 18.60 ± 6.54 ms for the HS event, 25.99 ± 7.61 ms for CTO, 37.97 ± 7.41 ms for HR and 29.14 ± 10.27 ms for TO gait event. The corresponding F1-Score metric reaches values of 92.10% ± 10.56%, 79.44% ± 10.29%, 85.31% ± 9.50% and 95.82% ± 5.36%, respectively. The CTO event is the most toughly predicted by this model with lowest value of F1-Score, due to the high number false positive predicted. The average number of total CTO events, among all subjects and folds, is 45.81 and the number of true positive detected by this model is 44.90. The computed of Recall score, indeed, is 98.14%. The average number of false positive events, however, is high (24.30), leading to a low value of Precision (67.79%). HS and TO events are correctly predicted, exploiting the performance of the binary MLP classifier. The average number of total gait events are 44.54 and 45.84, respectively. Instead, the total number of correctly classified events are 40.57 and 44.26, for HS and TO, respectively. The average number of false positive detected are 1.97 for HS and 2.17 for TO, leading to very high values for both Precision and Recall scores (and turn F1-Score). HR has been moderately correctly identified, with 44.37 true positive events (versus 45.55 for all positives), and 15.55 false positive events misdetected (Precision 76.79% and Recall 97.42%).
An example of the basographic signal predicted using the first architecture is reported in ***Figure 6. 4***.

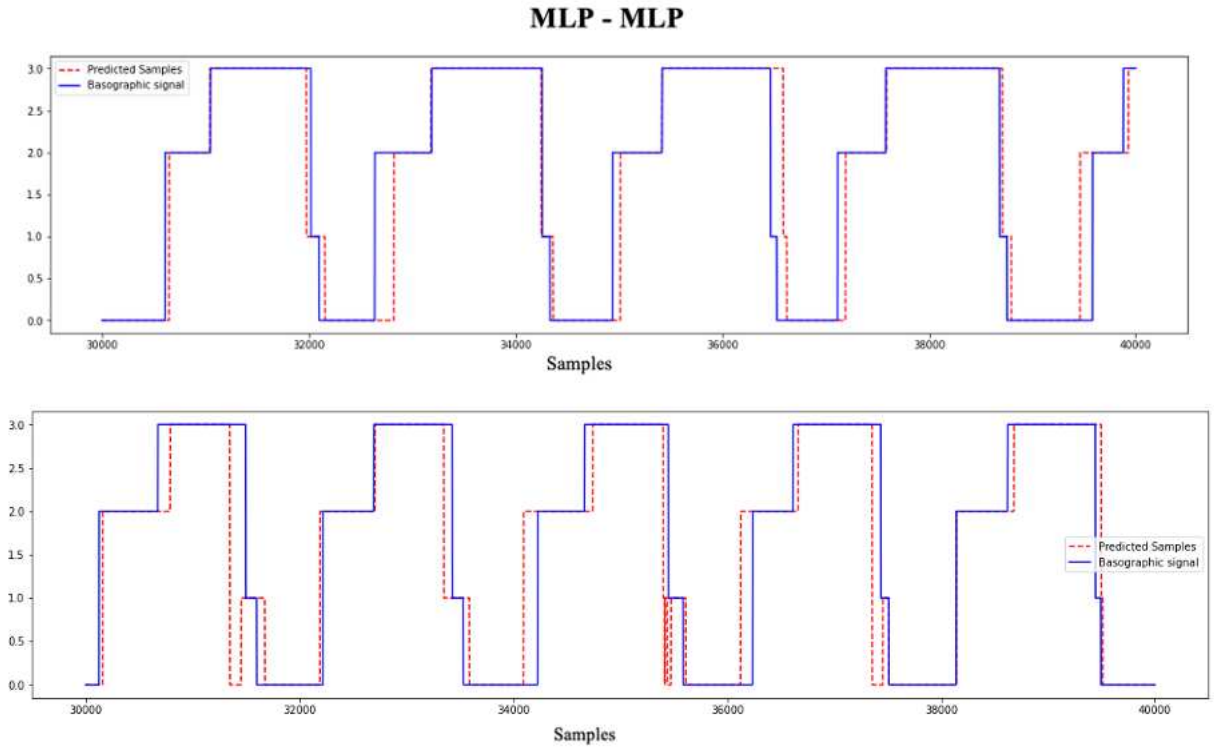

Figure 6. 4 *Example of the predicted basographic signal of the subject 28 (upper figure) and 31 (bottom figure) obtained with the MLP-MLP architecture. The predicted signal of subject 31 some errors are visible.*

More detailed information is reported in ***Table 6. 5***.

Table 6. 5 *Average values corresponding to the total number of actual positives, true positive, false positive and false negative. Precision, Recall and F1-Score metrics for the MLP-MLP model.*

MLP - MLP	***HS***	***CTO***	***HR***	***TO***
Positives	44.54	45.81	45.55	45.84
TP	40.57	44.90	44.37	44.26
FP	1.97	24.30	15.55	2.17
FN	3.97	0.92	1.19	1.58
Precision	95.33%	67.79%	76.79%	95.44%
Recall	90.42%	98.14%	97.42%	96.33%
F1-Score	92.10%	79.44%	85.31%	95.82%

The second proposed classifier has similar performances to the first one. The values of MAE reached by this second architecture are 18.49 ± 6.00 ms for HS, 26.06 ± 7.33 ms for CTO, 37.96 ± 7.28 ms for HR and 29.26 ± 10.84 ms for TO. The corresponding values of F1-Score are 91.53% ± 11.21% for HS, 79.61% ± 9.89% for CTO, 85.68% ± 9.64 for HR and 96.08% ± 5.50% for TO events. HS and TO events, as expected, are fairly well predicted with 40.14 (out of 44.54) and 44.85 (out of 45.81) true positive events identified (on average), respectively. The number of false positive events, however, remains low on average for HS (1.94) but significantly increases for TO (23.88) events. The corresponding value of Precision are 95.35% for HS and 67.97% for TO, while the Recall is 89.44% for HS and 98.04 for TO. CTO is the most difficult event to be predicted. The total number of true positive events are 44.86 versus 45.81 total positive. The number of false positive events are 23.88, leading to values of Precision and Recall of 67.97% and 98.04%, respectively. For what concerned the HR event, the total number of correctly predicted transitions are 44.29 (out of 45.55), with 14.99 false positive events. The corresponding percentages of Precision and Recall are 77.46% and 97.24%. More detailed information about the average number of actual positives, true and false positives and false negatives, as well as Precision, Recall and F1-score metrics are reported in the following table (***Table 6. 6***).

Table 6. 6 *Average values corresponding to the total number of actual positives, true positive, false positive and false negative. Precision, Recall and F1-Score metrics for the SVM-MLP model.*

SVM - MLP	***HS***	***CTO***	***HR***	***TO***
Positives	44.54	45.81	45.55	45.84
TP	40.14	44.86	44.29	44.27
FP	1.94	23.88	14.99	1.88
FN	4.41	0.95	1.26	1.57
Precision	95.35%	67.97%	77.46%	95.92%
Recall	89.44%	98.04%	97.24%	96.32%
F1-Score	91.53%	79.61%	85.68%	96.08%

An example of the predicted basographic signal of the subject 28 of the present study obtained using the second architecture, SVM-MLP, is reported in ***Figure 6. 5***.

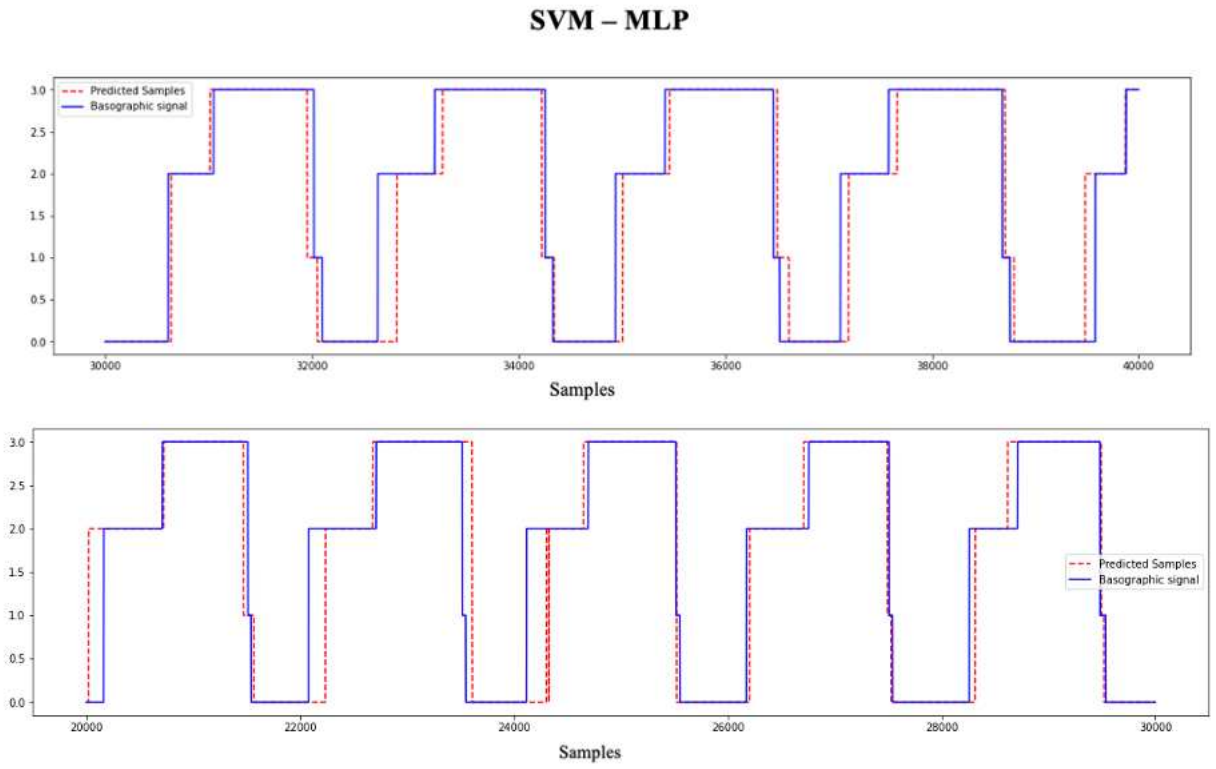

Figure 6. 5 *Example of the predicted basographic signal of the subject 28 (upper figure) and 31 (bottom figure) obtained with the SVM-MLP architecture. The predicted signal of subject 31 some errors are visible.*

Finally, the third architecture is assumed as the leading model for its high ability to detect also CTO transition events, significantly better than the other two previous approaches. The computed F1-Scores for all the gait events reach values of 89.93% ± 19.57% for HS, 88.10% ± 7.33% for CTO events, 91.61% ± 7.06% for HR and 96.08% ± 5.50% for TO transition events. The average number of true positive events detected by the binary classifiers are 39.77 (out of 44.54) and 44.27 (out of 45.84) for HS and TO, respectively. The number of false positive events detected by the third architecture remains very low for both HS (1.59) and TO (1.88), with values of Precision and Recall that are higher with respect to the previous models. Precision stands at 92.99% for HS and 95.93% for TO, while Recall metric is 88.38% for HS and 96.32% for TO. CTO go from 79.44% and 79.61%, in the previous two approaches, to 88.10%, in the present model. Thus, a significant improvement occurs for the F1-Score metric, corresponding to an improvement of 10.90% and 10.66%, respectively. The average number of true positive events for the CTO class is 44.65 against 45.81 total positives. The false positive events are 11.57 (lower than for the other two, 24.30 and 23.88), leading to acceptable values of Precision (80.89%) and Recall (97.54%). The Kruskal-Wallis test performed on the three non-normal distributions of F1-scores values for the CTO classes of the proposed models highlights statistical differences among the groups ($p = 7.53 \cdot 10^{-19} < 0.01$). The multiple comparison analysis demonstrates that the SVM-SVM model has a median value of F1-Score which is significantly better from the other two. For the HR transition events the true positive events detected are 44.06, on average, and the number of false positives is 7.08. Recall and Precision reaches values of 87.37% and 96.76%, respectively.

Table 6. 7 *Average values corresponding to the total number of actual positives, true positive, false positive and false negative. Precision, Recall and F1-Score metrics for the SVM-SVM model.*

SVM - SVM	***HS***	***CTO***	***HR***	***TO***
Positives	44.54	45.81	45.55	45.84
TP	39.77	44.65	44.06	44.27
FP	1.59	11.57	7.08	1.88
FN	4.77	1.17	1.50	1.57
Precision	92.99%	80.89%	87.37%	95.93%
Recall	88.38%	97.54%	96.76%	96.32%
F1-Score	89.93%	88.10%	91.61%	96.08%

Also, the HR transition event shows a significantly higher value of the mean F1-Score in the SVM-SVM model, as reported by the test statistic ($p = 4.35 \cdot 10^{-12} < 0.01$). More detailed information about this architecture is summarized in ***Table 6. 7***.

The MAE values computed for the third architecture are 18.73 ± 6.14 ms for HS, 27.67 ± 9.61 ms for CTO, 40.45 ± 8.95 ms for HR and 29.26 ± 10.84 ms for TO transition event. One can notice that for all the models proposed in the present study the value of the MAE increases as the corresponding F1-Score value increases, probably because a higher number of correctly predicted events leads to a less precise time localization of single events, on average. An example of the predictions of the basographic signal obtained from the third proposed architectures is shown in ***Figure 6. 6***.

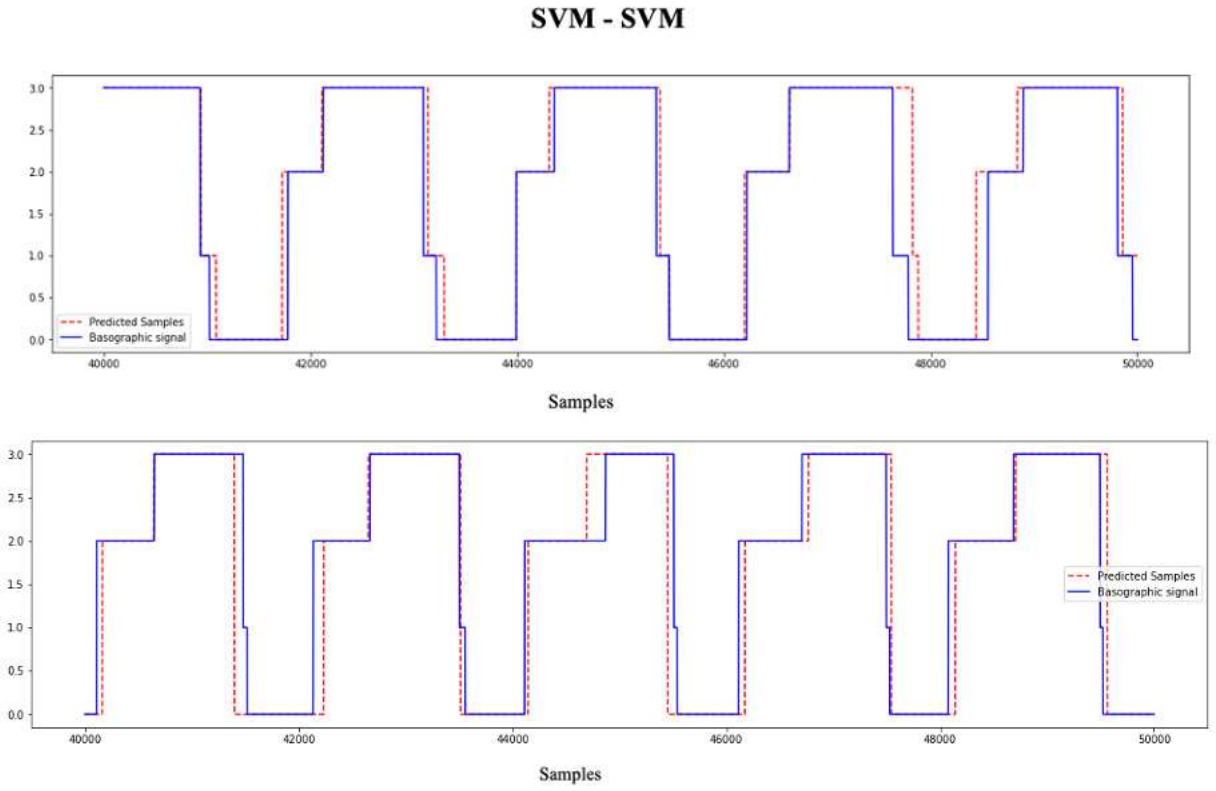

Figure 6. 6 *Example of the predicted basographic signal of the subject 28 (upper figure) and 31 (bottom figure) obtained with the SVM-SVM architecture. The predicted signal of subject 31 some errors are visible.*

Furthermore, the last column of ***Table 6.4*** reports the mean values of MAE and F1-Score calculated among the four different gait events for each of the proposed architectures. The mean F1-Score reaches the highest value in the SVM-SVM model at 91.43% (versus 88.23% for SVM-MLP and 88.17% for MLP-MLP). However, the MAE value is also the maximum for SVM-SVM which identifies many true positive events compared to the other two models.

6.3 Validation with standard 4-phase classifiers

Two additional 4-phases SVM and MLP classifiers are introduced to validate the performances of the proposed approaches. The results, in terms of mean prediction accuracy for each class of the 4-phase SVM model, are shown in ***Figure 6. 7***. The average accuracy is computed between all the subjects and folds considered in the present study. The mean Initial Stance accuracy is 57.27% ± 20.65%, 85.99% ± 8.15% for the Mid Stance accuracy, 81.71% ± 8.73% for the Terminal Stance, and 94.18% ± 2.77% for the mean Swing accuracy. The 3 stance sub-phases have an average accuracy which is comparable with the one obtained with the proposed classifier in the novel approach.

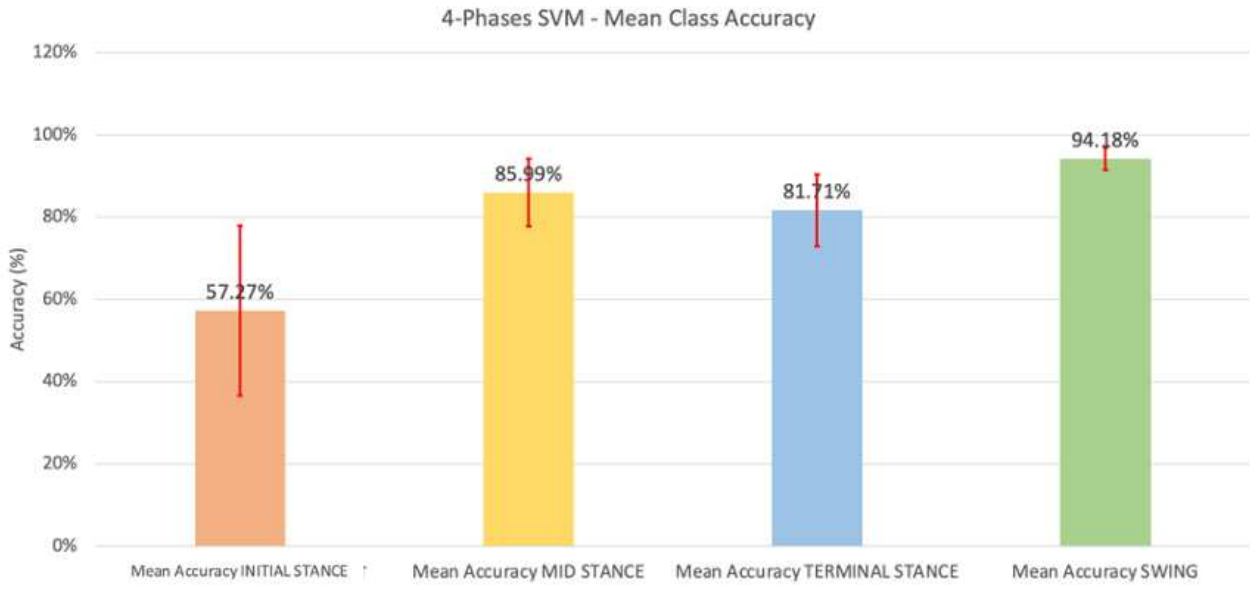

Figure 6. 7 *Class accuracy of the 4-phases SVM classifier*

In ***Figure 6. 8*** the same results of the 4-phases MLP neural networks are shown. The mean accuracies reached for each of the 4 gait sub-phases are reported in the following. The Initial Stance phase reached 58.88% ± 17.15% of accuracy, the Mid Stance phase 85.15% ± 7.71%, the Terminal Stance phase 82.80% ± 7.92% and 94.05% ± 2.74% for the swing phase accuracy. No statistically significant differences exist between the proposed reference approach, the one formed by the 2 cascaded SVM classifiers, and the two simple 4-phases SVM and MLP models. The Kruskal-Wallis test carried out among the non-normal distributions of the class accuracies in the three models (the proposed reference architecture, and the two simple 4-phase classification models) does not show significant performance differences in terms of mean accuracy for the classification of the three stance sub-phases (Initial Stance $p = 0.54 > 0.05$, Mid Stance $p = 0.49 > 0.05$, Terminal Stance $p = 0.35 > 0.05$).

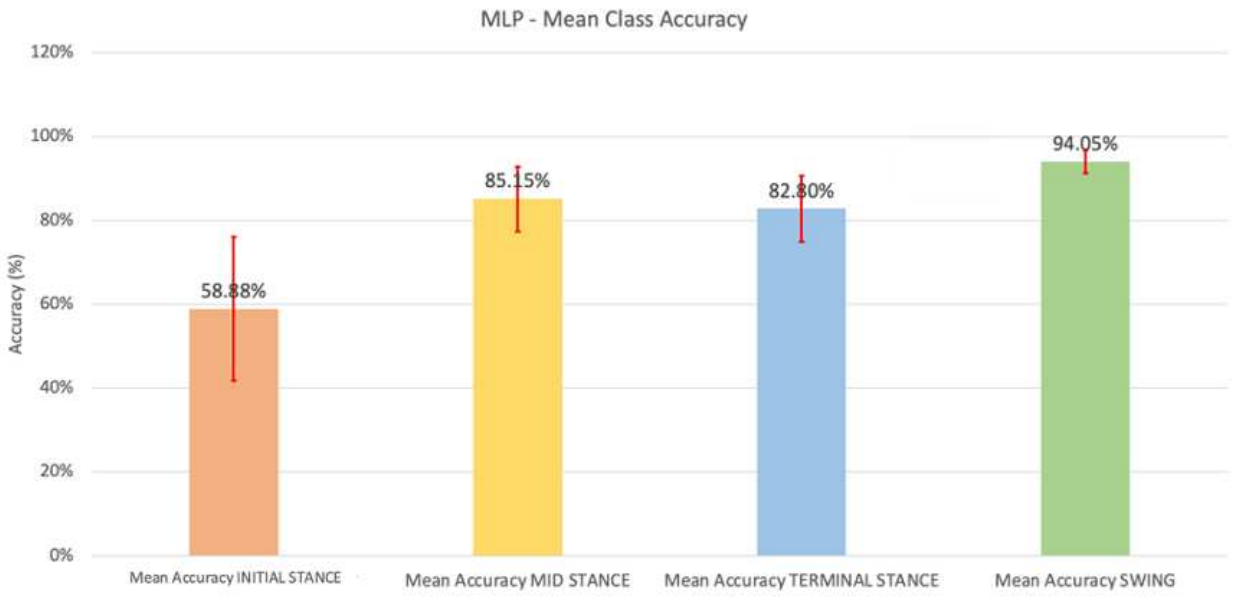

Figure 6. 8 *Class accuracy of the 4-phases MLP classifier*

The only exception exists for the Swing phase that is classified significantly better in the two simple SVM and MLP models. The median value of the proposed reference architecture for the swing class is statistically lower than the other two ($p = 3.22 \cdot 10^{-6} < 0.01$). However, the performance in the transition instants between subsequent gait phases is significantly better in the proposed architecture. In ***Table 6. 8*** the performances of the three model in detecting transition event are compared.

Table 6. 8 *Comparison between performances of the three models in detecting transition events.*

Model	***Metric***	***HS***	***CTO***	***HR***	***TO***	***Mean Values***
MLP	*MAE*	17.22 ms	26.03 ms	38.19 ms	26.98 ms	27.11 ms
	F1-Score	88.31%	79.34%	86.60%	82.23%	84.12%
SVM	*MAE*	17.04 ms	27.32 ms	40.52 ms	27.65 ms	28.13 ms
	F1-Score	86.57%	86.40%	91.76%	88.50%	88.31%
SVM - SVM	*MAE*	18.73 ms	27.67 ms	40.45 ms	29.26 ms	29.03 ms
	F1-Score	89.93%	88.10%	91.61%	96.08%	91.43%

The F1-Scores of the HS events are statistically different between the two simple 4-phases classifier and the reference approach reported in the study ($p = 1.98 \cdot 10^{-6} < 0.01$). The multiple comparison analysis shows that the SVM-SVM model behaves better in prediction of HS event (SVM has higher median F1-Score with respect to MLP). Moreover, the CTO and HR transition events have a F1-

Score which is comparable between the proposed architecture and the SVM model, while the MLP performs worst with respect to the previous two. The p-value computed for CTO and HR events is $p = 2.91 \cdot 10^{-15}$ and $p = 1.75 \cdot 10^{-9}$ (p-values < 0.01), respectively. The multiple comparison analysis demonstrate that no differences exist between the SVM-SVM classifier and the simple 4-phases SVM model, while the simple MLP model has a lower ability to detect HR and CTO transitions, presenting a significantly lower median value of F1-Score. Finally, the first binary model implemented in the proposed reference architecture behaves better in the identification of TO events, with a statistically higher median value of F1-Score ($p = 1.89 \cdot 10^{-38} < 0.01$) with respect to the simple SVM and MLP classifiers (SVM performs better than MLP). The test statistic used to evaluate the differences of model performances is the Kruskal-Wallis test carried out on non-normal distributions. The last column of ***Table 6. 8*** demonstrate the higher ability of the reference SVM-SVM model to predict gait events. The following summary table (***Table 6. 9***) reports the performance of all the 4-phase classifiers tested in the present study, allowing a direct comparison between the obtained results.

Table 6. 9 *Summary table: it reports the average values of MAE and F1-Score among each fold computed for each subject involved in the study. Results are divided for each gait events. The last column shows the average values of MAE and F1-Score among the 4 gait transition events reported on the other columns.*

Model	*Metric*	*HS*	*CTO*	*HR*	*TO*	*Mean Values*
MLP	*MAE*	17.22 ms	26.03 ms	38.19 ms	26.98 ms	27.11 ms
	F1-Score	88.31%	79.34%	86.60%	82.23%	84.12%
SVM	*MAE*	17.04 ms	27.32 ms	40.52 ms	27.65 ms	28.13 ms
	F1-Score	86.57%	86.40%	91.76%	88.50%	88.31%
MLP - MLP	*MAE*	18.60 ms	25.99 ms	37.97 ms	29.14 ms	27.93 ms
	F1-Score	92.10%	79.44%	85.31%	95.82%	88.17%
SVM - MLP	*MAE*	18.49 ms	26.06 ms	37.96 ms	29.26 ms	27.94 ms
	F1-Score	91.53%	79.61%	85.68%	96.08%	88.23%
SVM - SVM	*MAE*	18.73 ms	27.67 ms	40.45 ms	29.26 ms	29.03 ms
	F1-Score	89.93%	88.10%	91.61%	96.08%	91.43%

The table reports the value of F1-Score and MAE for each transition event. The last column shows the average MAE and F1-Score value among the 4 different events. As expected from previous

results, the SVM-SVM model performs better than the other models in terms of ability to detect transition events (F1-Score = 91.43%).

CHAPTER 7: Discussions and Conclusions

The aim the present study was the classification of the main four gait sub-phases (Initial Stance, Mid Stance, Terminal Stance and Swing) and the prediction of the related transition events (HS, CTO, HR, TO) through a novel machine learning approach applied to only sEMG signals. The use of only sEMG signals in the prediction of the foot-floor signal could contribute to reduce the number of sensors involved in the experiments, thus limiting the clinical encumbrance, time-consumption, and cost, especially in condition of neurological diseases in which the acquisition of sEMG signals is typically recommended. The proposed architecture consisted of two classifiers implemented in cascade, where a first binary classifier was used to identify the two main gait phases (stance and swing) and a second classifiers provided predictions on the further subdivision of the stance, identifying the three main sub-phases: Initial Stance, Mid Stance and Terminal Stance. The swing phase was obtained from the first binary classification. The signal used in the present work, to train the classifier, was essentially the difference between the RMSS obtained by the sEMG signals from right and left leg muscle pairs and known as the WSD signal a sEMG-derived [9]. The basographic signal acquired thorough foot-switch sensors was adopted as the ground truth. The use of footswitches allowed to acquire many strides during walking of the subjects involved in the study and to accurately measure spatial/temporal parameters of the gait, that are used as reference to predict and classify transition events between consecutive gait phases. At the end, predictions are chronologically concatenated and re-arranged to obtain the final output of the models, i.e., the foot-floor signal including the four gait subphases. To identify the best-performing approach for implementing the two classifiers in cascade, a preliminary evaluation of the performance in binary classification of two supervised learning algorithms was performed: a SVM classifier and a MLP neural network were chosen based on literature. The binary SVM was implemented using the parameters C and γ obtained by Ziegler at al. ($C = 25.902$ and $\gamma = 0.018$) from the intra-subject approach that better performed on different test subjects [14]. The binary MLP neural network was defined using one single hidden layer composed by 32 units, an input layer with 5 neurons (equal to the number of input vectors, 5 WSD signal) and 2 output neurons for the two gait classes [5]. The results were reported in ***Table 6. 1***. The average accuracy of the stance phase is 94.63% ± 3.27% for the SVM model and 94.71% ± 2.95% for the second MLP net. The swing phase reached 93.47% ± 3.18% and 93.55% ± 3.36% for SVM and MLP, respectively. The overall prediction accuracy for the two models is 94.09% ± 2.59% for SVM and 94.21% ± 2.42% for MLP. The obtained results demonstrated that the two proposed machine learning model were able to correctly identify and classify the main gait phases, with accuracy values that were almost comparable with those available in the literature. Nevertheless, the

prediction performances could still be improved by using a more complex architecture of the MLP network, for example a MLP network with 3 hidden layers composed by 512, 256 and 128 hidden units (best performing MLP neural network proposed by Morbidoni et al. [4] and Di Nardo et al. [7]), or through a parametric tuning of the SVM classifier (Ziegler et al. [14]). More complicated architectures and parameter tuning, however, require much longer calculation and execution times of the algorithms than the simple binary networks used in the present study. In particular, the SVM model trained on a large amount of data required very high computation times, for this reason the results obtained seem to be a good compromise between the simplicity of the proposed architecture and the overall accuracy levels achieved. The average overall accuracy reached by the four study that adopt the same intra-subject approach is 97.02%, against the best overall accuracy of 94.21% reached by the binary MLP model proposed in this work. Despite the lower percentage of error made by the works proposed in the literature, the simplicity of the models still offers acceptable performances, taking into account the fact that a future goal could consist in applying a post-processing algorithm to eliminate non-physiological phases from the predicted signal, achieving even higher levels of accuracy. The performance of the models in identifying transition events was also evaluated and the results were reported in ***Table 6. 3***. The MAE, defined as the average error between detected positive events, was computed for all the subjects and folds, used for the cross-validation strategy, involved in the study. The mean value was reported in the aforementioned table: 20.82 ± 7.01 ms for HS and 28.24 ± 10.09 ms for TO in the SVM binary classifier and 19.74 ± 6.21 ms and 26.69 ± 8.62 ms for HS and TO, respectively, using the binary MLP model. The results of the identification of transition events obtained by the two binary models were, also in this case, comparable with those present in the literature. In [7], Di Nardo et al. reached MAE values of 14.4 ± 4.7 ms for HS and 23.7 ± 11.3 ms for TO events. Post-processing algorithm can also improve prediction accuracy allowing to obtain better MAE values. The F1-Score metrics were evaluated, and results reported in ***Table 6. 3***. SVM had an F1-Score of 89.34% ± 8.87% in detecting HS events and 88.63% ± 9.55% for TO, while MLP reached values of 82.47% ± 11.64% and 81.91% ± 12.11% for HS and TO, respectively. These results highlighted how the SVM classifier was able to provide a better overall predictive capacity than the MLP network. After the analysis of the performances provided by two binary models, three different combinations of these two models were tested in order to achieve the best-performing cascaded classifier. The first architecture (MLP-MLP) is composed of two MLP neural networks, a simple binary MLP model, that predict stance and swing phases, and a second MLP that takes the predicted stance phases out of the first model and subsequently sub-classified it in Initial Stance, Mid Stance and Terminal Stance. The average classification results over the 5 folds on all the subjects were reported in ***Figure 6. 1***. As expected, the Initial Stance phases had the lower accuracy levels, 61.42%

± 15.28%, due to its very short duration (5-10% of the entire gait cycle). Because of the different duration of each gait phases, the number of samples belonging to each class remains heterogeneous and the final dataset is quite unbalanced. In fact, the sEMG data was segmented into 4 classes, following the definition of the gait sub-phases and thus, each class have a different duration (i.e., different number of samples). The Swing phase cover the biggest part of the dataset (40-45% of the gait cycle) followed by Mid Stance (20-30%), Terminal Stance (15-25%) and Initial Stance phase. Classifiers were trained with a small number of Initial Stance samples which affected their performance in the correct classification of this phase. The Mid Stance phase reached 85.44% ± 7.44% of accuracy, the Terminal Stance phase 82.19% ± 8.24% and the Swing phase reached 92.86% ± 3.21%. The mean overall accuracy reached by this first architecture was 86.71% ± 3.31%. The second proposed architecture (SVM-MLP) is formed by a binary SVM and by a three stance sub-phases MLP neural network. In ***Figure 6. 2*** were reported the average classification results computed for each gait phase. The results referred to the average accuracy per class over the 5 folds computed for each of the 31 subjects involved in the study. The Initial Stance phases accuracy worsened with respect to the previous architecture to a value of 60.84% ± 15.45% (versus 61.42% ± 15.28%), the Mid Stance accuracy is 85.46% ± 7.41%, the Terminal Stance phase reached values of 86.63% ± 8.49%, while the Swing phase accuracy is 92.74% ± 3.19%. The Terminal Stance phase underwent a notable improvement (5.04%) in performance in terms of class accuracy (86.63% ± 8.49 versus 82.19% ± 8.24%), but the Kruskal-Wallis test showed no statistical differences between the performances of the two architectures. The mean overall accuracy reached by the present architecture is 86.70% ± 3.38% that is comparable with the overall classification performances reached by the first proposed model. Thus, noticeable differences were not detected by these two proposed models in terms of prediction accuracy. A third architecture was introduced, formed by two cascaded SVM classifiers (SVM-SVM). The class accuracy results were reported in ***Figure 6. 3***. The four gait sub-phases were predicted with 59.69% ± 20.07% for Initial Stance, 86.16% ± 8.11% for Mid Stance phase, 81.47% ± 9.11% for Terminal Stance and 92.74% ± 3.19% for Swing phase. The Swing phase reached the same values of accuracy and variability obtained from the previous architecture since the same binary model was implemented. The swing predictions out of the first SVM classifier were exactly the same. The Mid Stance phase reached the highest value of class accuracy among the three proposed architecture while the Terminal Stance phase the lowest one. A statistical analysis of these results was also performed. The Kruskal-Wallis test, performed on the accuracy distributions of each class for the three proposed architectures, highlighted no statistically significant differences among the proposed approaches in classifying gait phases. These results suggests that the three models have a comparable behavior in the classification of gait phases and no significant differences exists.

Nevertheless, different performances between the three models were reported in terms of ability to correctly identify gait transition events. The two cascaded SVM classifiers outperforms with respect to the previous two architectures and results were reported in ***Table 6. 4***. The F1-Score metrics is a harmonic mean between Precision and Recall. Precision measures the overall number of correctly predicted events over the total number of predicted positive events, while the precision is the measure of correctly predicted events over the total number of actual positives. The number of correctly classified events (i.e., true positive events) is high in all the three architectures, and the values of the Recall metrics is almost very high. Differences between the three proposed classifiers exists in terms of number of false positive events detected. The F1-Score value for the HS events is 92.10% for the first architecture, 91.53% for the second and 89.93% for the third proposed model. Despite the F1-Score values being the lowest for the third proposed model, the statistical test did not show significant differences between the three distributions and the null hypothesis could not be rejected. The same results can be translated for the HR (first 85.31%, second 85.68%, third 91.61%) and the TO (first 95.82%, second 96.08%, third 96.08%). The CTO events, however, was significantly better predicted by the SVM-SVM model with a F1-Score of 79.44% against 85.31% and 79.61% for the first and second architecture, respectively. The Kruskal-Wallis test confirmed that the third architecture outperforms in terms of CTO prediction accuracy with respect to the previous two. For this reason, the two cascaded SVM classifier is assumed as reference model in the present study. The average results, in terms of MAE, for the reference architecture reported values of 18.73 ± 6.14 ms for HS, 27.67 ± 9.61 ms for CTO, 40.45 ± 8.95 ms for HR and 29.26 ± 10.84 ms for TO transition event, comparable between the three proposed models. Once the SVM-SVM has been identified as the best cascading architecture, this model had to be validated using two literature-based 4-phase classifiers, SVM and MLP [2,5]. Classification results for the two 4-phases classifiers were reported in ***Figure 6. 7*** and ***Figure 6. 8***. Significant differences are not observable, and it can be concluded that the proposed models perform in a comparable way with 4-phase models already suggested in literature. Comparison results in terms of prediction of transition events were reported in ***Table 6. 6***. The detection performances of the HS events did not change between the simple models and the proposed reference architecture, in terms of F1-Scores. Differences exists between the reference approach and the SVM classifiers, with respect to the MLP neural network, for the identification of CTO and HR events. The proposed architecture outperforms the MLP classifier in the identification of the transitions between Initial Stance and Mid Stance phases and between Mid Stance and Terminal Stance phases. Moreover, the reference approach has higher detection performance in the identification of TO events with respect to both the standard 4-phase classifiers (96.08% against 82.23% for MLP and 88.50% for SVM).

In conclusion, the present work successfully proposed a novel approach for the classification of the main four gait sub-phases and the identification of the corresponding transition events, based on the implementation of two SVM classifiers in cascade. Compared with two state-of-the-art models (MLP and SVM), the SVM-SVM architecture was able to overall outperform them, in particular in the prediction of TO events. This event is particularly significant in gait analysis because it plays a key role in the identification of the two main gait phases (stance and swing). Improving the reliability of stance vs. swing classification could be crucial in clinics or for evaluating the effects of a rehabilitation effort. Furthermore, MAE values up to 50 ms can be considered clinically acceptable because they correspond to a percentage of the gait cycle < 5%. The SVM-SVM approach provided mean MAE values ≤ 40 ms for all the transition events (18.73 ± 6.14 ms for HS, 27.67 ± 9.61 ms for CTO, 40.45 ± 8.95 ms for HR and 29.26 ± 10.84 ms for TO) suggesting the suitability of this approach in clinical practice. It is also worth noticing that WSD samples, used in this study to train the supervised learning model, provided a very high information content that allows to obtain very high prediction performances. Most of the works present in literature use different data preparation that usually involved feature extraction or signal windowing [4-8]. The classifiers usually are fed with temporal windows during training and each label is associated with more than one samples of the input vector, in order to exploit redundancy of data. In the present work, each label given to the classifier is assigned to one single sample of the input vector. The predictive potential of the WSD signal also deserves a positive comment and future development can improve the data preparation process, increasing the information content provided to the classifier. Despite the good performances provided by the proposed classifier, the classification accuracy in general can be improved using post-processing algorithms. A primary factor that could affect prediction performances of the classifiers is the large variability of the sEMG and basographic signals from footswitches. The eight shaped path followed by each subject during the experimental protocol introduces gait variability such as number of steps and cadence, walking speed and changes in sEMG activation, due to curves, reversing, acceleration, deceleration. The impact of this issue is partially limited considering a great amount of data to train the models (ten sEMG signals per subject). It can be considered a limitation from the performance standpoint, but it can also highlight the ability of the models to correctly classify gait phases despite this variability. Another future improvement consists in the implementation of an appropriate post-processing algorithm capable of eliminating non-physiological predictions (gait phases too short or too long) in order to increase both classification performance and the identification of transition events.

References

[1] L. Ying, G. Farong, C. Huihui, X. Minhua*, "Gait Recognition Based on EMG with Different Individuals and Sample Sizes"*, Proceedings of the 35th Chinese Control Conference, pp 4068-4072, China, 2016

[2] M. F. Ghalyan, M. A. Alher, M. J. Jweeg*, "Human Gait Cycle Classification Improvements Using Median and Root Mean Square Filters Based on EMG Signals"*, IOP Conference Series: Materials Science and Engineering, 2021

[3] M. Meng, Q. She, Y. Gao, Z. Luo*, "EMG Signals Based Gait Phases Recognition Using Hidden Markov Models"*, IEEE International Conference on Information and Automation, pp 852-856, China, 2010

[4] C. Morbidoni, A. Cucchiarelli, S. Fioretti, F. Di Nardo, *"A Deep Learning Approach to EMG-Based Classification of Gait Phases during Level Ground Walking",* Electronics, 2019

[5] C. Morbidoni, A. Cucchiarelli, V. Agostini, M. Knaflitz, S. Fioretti, F. Di Nardo, *"Machine-Learning-Based Prediction of Gait Events from EMG in Cerebral Palsy Children"*, IEEE Transactions on neural systems and rehabilitation engineering, vol. 29, pp 819-830, 2021

[6] C. Morbidoni, L. Principi, G. Mascia, A. Strazza, F. Verdini, A. Cucchiarelli, F. Di Nardo, *"Gait phase classification from surface EMG signals using Neural Networks"*, XV Mediterranean Conference on Medical and Biological Engineering and Computing – MEDICON 2019, Portugal, 2019

[7] F. Di Nardo, C. Morbidoni, G.Mascia, F. Verdini, S. Fioretti, *"Intra-subject approach for gait-event prediction by neural network interpretation of EMG signals"*, BioMedical Engineering OnLine, 2020

[8] F. Di Nardo, C. Morbidoni, A. Cucchiarelli, S. Fioretti, *"Influence of EMG-signal processing and experimental set-up on prediction of gait events by neural network"*, Biomedical Signal Processing and Control, 2021

[9] R. Luo, S. Sun, X. Zhang, Z. Tang, W. Wang, *"A Low-Cost End-to-End sEMG-Based Gait Sub-Phase Recognition System"*, IEEE Transaction on neural systems and rehabilitation engineering, vol. 28, pp 267-276 2020

[10] N. Nazmi, M. A. A. Rahman, M. H. M. Ariff, S. A. Ahmad, *"Generalization of ANN Model in Classifying Stance and Swing Phases of Gait using EMG Signals"*, IEEE-EMBS Conference on Biomedical Engineering and Sciences, pp 461-466, 2018

[11] N. Nazmi, M. A. A. Rahmana, S. Yamamotob, S. A. Ahmad, *"Walking gait event detection based on electromyography signals using artificial neural network"*, Biomedical Signal Processing and Control, vol. 47, pp 334–343, 2019

[12] P. Wei, R. Xiw, RO. Tang, C. Li, J. Kim, M. Wu, *"sEMG Based Gait Phase Recognition for Children with Spastic Cerebral Palsy"*, Annals of Biomedical Engineering, Vol. 47, pp 223–230, 2019

[13] P. Wei, J. Zhang, P. Wei, B. Wang, J. Hong, *"Different sEMG and EEG Features Analysis for Gait phase Recognition"*, IEEE Annual International Conference of the IEEE Engineering in Medicine and Biology Society, EMBC 2020, 2020

[14] J. Ziegler, H. Gattringer, A. Mueller, *"Classification of Gait Phases Based on Bilateral EMG Data Using Support Vector Machines"*, IEEE International Conference on Biomedical Robotics and Biomechatronics (Biorob), pp 978-983, The Netherlands, 2018

[15] S. Kyeong, W. Shin, M. Yang, U. Heo, J. Feng, J. Kim, *"Recognition of walking environments and gait period by surface electromyography"*, Frontiers of Information Technology & Electronic Engineering, vol. 20, pp 342-352, 2019

[16] R. T. Lauer, B. T. Smith, R. R. Betz, *"Application of a Neuro-Fuzzy Network for Gait Event Detection Using Electromyography in the Child With Cerebral Palsy"*, IEEE Transaction on Biomedical Engineering, vol. 52, pp 1532-1540, 2005

[17] A. Alamdari, V. N. Krovi, *"A Review of Computational Musculoskeletal Analysis of Human Lower Extremities"*, in *"Human Modelling for Bio-Inspired Robotics"*, J. Ueda and Y. Kurita, Elsevier Inc., pp 37-73, 2017

[18] J. Perry, *"Gait Analysis: Normal and Pathological Function"*, Slack Inc.: Thorofare, pp 9-130, NJ, USA, 1992.

[19] N. Stergiou, *"Biomechanichs and gait analysis"*, Elsevier Inc., pp 225-250, 2020

[20] U. Della Croce, P. O. Riley, J. L. Lelasc, D. C. Kerrigan, *"A refined view of the determinants of gait"*, in *"Gait and Posture"*, Elsevier, Inc., vol. 14, pp 79-84, 2001

[21] C. L. Brockett, G. J. Chapman, *"Biomechanics of the ankle"*, Orthopaedics and Trauma, vol.30, pp 232-238, 2016

[22] D. A. Neumann, *"Kinesiology of the Musculoskeletal System",* Journal of Orthopaedic & Sports Physical Therapy, vol. 40, 2010

[23] F. Flandry, G. Hommel, *"Normal anatomy and biomechanics of the knee"*, Sports Medicine and Arthroscopy Review, vol 19, pp 82-92, 2011

[24] M. T. Hirschmann, W. Müller, *"Complex function of the knee joint: the current understanding of the knee"*, Knee Surgery Sports Traumatology Arthroscopy, vol. 23, pp 2780-2788, 2015

[25] D. P. Byrne, K. J. Mulhall, J. F. Baker, *"Anatomy & Biomechanics of the Hip"*, The Open Sports Medicine Journal, vol. 4, pp 51-57, 2010

[26] J. V. Basmajian, C. J. de Luca, *"Muscles Alive: Their Functions Revealed by Electromyography"*, Williams & Wilkins, 1985

[27] H. M. Raez, M. S. Hussain, F. Mohd-Yasin, *"Techniques of EMG signal analysis: detection, processing, classification and applications"*, Biological Procedures Online, vol. 8, pp 11-35, 2006

[28] H. D. Dave, M. Shook, M. Varacallo, *"Anatomy, Skeletal Muscle"*, Treasure Island (FL), 2022

[29] V. M. Zatsiorsky, B. I. Prilutsky, *"Biomechanics of Skeletal Muscles"*, Human Kinetics, pp 12-59, 2012

[30] G. M. Cooper, *"The Cell: A Molecular Approach"*, 2nd Edition, Sinauer Associates, 2000

[31] P. Bolaños, J. C. Calderón, *"Excitation-contraction coupling in mammalian skeletal muscle: Blending old and last-decade research"*, Frontiers in Physiology, vol 30, 2022

[32] S. Pham, Y. Puckett, *"Physiology, Skeletal Muscle Contraction"*, Treasure Island (FL), 2022

[33] P. Konard, *"The ABC of EMG: A Practical Introduction to Kinesiological Electromyography"*, Noraxon Inc., USA, 2005

[34] C. Bischoff, A. Fuglsang-Fredriksen, L. Vendelbo, A. Sumner, *"Standards of instrumentation of EMG. The International Federation of Clinical Neurophysiology"*, Electroencephalography and clinical neurophysiology, Supplement vol. 52, pp 199-211, 1999

[35] R. Merletti, G. L. Cerone, *"Tutorial. Surface EMG detection, conditioning and pre-processing: Best practices"*, Journal of Electromyography and Kinesiology, vol. 54, 2020

[36] A. Sabharwala, B. Selmanb, *"Artificial Intelligence: A Modern Approach"*, Third Edition, Artificial Intelligence, pp 1-7, 2010

[37] J. Haugeland, "Artificial Intelligence: The Very Idea", Cambridge: MIT Press, 1985

[38] E. Charniak, D. McDermott, D. V. McDermott, "Introduction to Artificial Intelligence", Addison-Wesley, 1985

[39] R. Kurzweil, "The Age of Intelligent Machines", Kurzweil Foundation, 1990

[40] D. Poole, Alan Keith Mackworth, R. Goebel, "Computational Intelligence: A Logical Approach", Oxford University Press, 1998

[41] P. P. Shinde, S. Shah, *"A Review of Machine Learning and Deep Learning Applications",* Fourth International Conference on Computing Communication Control and Automation, pp 1-6, 2018

[42] S. Raschka, V. Mirjalili, *"Python Machine Learning: Machine Learning and Deep Learning with Python, scikit-learn, and TensorFlow 2"*, Second Edition, Packt Publishing Limited, 2017

[43] W. S. McCulloch, W. Pitts, *"A logical calculus of the ideas immanent in nervous activity"*, Bulletin of Mathematical Biophysics, vol. 5, pp 115–133, 1943

[44] P. Raj, P. Evangeline, *"The Digital Twin Paradigm for Smarter Systems and Environments: The Industry Use Cases"*, First Edition, Advances in Computers, Vol. 117, 2020

[45] S. Khandelwal, N. Wickstrasm, "*Evaluation of the performance of accelerometer-based gait event detection algorithms in different real-world scenarios using the MAREA gait database"*, Gait Posture, vol. 51, pp 84-90, 2017

[46] D. Trojanello, A. Cereatti, U. Della Croce, *"Accuracy, sensitivity and robustness of five different methods for the estimation of gait temporal parameters using a single inertial sensor mounted on the lower trunk"*, Gait Posture, vol. 40, pp 487-492, 2014